Seismic Response of Tunnels in Partially Degraded Ground

部分的な劣化地盤がトンネルの地震時挙動に及ぼす影響

Saddy Ahmed

2021

Seismic Response of Tunnels in Partially Degraded Ground

部分的な劣化地盤がトンネルの地震時挙動に及ぼす影響

By

Saddy Ahmed

A Dissertation Submitted to the Graduate School of Urban Innovation, Yokohama National University in Partial Fulfilment of the Requirement for the Degree of

Doctor of Engineering

Yokohama National University, Graduate School of Urban Innovation

Examination Committee

Associate Professor, Dr. Ying CUI (Chair)

Professor, Dr. Kimitoshi HAYANO

Professor, Dr. Koichi MAEKAWA

Associate Professor, Dr. Mamoru KIKUMOTO

Associate Professor, Dr. Chikako FUJIYAMA

September 2021

Preface

My continued pursuit of acquiring education is reflective of my commitment to learn and excel. I was able to achieve quality education with the help of my parent's guidance, my teachers, and the level of my commitment. It was difficult at times, as it is difficult in the beginning, but it has gradually moved to a smooth path. I had the opportunity to be exposed to the course of MSc Civil Engineering during my university period; I had the opportunity to study basic and advance courses related to underground development in the period of graduate study. This developed my interest to get higher education. So, I made my mind to get higher education in the field of Tunnel Engineering.

I am extremely thankful to the Ministry of Education, Culture, Sports, Science, and Technology (MEXT) Japan for the generous Grant-in-Aid for doctoral studies and thanks to Yokohama National University Japan as they gave me a chance to study for my desire degree.

I am indebted to my supervisor and examiner Associate Professor Dr. CUI Ying as she gave me a chance to work with such an interesting topic. I am extremely grateful to Professor Dr. Kimitoshi HAYANO and Associate Professor, Dr. Mamoru KIKUMOTO for their valuable support and guidance during the lab seminars.

In the end, I would like to say thanks to my wife, beloved parents, and my siblings. Furthermore, special thanks to my friends for their joyful company.

Yokohama, September 2021

Saddy Ahmed

Abstract

Past experiences in the field of tunnel engineering have suggested a high correlation between the presence of weak zones behind the tunnel lining and seismic damage of tunnels. Several tunnels have exhibited the presence of such weak zones as one of the prime reasons for tunnel failure. The formation of these weak zones usually is associated with poor workmanship, water erosion, improper backfilling, slacking of soil, and/or dynamic loadings caused by construction activities. This study has been conducted to confirm the existence of such correlations from an experimental perspective. To accomplish the task a two-dimensional shaking table test has been designed for a shallow circular model tunnel having weak zones behind the lining and subjected to uniform sinusoidal seismic waves. The tunnel model was equipped with several strain gauges to record the produced strain and changes in the strain for pre-weak zones creation, considering weak zones at static state as well as under dynamic conditions of the table. To measure the acceleration and displacement of the table, an accelerometer and a displacement sensor were attached to the table, while the ground's shear displacement was recorded with the help of a laser sensor. A high-speed camera was used to capture the image series during the shaking process. The images were then analyzed through Particle Image Velocimetry (PIV) technique to calculate the strains in the ground.

Herein, a weak zone is defined as a loose ground with a higher void ratio as compared to the surrounding ground. During laboratory experiments, the weak zone was created by removing the calculated amount of ground particles to attain a required value of the void ratio between the lining and the surrounding ground. During the experimental process three values of the void ratios i.e., 0.30, 0.45, and 0.60 have been explored and results have been compared with the case of full contact. Tunnel response was recorded after putting the weak zone at the prime locations of the tunnel such as the crown, shoulder, and springline positions. Later, a crack was introduced in the tunnel model to check the effect of a joint opening during seismic excitation and its position was varied with and without the weak zone to check the tunnel response. The crack is defined as a complete cut made along the length of the tunnel model. Aluminum rods with uniform length consisting of two sizes mixed have been used as a model soil material and all experiments have been performed at a shaking frequency of 1 Hz.

The seismic response of the tunnel was measured in terms of internal strains and bending moments. While the ground response was recorded in terms of strains produced in the model ground and shearing displacement during the shaking process. Results indicate that the weak zone behind the lining can change the stress state of the tunnel and in some cases, the bending moment can reverse its sign from positive to negative and vice versa. It has been observed that the internal strain at the point of the weak zone and crack location tends to change itself from tension to compression side which means the tunnel tends to bend towards the loose cavity's direction and this phenomenon intensifies with the increase of the void ratio of the weak zone. The shear displacement of the table shows significant changes with the introduction of the weak zone. The volumetric strain shows that with the introduction of the weak zone the ground volume changes considerably. It has been observed that during shaking of the table the ground particles move towards the weak zone location and as the number of cycles increases, more compression happened in the ground. Moreover, the increase of the void ratio of the weak zone produced more compression strain in the vicinity of the weaker part. Finally, a crack was introduced along the tunnel length and its effect was also checked on the tunnel and ground response. The bending behavior of the tunnel and the ground response due to the presence of the crack and the weak zone is different.

The above findings suggest a close relationship between large stress concentration in the structure as well as in the ground caused by the occurrence of the weak zones and the crack in the lining before and during an earthquake. The damages can be concrete cracking, concrete spalling, water infiltration resulting from joint opening, and/or even the complete failure of the tunnel. Based on these findings, early detection of loose cavities and placement of reinforcement where large stress concentrations can occur is crucial for preventing the seismic damage of tunnels.

Acknowledgment

This research would not have been possible without the encouragement and continuous support from my supervisor Associate Professor Dr. CUI Ying and the financial support provided by MEXT Japan.

I appreciate the understanding and support as well, received from Dr. CUI Ying when things were not going well at times.

I would like to thank my examiners Prof. Dr. Kimitoshi HAYANO, Prof. Dr. Koichi MAEKAWA, Assoc. Prof. Dr. Mamoru KIKUMOTO, and Assoc. Prof. Dr. Chikako FUJIYAMA for their deep insight and valuable suggestions during the pre-defense occasions to further improve the research.

The time spent at Yokohama National University wouldn't have been the same without the time shared with all other researchers in rooms 205 and 206, the ones that were already there, when I started, and those who arrived after I joined the Geotechnical Engineering laboratory.

I would like to very special thank you to Mr. Kobata, Mr. Usman Ali for their help in doing the laboratory testing.

Last but not least, thanks to my beloved parents, wife, fellow Ph.D. student Dr. Kim Minkoan and Dr. Saqib Ashraf who listened to me and shared interesting experiences from their studies as a Ph.D. student.

List of Figures

List of Tables

Table of contents

CHAPTER 1: INTRODUCTION

1.1 Research Background

Tunnels are very important structures built from one place to another species in hilly areas to create a path for railway and roads transportation. In urban areas, apart from transportation, they are considered as one of the main underground facilities for lifelines such as sewerage and waterworks, etc. While designing the main structure, major attention is being given to the design, selection of construction materials, and the durability aspects (Cui and Kimura, 2010). For an economical and safe design, it is required to estimate the accurate loads acting on the lining. In Japan, the load acting on the lining is estimated by Terzaghi's formula, or overburden load is adopted for further calculations (H. Mashimo, 2003). To evaluate the structural stability of the lining under dynamic conditions, it is required to predict the stresses induced by the seismic activities. When exposed to an earthquake, it is thought that tunnels are relatively safer than surface structures (Yasuda et al., 2019). However, some tunnels have experienced significant damages during recent earthquakes e.g. the 2016 Kumamoto (Zhang et al., 2018), the 2008 Wenchuan (Li, 2012), the 2004 Niigata (Yashiro et al., 2007), the 1999 Chi-Chi (Wang et al., 2001) and the 1995 Kobe (Asakura and Sato, 1996). The damages reported in these tunnels show that the failure mechanism of tunnels under seismic excitation is very important.

The tunnels constructed in hilly areas, when hit by massive earthquakes are prone to severe damage if they are built very close to a fault line and /or under special circumstances (Yashiro et al., 2007). The special circumstances include structural defects in the lining, shallow tunnel, poor geological conditions, and movement of an earthquake fault where the lining is constructed. Severely damaged tunnels, reported in the literature, have been found to have a minimum of one of the above-mentioned conditions. In Japan, the conventional tunnels constructed before NATM (New Australian Tunneling Method) are often presenting partial discontinuities or weak zones. There are two main reasons for the development of these weak zones as illustrated with the help of Figure 1-1. The first reason for the weak zone development is the procedure of the lining support in which a sheet pile was usually used as the principal support, frequently following in a gap

between the surrounding ground and the tunnel support. The second cause involves the procedure through which the lining structure was placed in which usually the concrete was poured at the upside of the tunnel steel form and then let it compact with the help of only gravity forces, resulting in large weak zones around the crown. Such weak zones between the lining and the supporting rock negatively affecting the performance of the lining structure (Meguid and Dang, 2009a); (Wang et al., 2014); (Meguid and Kamel, 2014).

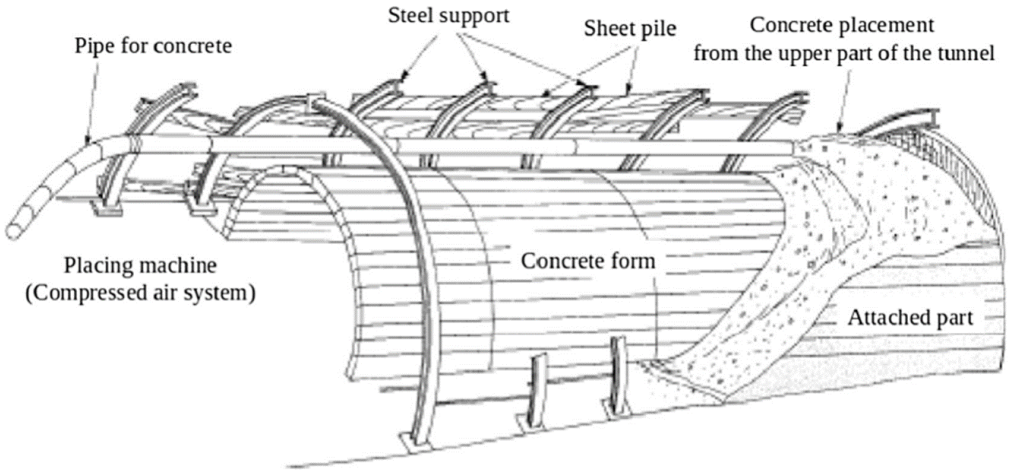

Figure 1-1. The conventional tunnel construction method in Japan (Takeuchi et al., 2013)

The latest method of tunnel construction includes three stages: the ground excavation, permanent support structure installation as a tunnel lining, and finally the placement of the overlaying soil on the tunnel lining. The excavation of ground mass causes the loss of soil support in the remaining soil material and ultimately produced a redistribution of stresses. The steps of tunnel construction by using a Tunnel Boring Machine (TBM) are illustrated in Figure 1-2. It can be seen that if the soil is immediately not backfilled it can produce a large settlement and loss of ground. While excavating the ground with the help of TBM, the size of excavation is usually kept higher than the actual size of the lining. This phenomenon produces a gap in between the surrounding soil and the tunnel lining. This gap starts directly above the tunnel crown in a crescent shape and moves towards the points, where the tunnel rests i.e., the invert of the tunnel. The size of the gap depends upon the underground soil conditions, the type of machinery, and the tunnel expertise involved in the project. For static analysis, the crown, which represents the highest point of the tunnel, the springlines, representing the horizontal edges of the lining, and the invert, representing the lowest point of the tunnel are considered the principal points of a tunnel (Lee et

al., 1992). While shaking in the horizontal direction the shoulders, which shows the upper diagonal point between the crown and the springline, the knees, which represent the lower diagonal point between the spring line and the invert are the principal points.

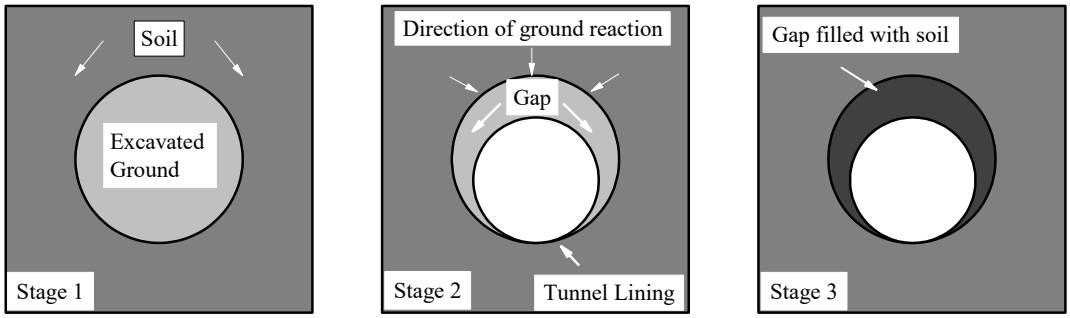

Figure 1-2. Steps of tunnel construction using Tunnel Boring Machine

The NATM technique of tunnels construction includes blasting, placement of temporary support, and provision of a permanent support system as illustrated in Figure 1-3. The blasting phenomena cause rock deformation which was later repaired with shotcreting. If the damages in the rock are not properly located and repaired, loose cavities in the form of weak zones can develop behind the liner.

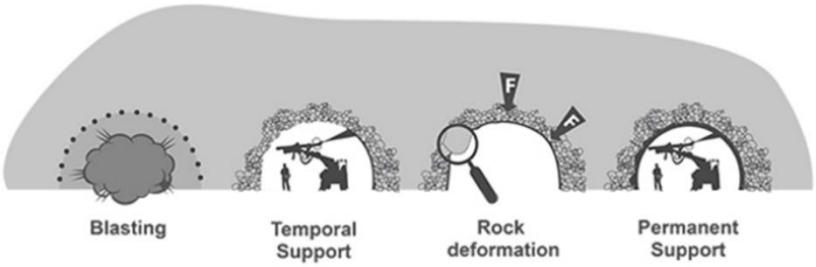

*Figure 1-3. Tunnel construction using NATM technique (*Rekindled NATM Debate, 2008*)*

The existence of gap/ weakened zones can be one of the most substantial sources of seismic damage to tunnels. Currently, the seismic design of circular tunnels based on time-domain finite element (FE) analysis (Pakbaz and Yareevand, 2005; Cai, 2008; Clot et al., 2016), deformation based static FE analysis (Hashash et al., 2005; Sedarat et al., 2009), and analytical solutions (Hashash et al., 2001; Bobet, 2010; Nejati et al., 2012). The above-mentioned solutions consider the full contact between the soil and the lining structure throughout the service life of the tunnel. However, weak zones may develop around the tunnels because of many reasons such as poor

workmanship, insufficient backfilling of supporting material, water erosion, and/or dynamic loadings caused by construction activities as mentioned above (Howard, 1991; Meguid and Dang, 2009; Gomes et al., 2015; Zhang et al., 2019). The damaging consequences of weak zones can be tunnel appurtenance corrosion, reduction in load-carrying capacity due to major deterioration, and even complete lining failure as the surrounding rock/soil gradually loosen around the weak zone (Helfrich, 1997; Leung and Meguid, 2011; Meguid and Kamel, 2014). Although the detection of such weak zones' location is not difficult the perfect renovation is not an easy task (Jifei et al., 2014). Thereafter, such sort shortcomings have gained much more vigilance from the earthquake engineering community but negligible from the design, construction and operation bodies as such deficiencies are often related to unforeseen phenomena (Xin et al., 2018). At present, the sizeable contribution of weak zones towards tunnel failure has started to attract the attention of many researchers (Wang et al., 2014).

To deal with the tunnel-weak zone interface problem in static and dynamic conditions, many researchers initiated weak zones' position detection projects with the help of different non-destructive approaches and techniques e.g. Davis et al., 2005; Aggelis et al., 2008. Undoubtedly, the weak zones behind linings are very common especially on crown positions (Yu et al., 2016). Furthermore, in many seismically severe regions, normally, the total length of weak zones behind the linings is more than 50% of the highway tunnel's length and more than 10% of the railway tunnel's length (Xiao et al., 2014). The complications resulting from the formation of weak zones can be described into three phases; appearance, expansion and, shrinkage and collapse, which ultimately results in reducing the load-carrying capacity and operational security of the lining (Huang et al., 2013). Thus, timely detection and renovation are very important for the tunnel's safety as many tunnels have already been constructed in earthquake-prone and weak zone concealing areas (Wang et al., 2015). Therefore, researchers need to examine the dynamic behavior of tunnel linings accompanied by loose cavities, aiming to achieve the protection of tunnels during and after seismic excitation. Because of this need, the current study targets the static and dynamic behavior of tunnel linings for different lining-weak zone interaction conditions. To accomplish this task, the authors had planned and conducted several tests on lining models using a shaking table by introducing the weak zones at tunnel crown, shoulder, and springline positions. The explanations of the laboratory tests covering experimental setup, test arrangements, ground material and lining model, stresses in the ground mass measured through particle image

velocimetry, and quantitative discussion on stress changes of lining under static as well as dynamic conditions are unveiled in this thesis. The outcomes of this investigation will be a useful contribution to references for future research work related to weak zone-inducing complications to tunnel linings.

1.2 Aims and Objectives of the Research

This research aims to provide an independent evaluation of the performance of the tunnel accompanying weak zones at various locations around its periphery by performing a series of laboratory testing and numerical simulations within the shallow overburden domain (i.e., $^{H}/_{D} \leq 2.0$ where H is the height of soil profile above the tunnel crown and D is the internal diameter of the tunnel). The ground created during the laboratory experiment was similar to dense sand or rock. The void ratio of the weak zone was set as the key parameter to represent the actual field conditions during physical testing. The key objectives of the research are:

a. Obtaining a general trend of stress redistribution in tunnel lining for a shallow overburden tunnel with weak zones behind the lining through laboratory testing under static and seismic conditions. The results of weak zones have also been compared with the crack on the lining.
b. Estimation of various types of stresses produced by the seismic excitation in the groundmass with different conditions of the weak zone.

The author has been very thorough and open in expressing not only the success but also the limitations and problems experienced during the research as such things often tend not to be included in the published literature thus reducing the chances of continuous improvement. Few of the results gathered during the present investigation have been previously published in various peer-reviewed conferences and journals.

1.3 Thesis Layout

This thesis has been divided into seven chapters organized as follows:

Chapter 1 Introduction

Problem statement formation, the review of the previously published literature in the field, and aims and objectives of the research.

Chapter 2 Literature review

A comprehensive study on the state-of-the-art literature available already related to the effect of the weak zone on tunnel response and the fundamental behavior of shallow overburden tunnel.

Chapter 3 Outlines of the experiment

A detailed explanation of the experimental setup including shaking table test, model ground, and tunnel behavior. The setting of various parameters which satisfy the basic rules and data acquisition system.

Chapter 4 Effect of weak zone position

The effect of weak zone location at different positions around the lining has been discussed in detail. The crown shoulder and springline positions have been explored.

Chapter 5 Effect of weak zone size and stiffness

This chapter included the results of the effect of weak zone size and stiffness. Two sizes have been checked and the ground as well tunnel responses have been documented. Similarly, weak zones with two different stiffnesses have been tested and compared with the case of full contact.

Chapter 6 Combined effect of the weak zone and crack

This chapter explains the results of crack and their comparison with the weak zone. Lastly, the combined effect of the weak zone and crack has been explored.

Chapter 7: Conclusions and Recommendations

In this chapter, the overall activities, results, and discussion of the study are summarized. Lastly, the gained benefits from the study and the improvement of the current study for future research have been pointed out.

CHAPTER 2: LITERATURE REVIEW

2.1 Introduction

Weak zone formation behind the tunnel lining has been a problem of rising apprehensions from owners and engineers' side. As stated in chapter 1 the possible issues caused by weak zones behind the lining can range from being a slight bother to complete collapse of the structure. In August 2006 The *Highway & Rail Transit Tunnel Maintenance & Rehabilitation Manual* ("U.S. Department of Transportation Federal Highway Administration. Highway and Rail Transit Maintenance and Rehabilitation Manual", 2005) released the mechanism of weak zone formation, and according to this one of the reasons is that the water can force the fine-grained particle to pass through the cracks thus creating the weak zone behind the lining. As a result of these weak zones, the surrounding structures can settle causing the development of unforeseen stresses from eccentric loading. Howard and Chairman, 1991; McDonald and Zhao, 2001; Davis et al., 2005 have mentioned that weak zones behind the lining are a very serious issue that can greatly affect the service life of the tunnel.

This chapter will summarize the review of case studies of weak zones around the tunnel lining. Most of the case histories presented in the literature are related to pipes. Moreover, as opposed to the tunnels the pipes can be excavated and the real scenario can be inspected more closely. Although the construction and underground conditions of pipes infrastructures are not identical as they are for tunnels, still there are enough similarities that exist so that one can extend the indications of the effects of the lining weak zone.

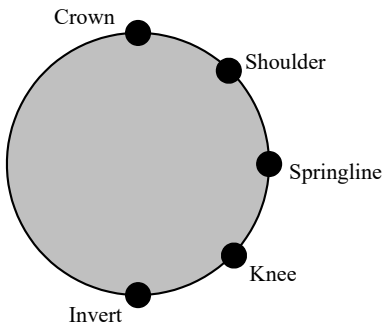

Figure 2-1. Different points of a tunnel

2.2 Development of Weak Zones Around Tunnels

The occurrence of weak zones has been documented within tunnel maintenance and rehabilitation literature. However, it's very surprising that only limited research has been done related to this problem. The published literature comprises case studies related to the mechanism of formation of the weak zone and their effects on the surrounding ground soil and/or tunnel lining. However, a lot of articles make no more than the introduction of the problem. Nevertheless, while citing the weak zones around the lining, the majority of the authors describe them as an area of loosened ground, initially caused by the moisture infiltration through cracks in the tunnel lining (Asakura and Kojima, 2003). As the moisture infiltrates into the underground structure, from the surrounding grounds, it carries with it fine soil particles. With the passage of time, the continuously eroding water can badly weaken the portion around the crack on the tunnel lining. This activity may head towards a ground loss and the overburden pressure will force the weak zone to collapse. The weak zone formed by the erosion may also cause the alteration in the distribution of the earth pressure and the resulting bending moments on the tunnel lining as the soil stresses try to readjust to the cavity formed by erosion in a process known in geotechnics as arching. This can also lead to ovalization of the tunnel and possibly cave-ins (ITA, 1991). McDonald and Zhao, 2001 stated that the weak zone formation caused a loss in the ground which leads to premature failure and this phenomenon can be explained by considering the soil support as integral to the underground structures. They also stated that the sand and the silts are the types of subsurface ground materials that are highly susceptible to this mode of deterioration. The reason is the size of the particles of these soil types as they may contain grains that are small enough to move through cracks but permeable enough to allow for high seepage flows. Delatte, 2003 described that a lot of tunnels are constructed below the water sources. The structures in such circumferences are more vulnerable to the hazards of water damage and the outcomes are hypothetically even more dangerous if the tunnel failure were to occur. Figure 2-2 shows the development of a weak zone caused by erosion on the outer side of a tunnel lining.

Many recorded case histories of soil erosion occurring in the ground on the outside of a tunnel lining. Development of such weak zones, in some cases, has been detected before any significant damage occurs to the tunnel lining. However, in the majority of the cases, they are only revealed while conducting post-failure forensic investigations. In an International Tunnelling

Association report published in 1991 (ITA, 1991) presenting and detailing case studies related to the effects of water contributing to the damages of the tunnel, at least 4 cases are cited in which the lining structure experienced the damage because of "a loss of support due to the transport of fines". One of these tunnels was constructed to convey the water and two were to transport the sewerage (all in the U.S.) and the remaining one was a transportation tunnel in Japan. The transportation tunnel was built without sufficient waterproofing because of unforeseen water levels. Soon after the completion of the tunnel, huge amounts of seepage started at the lining segment joints accompanying extensive amounts of ground particles. While this indicated substantial soil support loss at the tunnel springline, no noticeable damage occurred because the leak was promptly sealed and grouted. In all three cases in the U.S., the tunnels were built in silty or sandy soils. Each case experienced a loss of soil support on the sides and inverts of the tunnels. Loss of support at the tunnel invert was followed by increased cracking circumferentially and loss of support at the sides caused ovalization and longitudinal cracking. Further weak zones formed at the lower most of the tunnel triggered settlement of the lining contributing to more damage to the tunnel. Two out of three of the tunnels were restored with the help of pipe jacking or grouting. While in the case of the third one, the tunnel was to be abandoned mainly due to the huge amount of sediment that had flooded in through the lining.

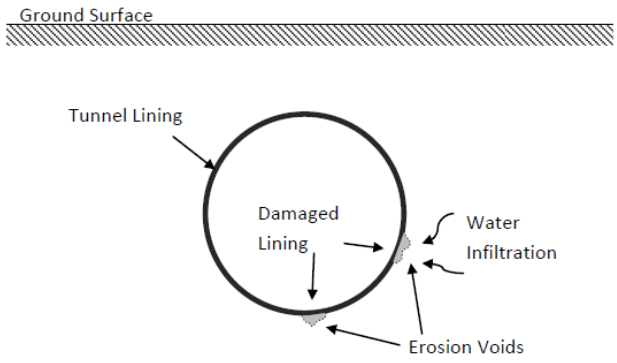

Figure 2-2. Development of weak zone at cracks in the tunnel lining (Cheehan Leung, 2009)

Davis et al., 2005 conducted tunnel lining inspections using non-destructive testing (NDT) methods. The developed methods were utilized in Buenos Aires, Argentina on a section of a water conveying tunnel. The methods included impulse radar and impulse response or transient dynamic response. In the above-mentioned case, the weak zones behind the tunnel lining were caused not

by erosion of water but improper grouting also played an important part. Davis et al., 2005 used impulse radar to determine whether the voids were of sufficient size to prevent hoop stresses from fully developing in the tunnel lining. The results did show some voiding occurring near the springline of the tunnel lining, but it was concluded that it was not large enough to cause significant damage to the lining. Figure 2-3 shows the reported impulse radar image.

Pipe infrastructure provides many good examples of the formation of the destructive potential of erosion voids. The reason is that there is more underground pipe infrastructure than tunnels, particularly those that are in a dire state of poor condition. Moreover, it is also generally simpler to excavate and substitute the damaged pipes. Even though there exist some dissimilarities in the earth pressure felt by pipe structures and by tunnel linings, mainly because of the different methods of construction, the similarities are close enough to draw a similarity between the two situations. The way of damaged experienced by pipe structures due to weak zones caused by erosion can be somewhat analogous in tunnel linings.

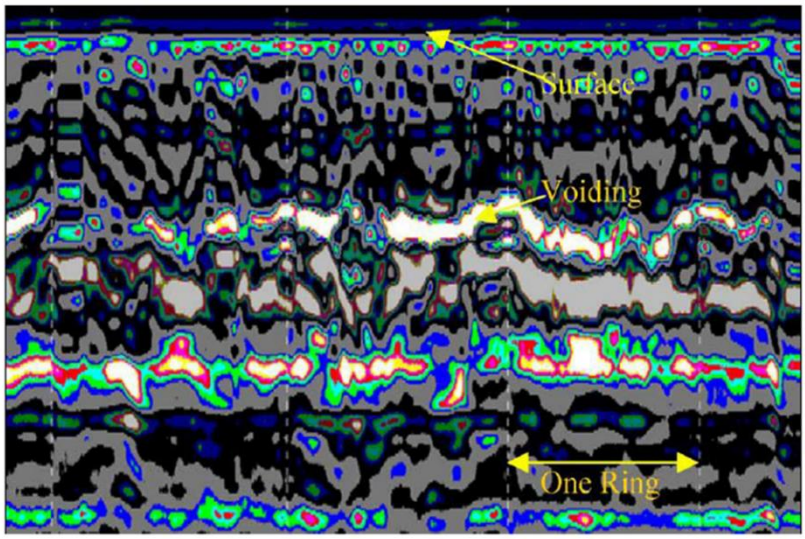

Figure 2-3. Detection of soil voids by Impulse radar method (Davis, Lim, and Petersen 2005)

Helfrich, 1997 performed an investigation into a failed 0.3 m diameter pipe constructed for sewerage purposes. In this particular case, the pipe was buried at depths from 3 to 6 m and was composed of vitrified clay. Due to incomplete subsurface investigation before the pipe design and installation, there was substantial settlement under the invert of the pipe. It was found that some lengths of the pipe were settled up to 50 mm and were therefore unable to maintain service. The main part of the pipe needs to eventually be replaced with a more thick layer of the backfill bedding underneath the bottom part. Talesnick and Baker, 1999 also presented the failure of a pipe whereby

the structure was failed because of excessive settlements below the invert of the pipe. As in the previous case, the pipe was collapsed because of insufficient support from the pipe invert. The pipe was made of a composite material composed of concrete and steel having a diameter of 1.2 m and was constructed in a stratum of clay over a backfill of granular bedding. The pipe was collapsed due to unsustainable downward deflection in a span of one year after its installation and was never used for its intended purpose. The post-failure investigation revealed that sections along the longitudinal axis developed some gaps under the invert with a height of around 200 mm. While the loss of the surrounding ground support for the pipe in the examples mentioned earlier may not have been due to erosion void formation, they still illustrate the potentially disastrous effects of a loss in soil support.

Davis et al., 2005 written a document that cataloged the different factors that can lead to the deterioration of pipes especially the rigid sewer. This comprehensive report highlighted many conditions which promote or mitigate the formation of weak zones around the pipes. They also summarize the steps involved in the deterioration of the sewer. Weak zones formed by erosion are not the only outlined form of sewer pipe deterioration, but they are, however, very much predominant which can head towards the other severe complications. Accordingly, Davis et al., 2005 included a comprehensive analysis of this issue.

Various authors including Hoffman and Lerner, 1992; Serpente, 1994; and Fenner, 2000 have thoroughly documented the stages of sewer failure. Davis et al., 2005 described three stages of pipe failure. The initial step includes a small, usually unnoticed crack or defect initiated by either construction oversight or excessive overburden. These cracks usually arise at the principal locations of the tunnel lining located at the crown, springlines, and invert due to the disproportionate bending moments at those locations. Although the defects of stage one are minor and even the pipe still maintains complete soil support and its structural integrity. However, they cause further disintegration to happen.

The second stage of pipe failure is primarily the ongoing and sometimes quick decline of the lining of the sewer. This is mainly due to the loss of side support because of moisture inflow and continuous transport of fine grains into the structure from the neighboring soil. This can also be responsible for substantial soil loss. The loss of ground will impose extra stresses on the lining structure and inside the ground material itself. Eventually, the removal of side ground support can enlarge the previous cracks into ever-larger fractures on the sewer lining, permitting more and

more seepage flow. This stage of pipe failure can also be spotted by a possible although insignificant ovalization of the pipe structure.

The final and the third stage of failure is the complete collapse of the pipe. This occurs when additional deformation movement of the pipe lining exceeds 10% of the initial positions. At reaching this stage, the pipe is at a high chance of failing. Generally, the failure itself is not because of the above-mentioned soil erosion mechanisms. Instead, it is happened by a sudden alteration in conditions on the sewer pipe such as an abrupt excessive surcharge or nearby excavation causing the release of supporting soil stresses. The presence of large weak zones caused by erosion around the outside of the lining can be expected before the failure. This loss of soil support for the pipe structure is the reason for the increased chance of failure. At this point, the pipes will cease to function properly and be in dire need of repair or replacement Figure 2-4 shows the development of the three stages of sewer failure.

2.3 Influence of Weak Zone

Tan, 2007 carried out a finite element analysis (FEM) to explore the impact of soil weak zones on the bending moment and the circumferential forces of a pipelining. Weak zones of different sizes paced at the springline of a rigid pipe were examined under plane strain conditions. By considering both linear elastic and elasto-plastic illustrations of the soil material a finite element model (FEM) was developed. The weak zones in the ground were considered as idealized circular shapes at contact angles on the pipe surface of 30°, 60°, and 90°. The granular ground material was adopted and the weak zones represented included those up to the highest size observed before ground settlement and surface changes were noticed (Spasojevic et al., 2007). Figure 2-5 illustrates the size and shape of the modeled weak zones.

Moore, 2008 presented the results of the finite element analysis. during all simulations, the primary factor was the contact angle on which the weak zone traversed the pipes. For the weak zone angle, it was observed that as the internal angle increased, the circumferential stresses and bending moments increased in the pipe structure. The increase of the circumferential stresses exceeded 100% of the initial values at the largest contact angle was simulated on the pipe. Since the majority of the pipes are constructed with a factor of safety around 2, it was concluded that an increase of over 100% should be enough to prompt cracks in the pipes lining. Figure 2-6 shows an example of one of the simulations. The plotted data show the changes in circumferential

compression and tension stresses on the crown of the pipe as the contact angle with the erosion void increases.

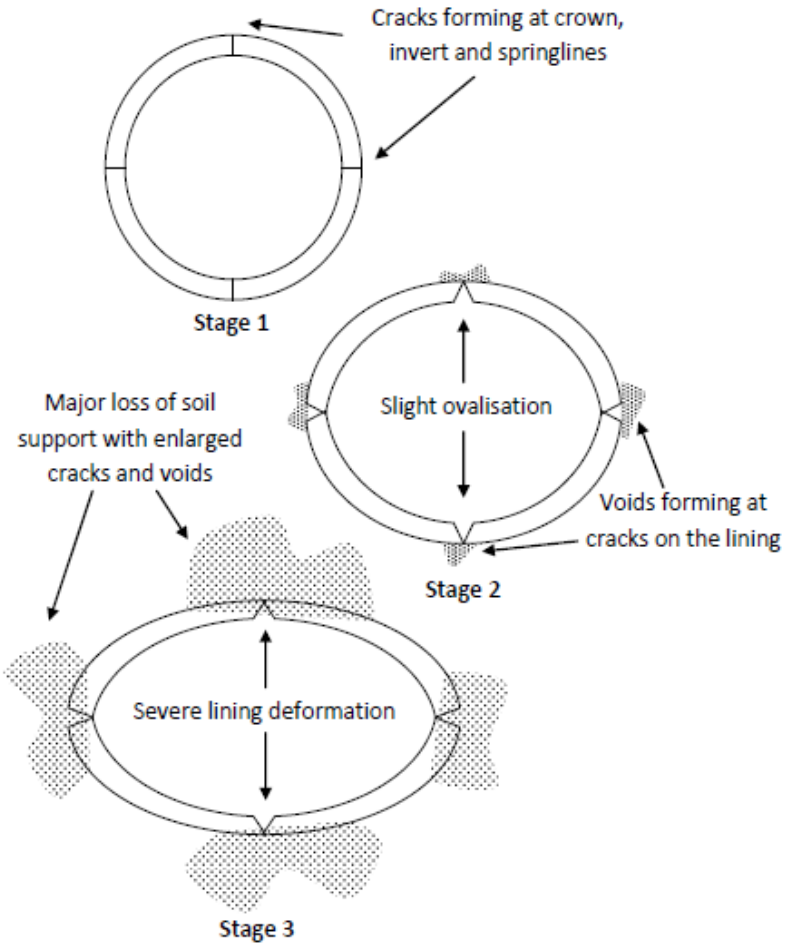

Figure 2-4. The stages of sewer pipe failure (Adapted from (Davis et al., 2005)

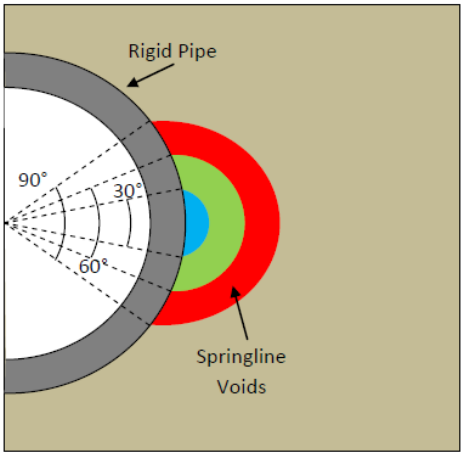

Figure 2-5. FEM voids on a pipe springline (Tan and Moore, 2007)

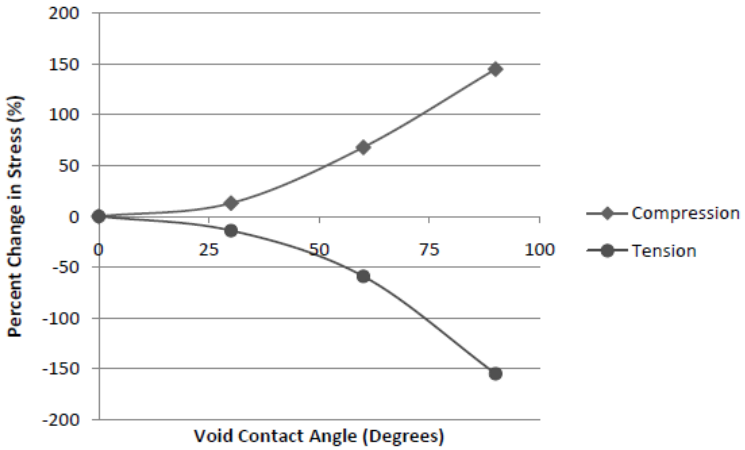

Figure 2-6. Circumferential stress changes at the crown (Moore, 2008)

Meguid et al., 2008 performed the numerical simulations to explore the action of weak zones caused by erosion on the circular tunnel linings as the simulations performed by Tan and Moore, 2007, the tunnel linings were examined under plane strain conditions using finite element analysis. In this case, the weak zones appearing on both the springline and invert of the tunnel were considered. The weak zones caused by erosion were exemplified as a series of circular shapes arising on the outer surface of the tunnel. These weak zones vary in size by the percentage of the tunnel circumference and range from 3% to 15%. For this specific model, the tunnel was considered to be constructed in soft ground and to be a shielded bored tunnel. The model tunnel was located 10 meters below the ground surface with a diameter of 4 meters. Meguid and Dang, 2009a also checked the effect of the flexibility ratio of the tunnel lining, accounting for the effect of erosion voids on tunnel linings of differing flexibility. In conclusion, in this model study, a tail void volume loss of 1% was assumed which is good correspondence with observed field values. Figure 2-7 illustrates the weak zone simulated around the lining.

The results reveal that the weak zones can cause unaccounted-for changes in the bending moments and the thrust forces on tunnel linings. The observed changes were found to be mainly dependent on the size of the weak zone. It is also worthy to note that the changes in the bending moment were more prominent than axial forces. The springline suffered a maximum increase in bending moment whereas there was also a reversal from negative bending moments to positive at the invert position. This reversal of bending moment is a crucial finding because the section of the tunnel lining that is designed to resist compression loads could easily fail under tension as the concrete strength is different under tension and compression situations. It was concluded that due

to these findings careful attention must be given to detect and repair weak zones in existing tunnels. However, it is also important to note that these finite element models are just simulations based on theoretical equations and need to be verified through laboratory and physical testing. Figure 2-8 - Figure 2-10 show some of the findings from these simulations.

The flexibility ratio of the tunnel and the length of the weak zone were the variables and the effects on the lining bending moment and the axial thrust were checked. It can be seen that the tunnels with a less flexibility ratio attract more bending moments as compared to ones with higher flexibility ratios. The increasing length of the weak zone caused more changes in the lining stresses. While comparing the position of the weak zone it was found that the maximum changes in the bending moment occurred on the springline positions.

Yasuda et al., 2017 conducted the two-dimensional analysis of the weak zone on the tunnel response using a numerical approach. The authors concluded that, under isotropic compression, the lining is in a state of stress where axial thrust dominates and bending moment is low, the presence of a void leads to large stress concentration on the lining and in turn causes undesirable deformation and stress in the lining. In contrast, under shear-type loading, where the stress state of the lining is low axial thrust and high bending moment, the presence of a void does not lead to a large stress concentration on the lining.

Yasuda et al., 2019 investigated the three-dimensional seismic response using the numerical method, for a cylindrical tunnel accompanying the weak zones behind the lining. In this study, a deep circular tunnel was considered. The weak zone was defined as a non-contact boundary as illustrated in Figure 2-11 and the point matching method was used to draw the solutions. Figure 2-12 shows the circumferential stress distributions of the inner, middle, and outer surfaces of the lining at a cross-section of $z = 0$ when the maximum principal stress at the cross-section is maximum under S1- wave incidence at an incident angle of 75°. The frequency f is 1.0 Hz and 5.0 Hz. The effect of a void is the largest at a cross-section $z = 0$, which is the center of the void in the longitudinal direction. For any condition of the weak zone, the frequency almost does not affect the circumferential stresses around the lining. This is maybe due to the reason that the wavelength of the wave is considerably higher than the weak zone size. From this study, high correlations between stress concentration and weak zone were suggested and the reinforcement of the lining is very crucial to avoid damage in the lining structure.

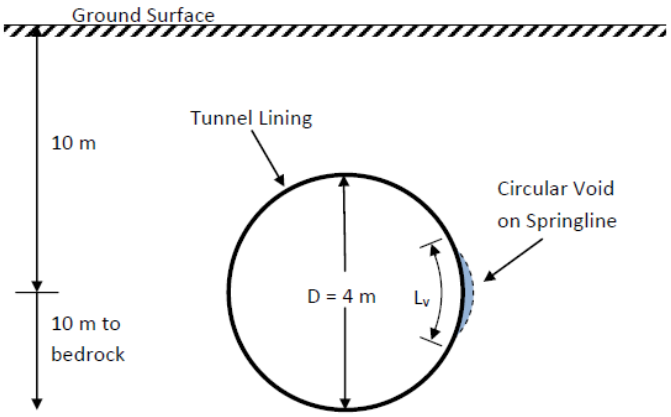

Figure 2-7. illustration of FEM tunnel accompanying a weak zone (Adapted from (M. A. Meguid and Dang 2009a)

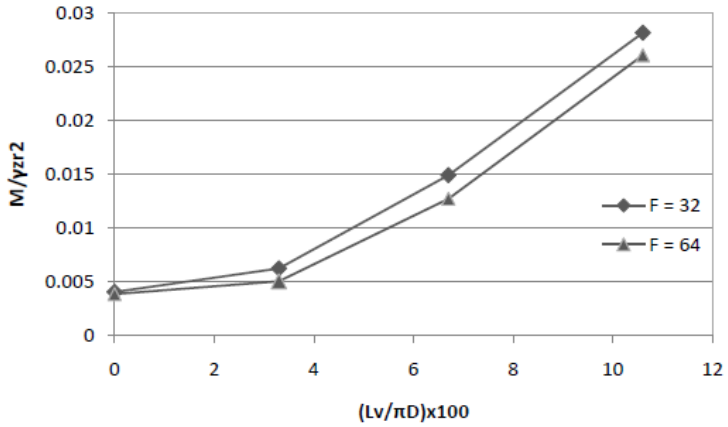

Figure 2-8. Change in bending moment at springline with void size and flexibility ratio (Meguid and Dang, 2009a)

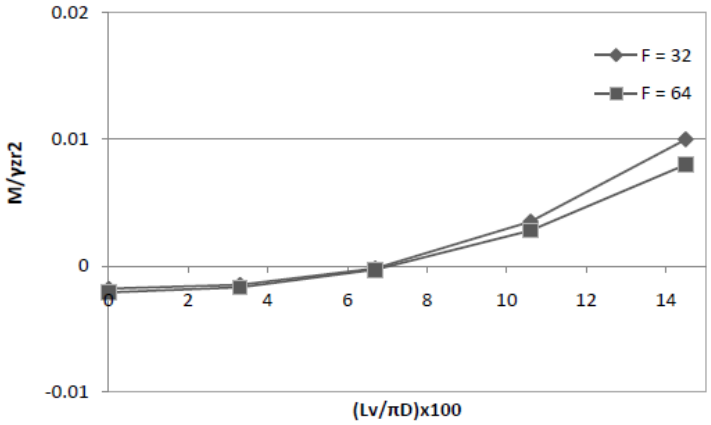

Figure 2-9. Change in bending moment at invert with void size and flexibility ratio (Meguid and Dang, 2009a)

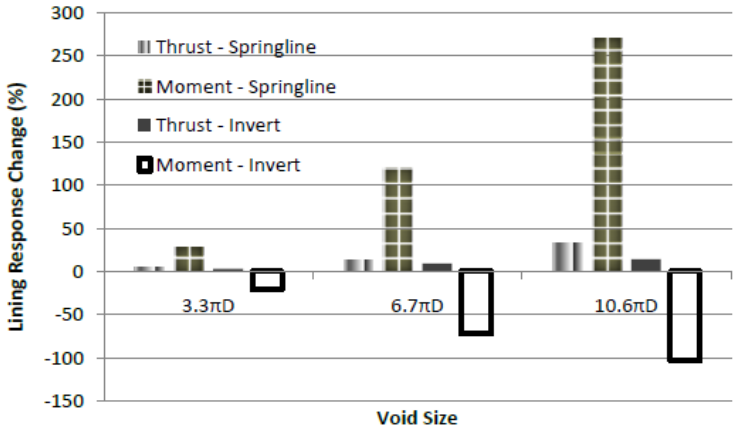

Figure 2-10. Summary of lining response changes with void size (Meguid and Dang, 2009a)

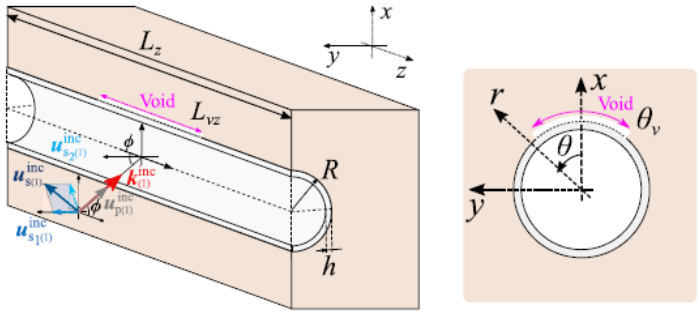

Figure 2-11. A cylindrical tunnel with a void behind the lining subjected to an obliquely incident plane harmonic seismic wave (Yasuda et al., 2019)

Fu et al., 2019 performed numerical analysis using the Extended Finite Element Method (XFEM) to illustrate the development of cracking directions and patterns on the existing tunnel lining in the vicinity of the cavity. The presence of cavities behind the lining is one of the essential factors for lining cracking. The stress distributions of the tunnel lining with a cavity behind are different from the lining which is fully in contact with the surrounding rock. Due to the loss of reaction force at the cavity area, the tunnel lining deforms squeezing outwards to the cavity. Such behavior leads to an increase in bending tension stress of the lining at the cavity area so that stress concentration near the exterior of tunnel lining was very obvious and crack is initiated when maximum principal stress is higher than the tolerable tensile strength of concrete. Moreover, Cracks are majorly developed at the intrados of tunnel arch shoulder symmetrically which is found to be in good agreement with the field observations. There is a potential that the crack initiation starts at the extrados of the tunnel crown when the cavities are majorly behind the vault area. The cracking initiate at the exterior of the tunnel lining was highlighted and should be paid great

attention to as such cracking performance is difficult to be detected in the field. It is also important that it will define the position of the reinforcement for repair purposes.

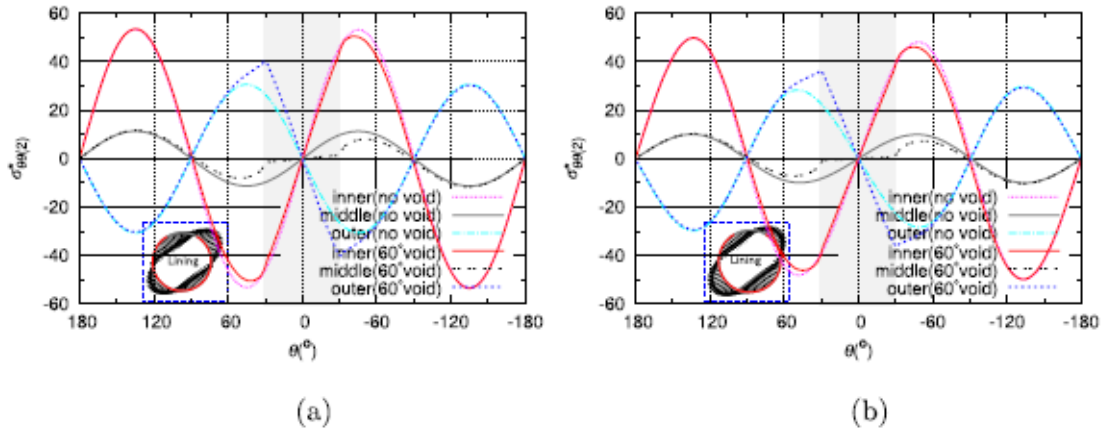

Figure 2-12. Circumferential stress distributions of the inner, middle, and outer surfaces of the lining at the cross-section z = 0 under S_1-wave incidence when the maximum principal stress at the cross-section becomes maximum (φ= 75°, θ_v = 60° and L_{vz}= 3R): (a) f = 1.0 Hz and (b) f = 5.0 Hz. (Yasuda et al., 2019)

Asakura and Sato, 1996 performed a laboratory test to check the effect of the weak zones behind the lining on its cracking performance. The tunnel model was made of concrete and the circumferential loads were applied using a series of jacks around the tunnel as illustrated in Figure 2-13. The weak zone was created by reducing the jack pressure and its effect was a check for various cases. The response of the tunnel was estimated in terms of axial thrust and bending moment.

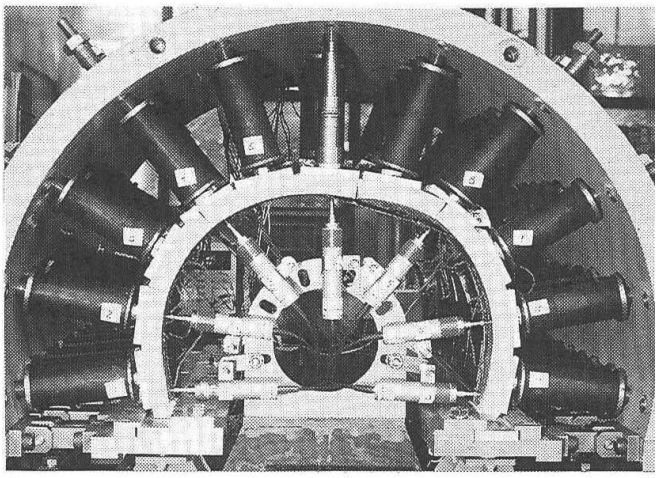

Figure 2-13. Experimental setup used for testing the lining using jack pressure (Asakura and Sato, 1996)

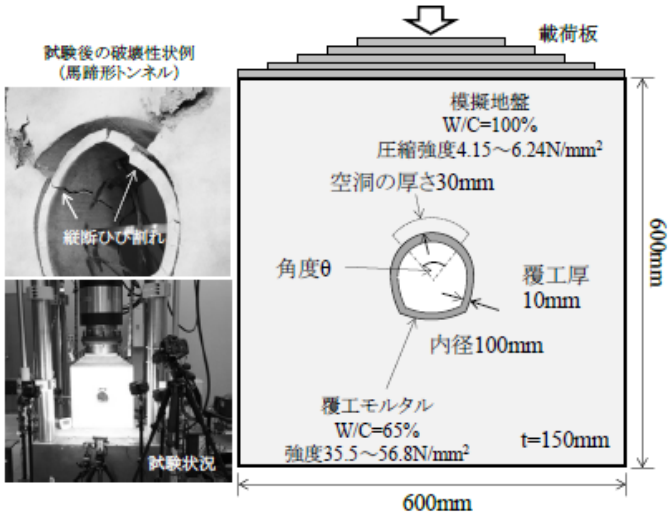

Figure 2-14. Experimental setup used for testing a horseshoe tunnel (Mori et al., 2014)

2.4 Lining Response to the Soil

Peck, 1969 illustrated the theoretical situation of soil-lining interaction for a typical circular tunnel lining with two different types of lining i.e., flexible, and rigid lining. The rigid lining represents an exceptionally strong and completely rigid structure. The flexible lining was assumed to be entirely flexible but strong enough to resist the substantial compressive stresses. The linings are placed at a certain depth z from the natural surface level and to counteract the incoming soil pressure at first, they were filled with the soil. The lateral earth pressure coefficient (K_o) was supposed to be less than unity. Since for naturally occurring underground soil conditions seldomly has K_o higher than 1 so the assumption was made quite reasonably.

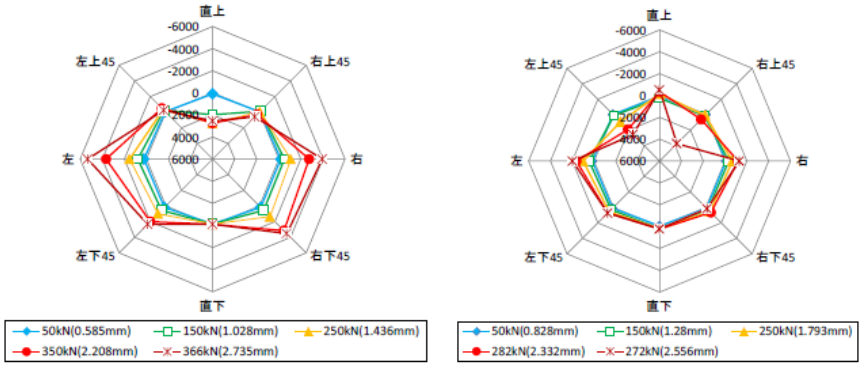

Figure 2-15. Internal strain distribution for tunnels with and without weak zone (left side without weak zone and right-side weak zone at crown) (Mori et al., 2014)

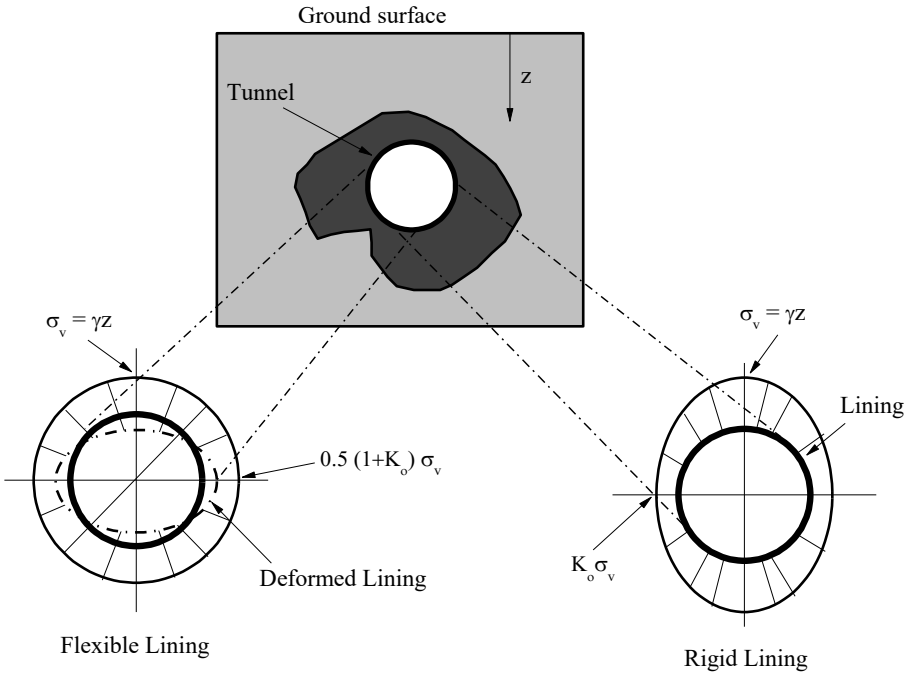

Figure 2-16. Ground pressure distribution around flexible and rigid tunnel lining

In the initial state when the soil was present in the lining, the system was in an equilibrium position. However, the removal of soil material forces the system to readjust itself to attain the equilibrium position. In the case of flexible lining, this phenomenon will generate an extension of the horizontal axis and compression of the vertical axis. However, in the rigid lining, the ground pressure will produce bending moment instead of lining distortion as illustrated in Figure 2-16. The bending moment developed in rigid lining would be positive at the springlines positions and negative at the crown and invert positions. However, the diagonal positions don't show the appreciable increase in bending moment as demonstrated in Figure 2-17. Finally, it can be imagined that the lining fibers present at the springline positions will experience tensile stresses on the outer side and compressive stress on the inner side. Conversely, the fibers present at the crown and invert position will experience the compressive stress on the outer face and tension on the inner face of the lining.

The situations mentioned earlier are very idealized and the lining response to earth pressure can be judge accordingly. Although the above-mentioned scenarios are very helpful to understand the interaction between the soil and the lining, however, the real tunnels are rarely completely flexible or rigid. Generally, they are a combination of both hence can exhibit different behavior.

To get the realistic picture, both are required superposition of their idealized lining response reactions. This implies that the lining can deform slightly and can retain the bending moment. To investigate the behavior of the model tunnel at rest conditions, the tunnel was tested in a biaxial compression test. The bending moment measured at different positions around the lining shows that at the crown and invert positions increases in the negative direction while at springline positions it increases positively. Moreover, the diagonal positions (shoulders and knees) don't exhibit a significant change in bending moment. The initial (at the start of the test) and final (when the maximum load reaches) bending moment are presented in Figure 2-18. The crown and invert show the negative bending moment while springline locations show the positive bending moment. Furthermore, the diagonal positions show very small bending moments. However, the top diagonal positions show a slight value which may be due to the vertical displacement of the tunnel. The deformations and development of the bending moment are in good agreement with each other as shown in Figure 2-19.

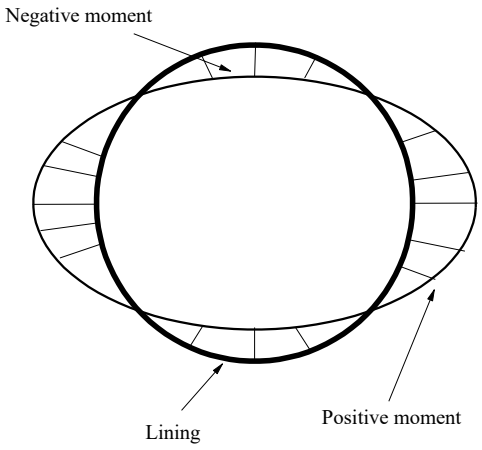

Figure 2-17. Development of bending moment around a rigid lining

2.5 Factors Influencing the Load on the Lining

Tunnel lining is designed to withstand the load acting directly on it and some percentage of the horizontal pressure. Normally, the structure of the primary lining is proportioned to withstand all sorts of loads generated by short-term soil loads as well as construction activities. The secondary lining is provided for the safety of the tunnel from further loadings caused by the future fluctuations in the global physical conditions and the possible increment in long-term soil loadings. If no soil settlement happens before, during, and after lining structure placement and the

gravitational stress gradient from the top part (crown) to bottom part (invert) is not considered, the lining load, T, acting on the lining is expressed as follows.

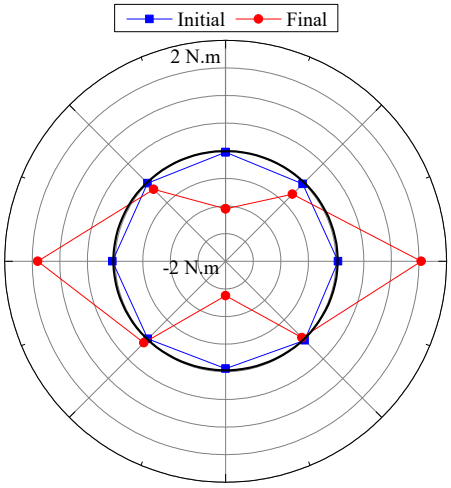

Figure 2-18. Summary of bending moment distribution around the lining

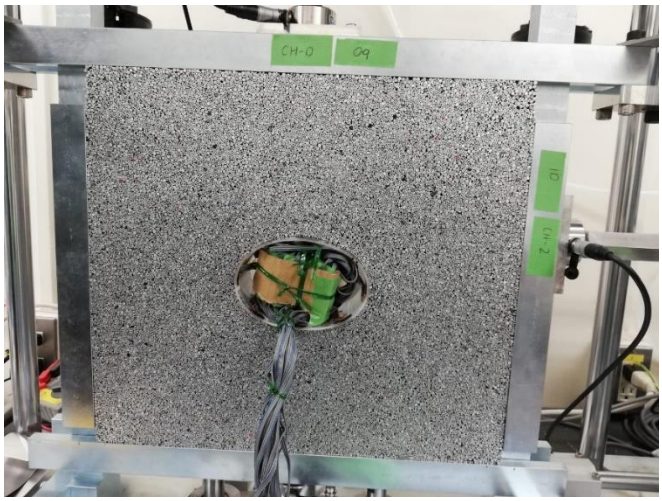

Figure 2-19. Tunnel deformation behavior under biaxial compression test

$$T = PR \tag{1}$$

$$P = \frac{1}{2}\gamma H\{(1 + K_o) + (1 - K_o)cos2\theta\} \tag{2}$$

Where,

$P =$ pressure acting in the radial direction

R = outer radius of the lining

K_o = coefficient of earth pressure at rest

θ = clockwise angle measured from crown to point of interest

γ = soil unit weight

H = tunnel depth from the ground surface to the tunnel springline

However, the lining is rarely carrying the whole load of the overlying soil. The rock/soil material laying over the tunnel structure is fractionally supported by the lining structure. In reality, whenever an opening is made in the ground in the form of a tunnel, due to the continuity of the ground and the inherent shear strength, the in-situ stresses are redistributed around that opening. This shifting of load from yielding soil mass to the surrounding portions is knowing as the arching effect. Hypothetically, the lining structure gas to withstand only those forces not arched to the surrounding rock/soil mass.

Due to the arching effect of the ground, tunnel linings occasionally withstand the complete load of the overlying soil. Many factors are causing the difference in loading on the lining of different tunnels. To predict the accurate and reliable loads acting on the tunnel, the important factor is to understand the impact of such factors. Here are the important factors affecting the loads on the lining.

2.5.1 Geology

For tunnel construction, the most important factor is probably the geology of the area. It is very rare to encounter similar geological conditions for the construction of any two tunnels. The geology of the area differs in the vertical direction and along the horizontal tunnel direction. It is well established that as the ground strength increases the support need decreases. In fact, in Sweden and Norway due to the high strength of soil, many tunnels have been constructed without the lining structure. The lining load would have been negligible if the lining structure were placed in those tunnels. Terzaghi, 1946 classified the rocks into different groups: intact, stratified, moderately jointed, blocky, and seamy, crushed, squeezing, and swelling. For each group, the anticipated approximate values of loads have also been provided. Although the classification system was very general without numerical valuation of the rock mass, the system indicates that with the decrease of rock strength the lining load increase.

Ward and Pender, 1981 deliberated the performance of a tunnel in various soft soils circumstances and their findings associated with the lining loads are concise as follows: tunnels constructed in gravelly or dense sandy material having minor cohesion and appropriate drainage behave in the same way to tunnels in non-swelling or stiff rock with smaller lining load as compared to those in clays and silts. The lining loads still even out rapidly after placement of the lining structure with the load depending on the stiffness of the lining, but considerably smaller than that equivalent to the overburden pressure. Tunnels constructed in immensely over consolidated swelling clays have lining pressure nearly comparable to the complete overburden stress even though the lining load may only correspond to about half of the overburden pressure in the 1st year of the construction. In the case of tunnels built in slightly over consolidated clays, with time lining loads tend to rise. The lining loads are related to the lining structure's stiffness but smaller than overburden loads.

In conclusion, in certain projects, geology has a key character in dropping the lining loads. However, stiffness of the lining structure is also an equally contributing factor as mentioned earlier, and not only the geological conditions of the ground.

2.5.2 The relative rigidity of the lining concerning the surrounding ground

The load acting on the lining structure is dependent on the lining stiffness comparative to that of the surrounding ground. The stiffer lining structure attracts more load, a mechanism that can be demonstrated with the help of the convergence-confinement method. There is a requirement to consider both stress-strain behaviors of the lining structure and the neighboring ground because a lining that is flexible concerning very stiff clay may show the stiff behavior in a soft clay as described by Peck et al., 1972. Under symmetric or uniform loading conditions, the compressibility ratio, C, is defined as a relative stiffness of the ground-support system.

$$C = \frac{ER(1 - v_l^2)}{E_l A_l (1 - v^2)} \tag{3}$$

Where;

E and v = Young's modulus and Poison's ratio of the ground

E_l and v_l = Young's modulus and Poison's ratio of the lining

R = Tunnel radius

A_l = The average cross-sectional area of the ground/lining unit length

The relation between compressibility and normalized lining load is illustrated in Figure 2-20. The loads plotted in the figure are calculated for the no-slip boundary condition based on the theory explained by Einstein and Schwartz, 1980. As the results are calculated for the springline position that's why the in-situ stress ratio, K_o, does not affect the results. The plotted results show that as the compressibility ratio increases the normalized lining load decreases very rapidly. Further, it is clear that when compressibility ratio exceeds 20 , the drop in normalized lining load is insignificant. Eisenstein et al., 1979 noticed that for the same ground conditions the lining load on the segmented lining is higher than the rib and lagging system due to the higher stiffness of the structure.

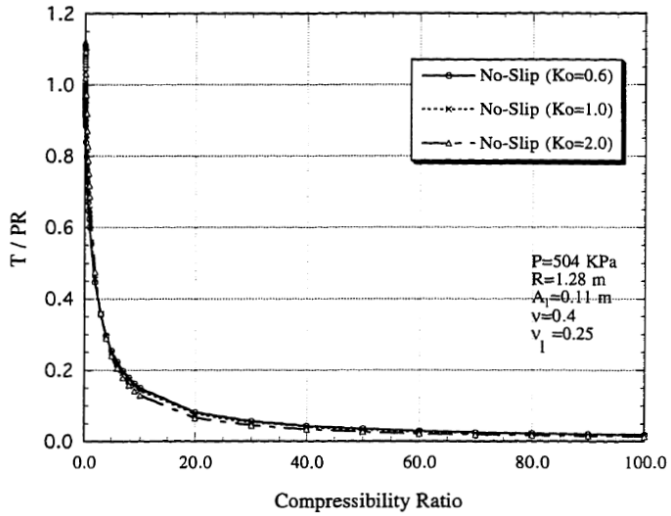

Figure 2-20. Lining load at tunnel springline for various compressibility ratios (Einstein and Schwartz, 1980)

2.6 Literature Review Summary

The review of the literature illustrates that even if the tunnels have drainage systems considerable pore water pressures can develop around tunnel linings. In the surrounding soils, drained tunnels generated higher water seepage forces. Usually, these forces are enough to carry and move away from the loose soil particles, ultimately causing the weak zones behind the lining.

In the literature, many case histories related to the occurrence and the effects of weak zones have been documented. In many of these cases, weak zones were found to be the major cause or a major contributing factor to the ultimate failure of subsurface structure i.e., pipes and tunnels. It

was also observed that the weak zones usually occurred at tunnel extremities, which are the most vulnerable positions of a lining to the fractures.

Even with so many recorded cases of weak zones and the resulting damages, minimal studies and very few experiments have been performed. The majority of the published research papers and thesis found relevant to weak zones were simulations and numerical analyses conducted to investigate their effect on pipes and tunnel linings. All these papers determined that the lining forces and ground stresses would increase in the areas adjacent to weak zones and the other parts as well. However, the maximum response has been observed around the periphery of the weak zones.

Regarding laboratory experimentation, very few studies were found considering only the static state conditions. An experimental study to investigate the effect of weak zones on the tunnel response under static as well dynamic conditions was therefore necessary. Hence this study will bridge the gap between the existing literature and the problems related to the weak zones in the tunnel structures.

CHAPTER 3: OUTLINES OF THE EXPERIMENT

3.1 Introduction

An effective and economic way to explore the geotechnical phenomena happening in underground structures is to perform physical modeling. For many years, it also served as the main method to verify geotechnical theories. To conduct the physical modeling there are various methods presented in the literature. It also includes the experiments performed on small-scale models instead of full-scale structures called prototypes. A comprehensive review of the physical modeling of tunnels in soft soils has been presented by Meguid et al., 2008. From the presented methods it can easily be seen that each method has its benefits and shortcomings. In the current study, a scale tunnel has been tested under 1g conditions. It is worth observing that the small-scale model can offer only the deep insight into the probable outcomes and trends of a full-scale test rather than providing the actual in-situ conditions.

The vital aspect of physical testing is to establish precise ground conditions. While performing this experiment all-important parameters were considered and careful planning has been done, to represent the true behavior of weak zone on the tunnel lining. The most important and difficult parameters of the design and realization of laboratory testing include the formation of homogenous ground in all tests, the creation of weak zones behind the lining with accurate void ratio, and the placement of the tunnel on the exact location for each trial.

Lastly, to get reliable results, each test trial needs efficient data recording and careful monitoring of the whole procedure during the laboratory activity. To record the data, several strain gauges, displacement sensors, accelerometer, and camera were used. Each sensor was precisely calibrated and accurately positioned before the start of the test. All devices were then connected to different data loggers and a computer to record the readings.

The target of this experimental activity was to physically model a tunnel constructed in sandy soil having a weak zone behind the lining. This chapter includes in detail the complete experimental program which will consist of a shaking table, the sensors and data acquisition system, tunnel model, formation and properties of the model ground, creation of weak zone around

the lining, calculation of the exact void ratio of the weak zone, and the procedure explaining the conduction of experiments.

3.2 Shaking Table Apparatus

The tests were performed with the help of a shaking table which is mainly made of steel plates, bolts, and beams. Shaking table tests are often performed to examine the dynamic behavior of tunnels and soil structures (Chau et al., 2009; Chen et al., 2012; Guoxing et al., 2015; Xu et al., 2016; Kheradi et al., 2018; Hassanzadeh et al., 2018; Xin et al., 2018). The apparatus used for testing at Yokohama National University is a 2-dimensional shaking table that can be accelerated with the help of an electric actuator and controlled by a digital control module as shown in Figure 3-1. The internal dimensions of the table measured $500\ mm$ long, $500\ mm$ deep, and $60\ mm$ wide. To represent the two-dimensional plane strain conditions, the table was designed much longer and deeper than its width. However, it is wide enough to accommodate the tunnel model and soil material. It consists of twenty steel blocks racked on one another. These blocks have been connected through smooth movable bearings resulting in frictionless roller supports which allow them to move without any restriction in either direction. The whole assembly is mounted on a horizontal platform which is bolted from all sides with the help of beams. The main assembly and the tightening beams are separated by a clear space of around 50 mm on both sides and the top surface. The whole apparatus is resting on six square steel footings made of $50\ mm$ firmly embed in the ground. On the ends of every footing, adjustable leveling screws are attached to level the table on slanted floors. On the front side, an adjustable assembly is attached to adjust the camera to captures the photos during excitation. The camera position can be adjusted in any direction and during the current study, it was set to capture the photos of the central part. To satisfy the boundary condition which says that the tunnel should be placed a minimum of one diameter above the rigid base, before the start of the testing, the tunnel position was decided and set at 175 mm above the top of the iron table. To check the effect of the bottom boundary, several tests were conducted by varying the height between the tunnel invert and top of the iron table, and it was observed that the height (175 mm) is enough to avoid the effect of the bottom boundary. To attain the symmetric loading conditions in the horizontal direction the tunnel model was placed at the center of the moving table. There is an important feature to note that there is clear gap between the soil and the front side of the table. To maintain this clear gap a wooden board was placed in between the ground

material and the table front side which was later removed. The reason of this gap is that there was a concern that the skin friction resulting from the front side and the soil material could affect the results.

The table can oscillate in a sinusoidal pattern from 0.5 Hz to 2 Hz with a maximum displacement of 25 mm from its mean position. While shaking, the data logging devices were capable to record displacements, accelerations, and strain data from the test model.

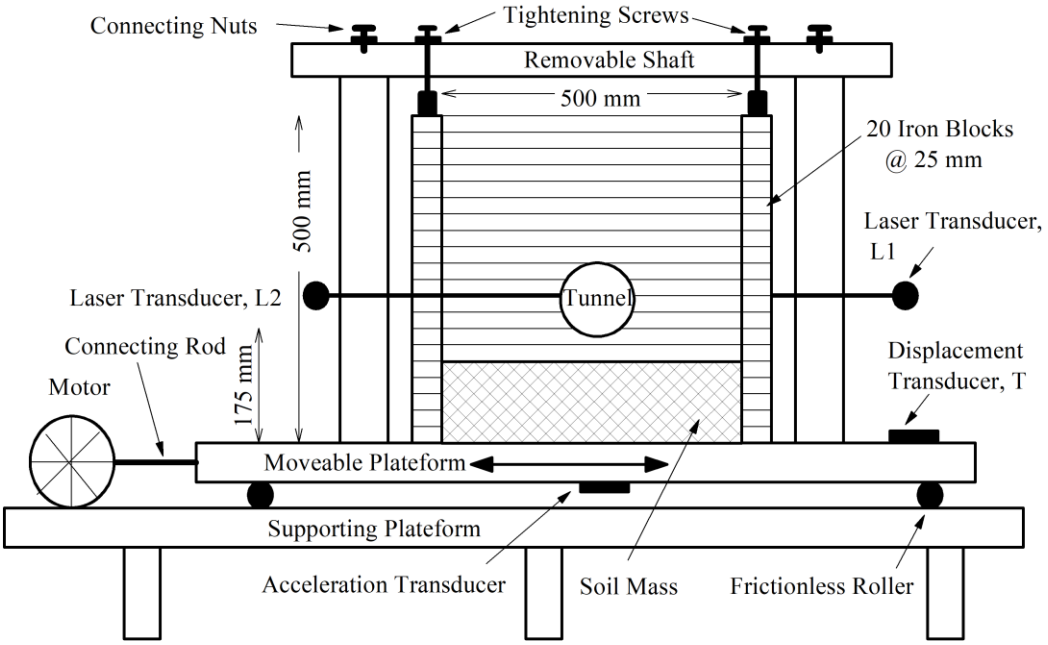

Figure 3-1. Schematic diagram of the shaking table test apparatus

The input wave is a typical sinusoidal wave with a frequency and maximum amplitude of 1 Hz and 25 mm respectively as shown in Figure 3-2. The table rotation was recorded for continuous 30 cycles. In each test, initially, the table was positioned at its mean position and then start to shake in the horizontal direction. The direction of the rotation is as follows; from the mean position to the extreme left side, from the left extrema to the right extrema, and finally comes back to the mean position to complete one cycle. It means that the negative values of displacement indicate the direction of motion towards the left side and vice versa. In the first cycle, due to low-level excitation, there is a delay of about 0.33 sec which makes the first cycle duration around 1.33 sec instead of 1 sec. The rest of the cycles are evenly distributed over time with a constant duration of 1 sec. During shaking, the data was recorded at a frequency of 0.001 s and the table positioned was determined very precisely at each time step.

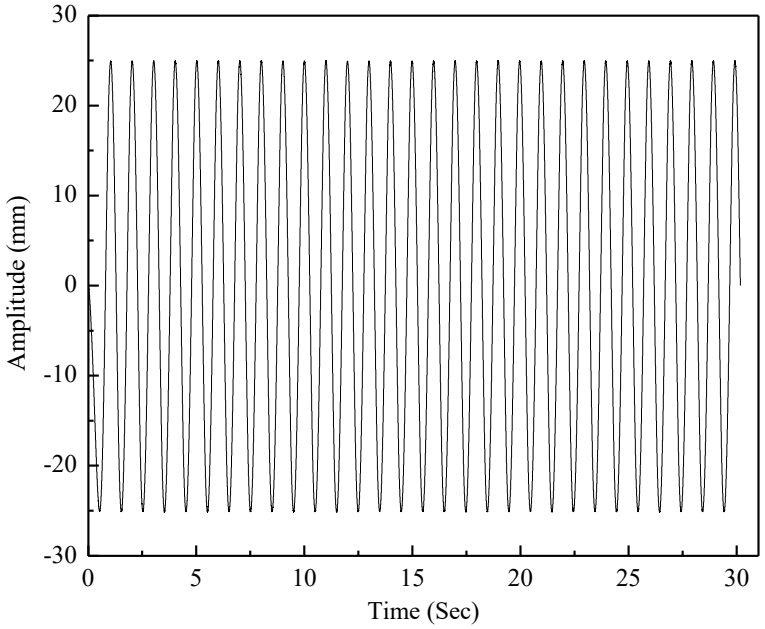

Figure 3-2. Input displacement of shaking table

As the table oscillated at a frequency of 1 Hz here to confirm that whether the table is oscillating at the provided frequency, the Fast Fourier Transformation (FFT) analysis was carried out and the results have been drawn in Figure 3-3. The predominant frequency determined through FFT analysis of displacement reveals that the table is shaking exactly at 1 Hz which is the same as the excitation frequency of the table. After confirmation of the excitation frequency, the input waves were kept the same throughout the testing activity.

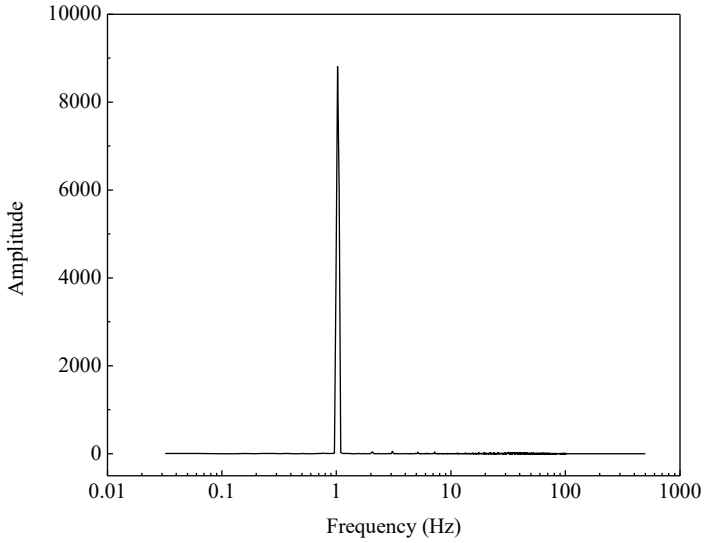

Figure 3-3. Fast Fourier Transformation (FFT) of the displacement curve

3.2.1 Tunnel model

The tunnel model consists of a polyethylene acrylic resin having a circular cross-section with 100 mm diameter, 2 mm thickness, and length of 60 mm. Figure 3-4 shows the tunnel used in this experimental setup. To observe the detailed behavior, the model tunnel was decided to be a flexible w.r.t. the surrounding ground. The behavior of the tunnel captured through bi-axial compression testing as indicated in Figure 3-5 shows that it has less stiffness as compared to the surrounding ground. The important characteristics of the model tunnel have been listed in Table 3-1.

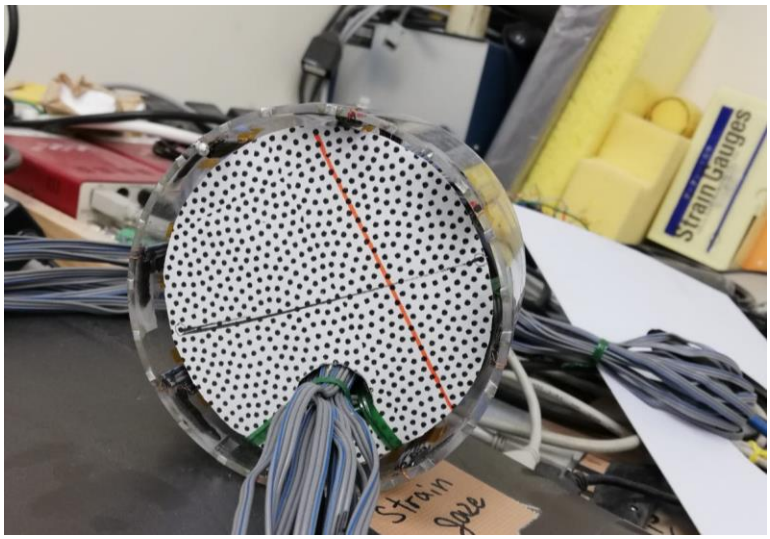

Figure 3-4. Polyethylene acrylic resin tunnel model

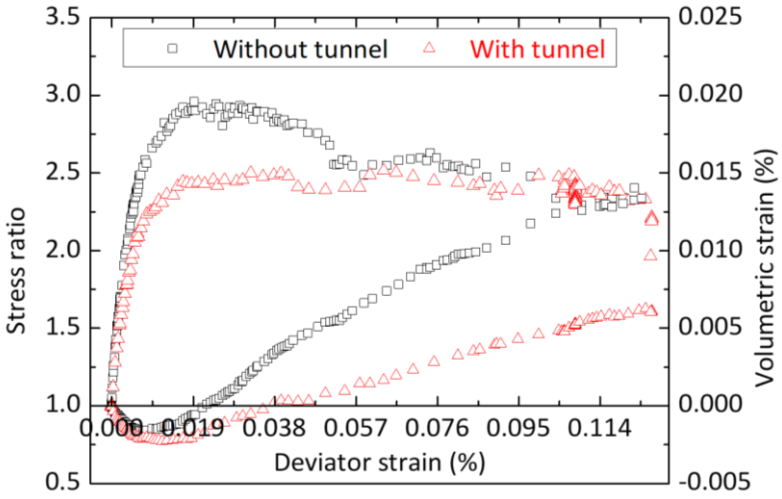

Figure 3-5. Comparison of Model ground behavior with and without tunnel model under bi-axial compression

Table 3-1. Characteristics of model tunnel

Item	Unit	Value
Diameter	mm	100
Thickness	mm	2
Length	mm	60
Bending stiffness	$N - mm^2$	1.26×10^5
Axial rigidity	N	3.76×10^5

Table 3-2. Properties of model tunnel's material

Item	Unit	Value
Young's modulus	GPa	3.14
Flexural strength	MPa	45
Tensile strength	MPa	40
Density	KN/mm^3	10.8

3.2.2 The construction process of the tunnel

In this study, the construction of the tunnel is slightly different from the actual field construction techniques. Usually, in the field, the tunnels are constructed by using the cut and cover method or NATM (New Australian Tunneling Method) techniques. However, here the tunnel and ground construction process has been illustrated in Figure 3-6 and the different steps have been explained as follows:

- Positioning of the shaking table at the mean position and cleaning it from dust or any clay material.
- Placement of a wooden board with $25\ mm$ thickness in front of the table to avoid the direct contact of the ground material and the table upfront.

- Weighing of the required amount of the material to be placed on the table up to nearest 1g.
- Placement of the ground material from the bottom to the position of the tunnel bottom in a layer-by-layer manner.
- Checking the ground density for each layer and providing the required compaction energy to get the target density for each layer.
- Positioning and the placement of the tunnel model above the ground.
- Placement of the remaining surrounding and similarly overlaying ground material.
- Marking of the weak zone around the tunnel with the help of a black marker.
- Removal of the wooden board, fixing of the top beam and tightening of all screws.
- Recording of the strain data to capture the effect of overburden pressure.
- Withdrawal of the calculated amount of the material to create the weak zone.
- Recording of the strain data to check the effect of the weak zone under static state conditions.
- Shaking and recording the strain, displacement, acceleration, and photos for continuous 30 cycles.

The removal of the ground and the tunnel was done as follows:

- Removal of the overlying and surrounding ground material
- Removal of the tunnel model completely out of the ground
- Removal of the remaining ground material

For each test trial, a similar method was adopted which was found to be convenient due to the small scale of the shaking table and the tunnel model. Before placing the tunnel in the ground, all strain gauges were initialized by putting it on the flat surface in the vertical plane.

3.2.3 Instrumentation

To measure the internal strain and the bending moment, the lining was instrumented with sixteen strain gauges S1 ~ S16 in a clockwise manner starting from the crown position as illustrated in Figure 3-7. It means that two strain gauges were glued at one section i.e., one inside and one outside of the lining structure. The acceleration and displacement responses of the table were recorded with the help of electronic transducers attached to it. Shear displacement (Δ) of the ground was documented by laser transducers (L1) as illustrated in Figure 3-1. To capture the

photos the orientation of the camera was held perpendicular to the displacement direction and the time interval between two consecutive photos were kept at 0.01 s. To improve the visibility and photo quality, artificial lights were also placed on the backside of the camera. During the experimental phase, the acceleration, displacement, and strain data were collected with the help of data loggers at a sampling frequency of 1000 values per second.

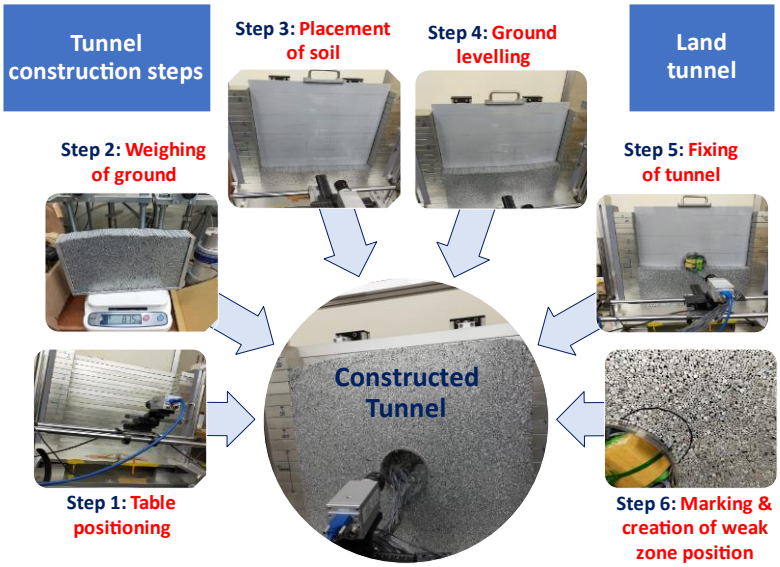

Figure 3-6. Steps involved in the tunnel construction process

To nullify the temperature effect on the strain gauge's performance, all experiments were conducted at a constant room temperature of 20 ℃. The strain gauges were glued on the tunnel surfaces and wires were running out of the tunnel to data loggers. It was found that due to the movement of the data wire the strain data contained more noise than acceleration and displacement. As the reliability of shaking table tests depends on the circumstances of the data logging devices to record the signals during the excitation process, therefore all the recorded strains were filtered using MATLAB (MATLAB, 2003) for further analysis.

3.2.4 Data acquisition system

The data acquisition system is an integral part of the test setup which is employed to record the whole readings from different sensors. To check the changes in table position in the horizontal direction, two laser transducers with the least count of 0.0001 mm and a table transducer having the least count of 0.001 mm were constructed and mounted on the table. The table displacement transducer was responsible to record the displacement of the table from its mean position, while

the laser transducer S1 was placed to check the movement of soil block at tunnel springline height. The laser transducer S2 was mounted on the opposite side of S1 to measure the tunnel position. All the sensors were calibrated before the start of the testing process. The table acceleration was recorded with the help of an accelerometer placed at the top surface of the iron platform. The data loggers are directly connected with the computer as shown in Figure 3-9.

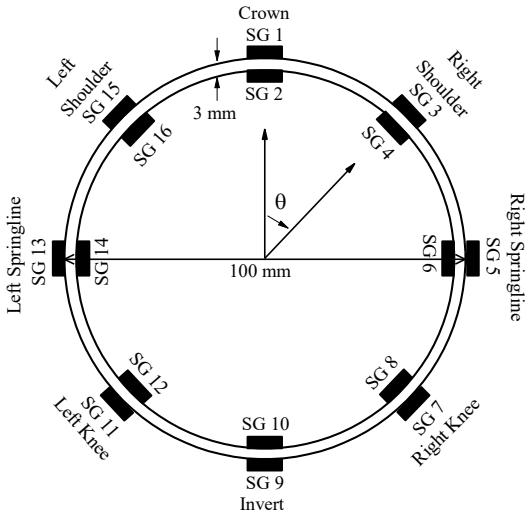

Figure 3-7. Position of strain gauges around the tunnel model

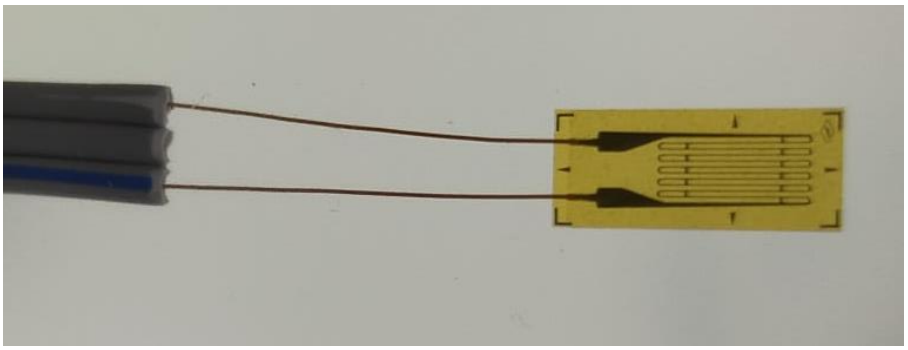

Figure 3-8. Description of strain gauge

Before the start of the testing, laser coefficients were assigned to the lasers to get the same value of the displacement as of the table transducer. These coefficients were established by the hit and trial method and have been listed in Table 3-3. Firstly, the table was placed at its mean position and its displacement reading was set to zero. After setting a random value of the laser coefficient, the laser beam of a laser transducer was positioned at a fixed point on the table and initialized to zero. The table was then moved around its mean position and both displacements were recorded for several cycles. After stopping the table both displacements were analyzed. If the displacements

were found to be different the coefficient was changed accordingly. After performing this exercise several times, the laser coefficient which gives the same displacement was found out. Additionally, the table transducer's coefficient was 1 but to increase the precision it was set equal to 10 hence the values were raised by ten times.

Figure 3-9. The data acquisition system

Table 3-3. Laser coefficients

Sr #	Laser model	Accuracy	Company	Range	Coefficient
1	IL-600		Keyence		78.4
2	IL-300		Keyence		27.78

The micro strain, displacement, and acceleration per volt were recording using the strain gauges, displacement transducers, and the accelerometers attached around the tunnel model and the shaking table. To get the value of the strain produced in the model tunnel, the values obtained from the strain gauge were multiplied with their respective coefficients. The strain values were calculated using Eq (4). In this expression, the number 0.95238 is a constant (provided by the manufacturer and is relevant to the strain gauge type.

$$Strain = 0.95238 \times 10^{-6} \times strain\ per\ volt \qquad (4)$$

3.2.5 Calculation of bending moment from strain data

Experimental calculation of bending moment from strain data was made using surface integration. The tunnel section along with the behavior under flexural loading is shown in Figure 3-10 and is used to derive the formula for the calculation of the bending moment. The detailed derivation is expressed in Eq. (5) – Eq. (9). The outcome of the derivation is the same as previously mentioned by (Munro et al., 2009).

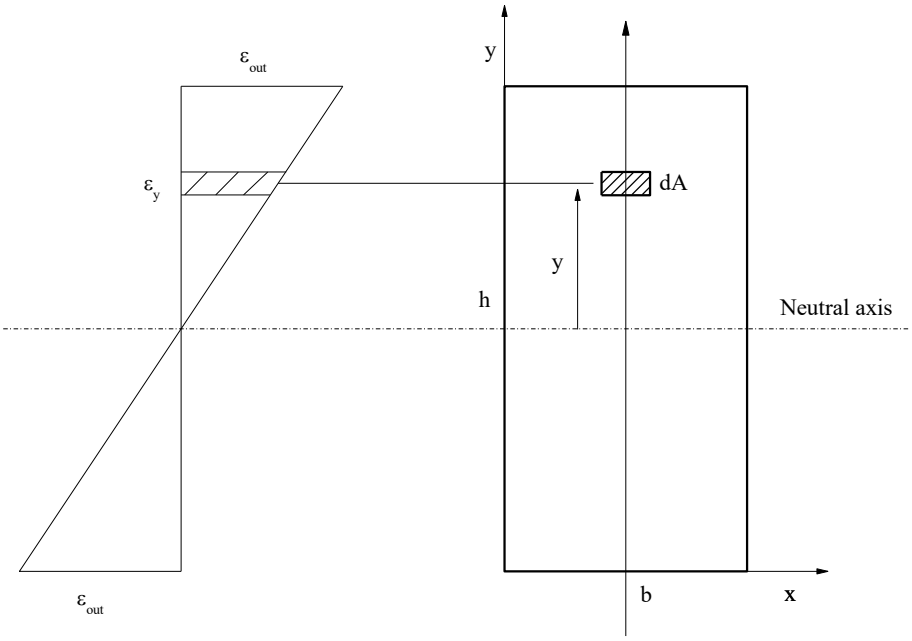

Figure 3-10. Flexural behavior of tunnel section

$$\varepsilon_y = \frac{(\varepsilon_{out} - \varepsilon_{in}) \times (\frac{h}{2} + y)}{h} + \varepsilon_{in} \tag{5}$$

$$M = \int_{-\frac{h}{2}}^{\frac{h}{2}} \int_{-\frac{b}{2}}^{\frac{b}{2}} E \times y \times \varepsilon_y \, dxdy \tag{6}$$

$$M = E \int_{-\frac{h}{2}}^{\frac{h}{2}} \int_{-\frac{b}{2}}^{\frac{b}{2}} y \left[\frac{(\varepsilon_{out} - \varepsilon_{in}) \times (\frac{h}{2} + y)}{h} + \varepsilon_{in} \right] dxdy \tag{7}$$

$$M = Eb \int_{-\frac{h}{2}}^{\frac{h}{2}} \left[\frac{(\varepsilon_{out} + \varepsilon_{in})}{2} + \frac{(\varepsilon_{out} - \varepsilon_{in})}{h} \mathrm{y} \right] y dy \quad (8)$$

$$M = EI \frac{(\varepsilon_{out} - \varepsilon_{in})}{h} \quad (9)$$

wherein E is the young's modulus of the tunnel, I is the second moment of area, ε_{out} and ε_{in} are the strains measures at the outer and inner face of the tunnel.

3.3 Model Ground

3.3.1 Preparation of Model Ground

During this research, model tests have been conducted for different B/D, where B is the soil cover from the top of the lining to the ground surface and D is the diameter of the tunnel. In the course of ground preparation, aluminum rods with a uniform length of 50 mm have been chosen as soil mass. This material has previously been used by many researchers for soil modeling (Nakai et al., 1999; Nakai and Hinokio, 2004; Shahin et al., 2004, 2011) and laboratory experiments (Nakai et al., 2007; Meguid et al., 2008; Kishida et al., 2016). The particles have a size of 1.6 and 3.0 mm mixed in a ratio of 3:2 by weight, which generated a ground having a unit weight of 22.3 kN/m^3. The other important physical properties of the ground have been illustrated in Table 3-4. To guide the preparation of the uniform ground and to avoid the fall of some aluminum rods, a temporary wall made of wood was attached to the back of the table before placing the ground material. Before the start of the shaking process, this wall was removed. The soil material was placed on the table manually from the bottom to the top in a layer-by-layer fashion keeping the uniform layer thickness of about 50 mm. To assure the even ground with constant unit weight, each layer was tempted with the help of a temping rod. The void ratio of the model ground was found to be 0.18 and special attention was given to keep this uniformity during ground preparation for each test. The front view of the compacted ground is shown in Figure 3-11. The characteristics of the prepared ground were similar to dense sand/rock (Shahin et al. 2011). For each test trial, the same material was used and after finishing the test it was properly covered with the help of clothes to avoid rusting.

3.3.2 Model soil behavior

The biaxial tests were conducted on a mass of aluminum rods to observe the stress-strain dilatancy and to calculate the important characteristics of the model ground. The schematic diagram of the biaxial test is shown in Figure 3-12. To carry out the biaxial test constant minor principal stress ($\sigma_2 = 19.6$ kPa) and the results have been shown in Figure 3-13. The plotted data shows the relationship between deviatoric strain (ε_d), major-minor principal stress ratio ($^{\sigma_1}/_{\sigma_2}$) and volumetric strain (ε_v). The arranged data show that the model ground formed by the mass of aluminum rods shows negative and then positive dilatancy similar to a medium or dense sandy soil.

Figure 3-11. A view of a compacted soil mass

Table 3-4 Properties of the model ground

Item	**Unit**	**Value**
Density	kN/m^3	22.3
Cohesive strength	MPa	0
Friction angle	-	31^0
Young's modulus	MPa	7.5
Void ratio	-	0.18

3.3.3 Preparation of weak zone and tunnel crack

Previous studies suggest that whenever a weak zone is mentioned in tunnels, it represents an area of weakened soil caused by various activities such as erosion, vibration, etc. (Asakura and Kojima, 2003). Therefore, the weak zones around the tunnel periphery were made by increasing the void ratio of that specific location to represent the field condition as illustrated in Figure 3-15. To achieve this task, the calculated numbers of aluminum rods were removed uniformly and the effect of three void ratios, 0.30, 0.45, and 0.60 was checked. For each value of the void ratio, three tests were performed by introducing the weak zone at crown, shoulder, and springline positions. For symmetricity, only these locations on the upper right side (i.e., only a quarter tunnel) were tested.

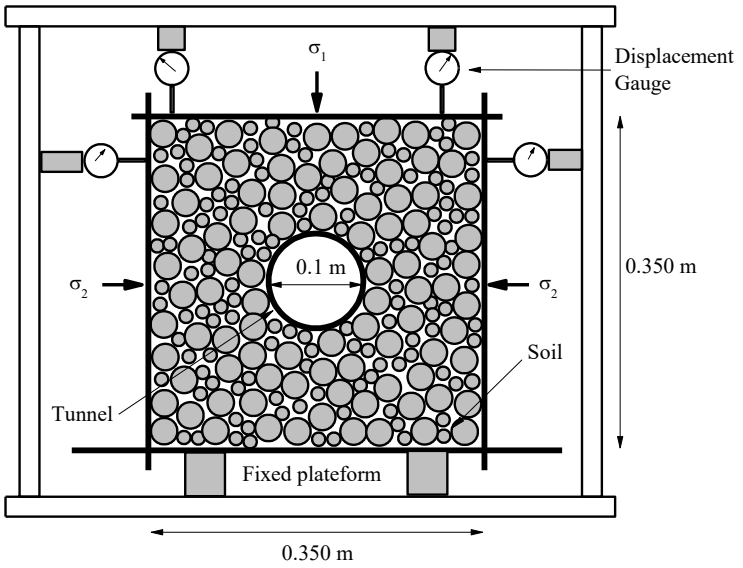

Figure 3-12. Schematic diagram of the biaxial test

The size of the weak zone was defined with the help of the internal angle θ and the height above the tunnel surface as shown in Figure 3-14. In this study, the tests have been conducted for two different sizes of the weak zones in which the internal angle was 51^0 and 90^0 respectively while the height was the same and kept equal to 20 mm. The effect of the void ratio on the elastic modulus has been confirmed by performing the biaxial tests where two different void ratios have been tested and the results have been presented in Figure 3-16. It can be seen that the ground with a higher void ratio shows lower peak strength as well as the slope of the stress-strain curve. Hence, the stiffness is related to the void ratio which means that the soil with a high void ratio will be

treated as less stiff and vice versa. The tests were conducted for void ratios 0.30, 0.45, and 0.60, and the effect has been checked on different properties under static as well as dynamic conditions.

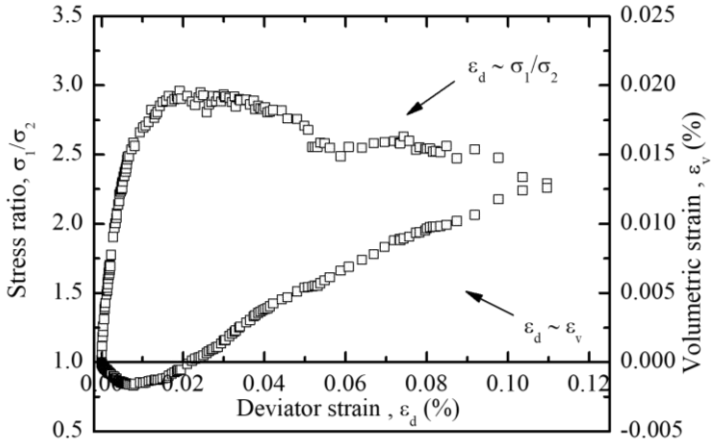

Figure 3-13. Model ground behavior in biaxial test

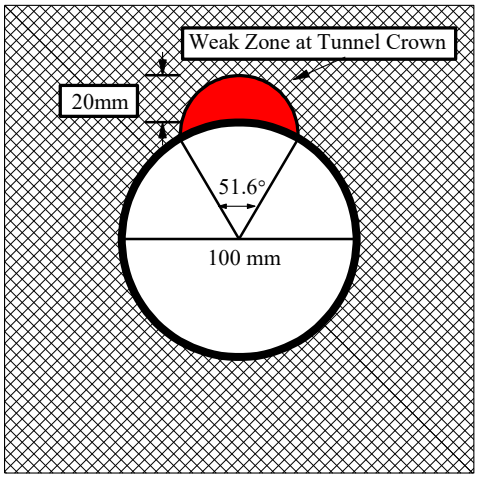

Figure 3-14. Model ground with the weak zone placed at tunnel crown.

3.3.4 Estimation of actual void ratio

While creating the weak zone its boundary was disturbed and the actual void ratio was also altered. Before shaking the table, the photos were captured, and later the actual void ratio was estimated. The results of the actual void ratio for overburden height 1D have been presented in Table 3-5. The weak zones having the same void ratio but with higher sizes have been illustrated with the additional letter S2 after their name. The results show that the actual void ratios of the weak zones are lesser than the targeted void ratios. The results of the other cases have been shown in Table 3-6 and Table 3-7.

Figure 3-15. Ground condition before and after the creation of the weak zone

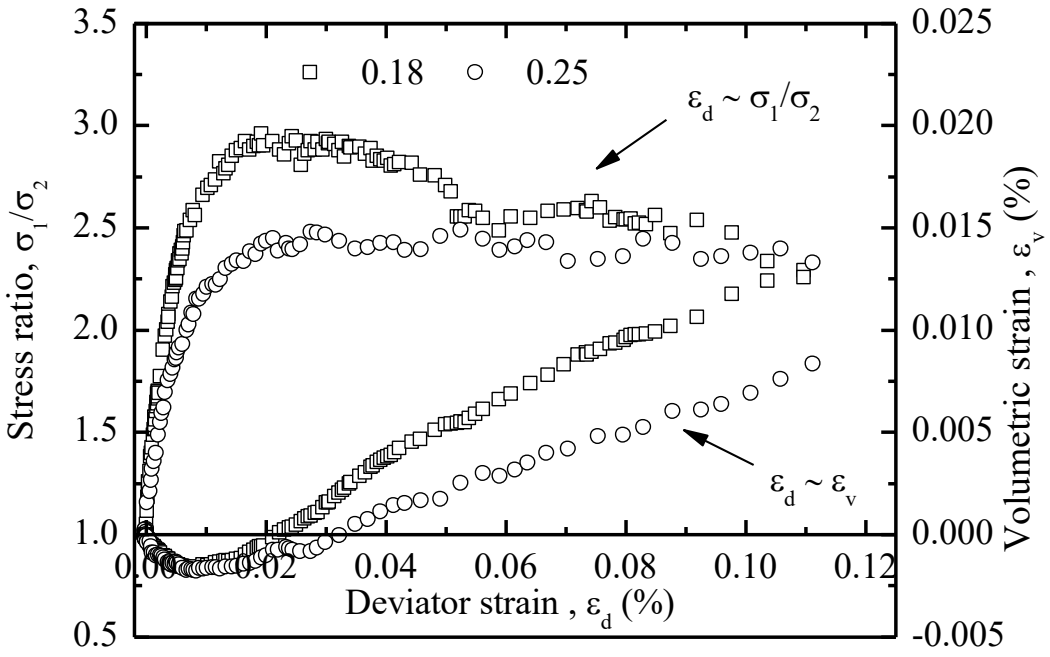

Figure 3-16. Stress-strain dilatancy relation of model soil

Table 3-5. Actual void ratio along with set void ratio for small and large size of the weak zone and overburden height 1D

Weak zone position	**Set void ratio**	**Actual void ratio**
No weak zone	0.183	0.179
Crown	0.30	0.275

Shoulder	0.30	0.292
Springline	0.30	0.289
Crown	0.45	0.42
Shoulder	0.45	0.43
Springline	0.45	0.41
Crown, S2	0.45	0.428
Shoulder, S2	0.45	0.421
Springline, S2	0.45	0.435

Table 3-6. Actual void ratio along with set void ratio for the small size of the weak zone and overburden height 2D

Weak zone position	**Set void ratio**	**Actual void ratio**
No weak zone	0.183	0.177
Crown	0.30	0.27
Shoulder	0.30	0.288
Springline	0.30	0.285
Crown	0.45	0.40
Shoulder	0.45	0.425
Springline	0.45	0.40
Crown	0.60	0.53
Shoulder	0.60	0.55
Springline	0.60	0.545

Table 3-7. Actual void ratio along with set void ratio for the large size of the weak zone and overburden height 2D

Weak zone position	Set void ratio	Actual void ratio
Crown	0.30	0.28
Shoulder	0.30	0.29
Springline	0.30	0.289
Crown	0.45	0.415
Shoulder	0.45	0.43
Springline	0.45	0.423
Crown	0.60	0.55
Shoulder	0.60	0.565
Springline	0.60	0.555

3.3.5 Test pe-preparations

Before the experiment could start, the tunnel and shaking table was cleaned properly from dust and inspected thoroughly. The wires which are coming out of the tunnel model are tied together to avoid the disturbance caused by their movement. Motor frequency was set to 1 Hz by rotating the adjusting knob. The camera position was established to capture good quality images. To improve the particles focusing, the camera was aided with artificial lights. All the sensors were checked thoroughly, and the readings were initialized.

3.4 Similarity relationship and parameters

While designing the shaking table test, usually the similitude analysis is the first step, and the satisfaction of some necessary similar parameters is essential. However, it is tough to meet all the similarity laws in model tests; thus, some settlements have to be accepted (Yan et al., 2015). The law of similarity for underground structures explained by Iai, 1989 has been used while deriving

the similarity relations between prototype and model. In the current study, special consideration is paid to the parameters affecting the bending rigidity. To guarantee the identical values of the strain of prototype and model, the strain similarity ratio C_ε was kept equal to 1 as also adopted by Tiecheng et al., 2011. The model dimensions were decided by scaling down a circular tunnel having a diameter and thickness of 10,000 and 200 mm respectively, as the size of the majority of railway tunnels in Japan lies in this range (Koyama, 2003). Keeping in view the geometry of the tunnel prototype, depending on the dimensions of the shaking table, a geometry model scale of $^1/_{100}$ was selected. The similarity ratios between different variables of the model tunnel are listed in Table 3-8 while the model ground is given in Table 3-9.

Table 3-8. Similitude analysis of model tunnel

Items	**Scaling factor (prototype/model)**	**Value**
Strain	-	1
Dimensions	λ	100
Displacement of structure	$\lambda^{1.5}$	1,000
Flexural rigidity	$\lambda^{3.5}$	100,000
Longitudinal rigidity	$\lambda^{1.5}$	10
Bending moment	λ^{3}	1,000,000
Axial force	λ^{2}	10,000

3.5 Particle Image Velocimetry (PIV)

Particle Image Velocimetry (PIV) is a visual surface velocity-estimating approach primarily established to visualize the two-dimensional deformations in the field of fluid mechanics (McKenna and McGillis, 2002; Adrian, 1991). Several researchers e.g. Allersma, 1996; White and Take, 2002 have highlighted the importance of the PIV technique to geotechnical applications. During soil analysis, in contrast to fluids, the grains themselves serve as tracers so it does not need any intrusive indicators to be mixed in the soil mass (White et al., 2003). High-resolution

observation of various deformations can be found through the analysis of serial digital pictures captured by the camera (Niedostatkiewicz et al., 2011). Initially, the image is divided into a mesh of interrogation cells. A local displacement vector for every interrogation cell is composed through a cross-correlation function between two consecutive images (Slominski et al., 2007). After the development of the cross-correlation function, the possible displacement can be estimated. A detailed explanation and related equations have been presented in Appendix A.

Table 3-9. Similarity relations of model ground

Items	**Scaling factor (prototype/model)**	**Value**
Density	-	1
Strain	$\lambda^{0.5}$	10
Stress	λ	100
Displacement of ground	$\lambda^{1.5}$	1,000
The bulk modulus of soil grains	$\lambda^{0.5}$	10

3.6 Repeatability Analysis

As the dynamic analysis is very sensitive and the reliability of the results lies in the repeatability. To ensure the repeatability of the tests, every test was performed more than two times under the same conditions. It was decided that the same type of test, will be performed on the same day by the same observer for apple-to-apple comparison. After plotting the tests with good repeatability have been chosen for further analysis. Results from selected tests were plotted to show the repeatability and have been placed in Appendix A.

CHAPTER 4: EFFECT OF WEAK ZONE POSITION

4.1 Examined Positions

The position of the weak zone around the tunnel was defined very carefully to capture the tunnel and ground behavior. As in this research activity a circular tunnel has been used which is doubly symmetric. By considering the symmetricity in the horizontal as well vertical direction, weak zones were placed only at the quarter part of the tunnel. Hence, the tests were conducted by placing the weak zone at tunnel crown, shoulder, and the springline positions as shown in Figure 4-1. However, the measurements of the strain were taken at each point around the lining. Similarly, the camera was positioned to capture the whole tunnel and surrounding ground to get the ground response under seismic excitation. The measurement of the strain was made on the inner and out surface of the tunnel. For no weak zone case, the distribution of the inner strains around the tunnel has been illustrated in Figure 4-2 and the outer strains have been displayed in Figure 4-4. It can be seen that the strains measured at the inner and the outer surface have similar distribution but with opposite nature i.e., when inner strain is positive the outer is negative and vice versa. The strains measured at the diagonal positions i.e., shoulders and knees are sinusoidal while the strains at points other than diagonals i.e., crown, springlines and invert are unidirectional which means that either they are positive and remain positive or negative and remains so during the complete cycle of the shaking. The nature of the strains depends upon the direction of the shaking table e.g., when the table starts shaking, first of all, it goes to the left-hand side and the inner strain at the left shoulder is negative (compressive) and at the right shoulder, it is positive. Conversely, the outer strain at the left shoulder is positive and at the right shoulder, it is negative. The strains at the left and right knees follow the opposite direction of the respective shoulders.

Figure 4-1. Positions of the weak zone around the tunnel

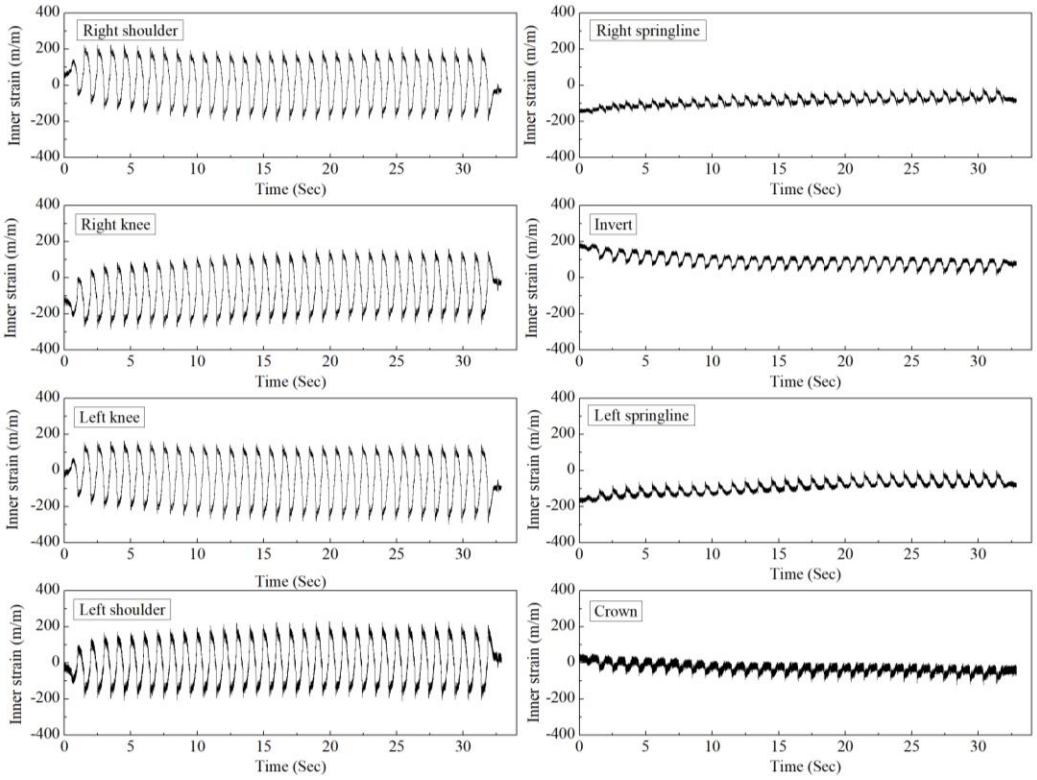

Figure 4-2. Distribution of internal strain for no weak zone and overburden height 1D

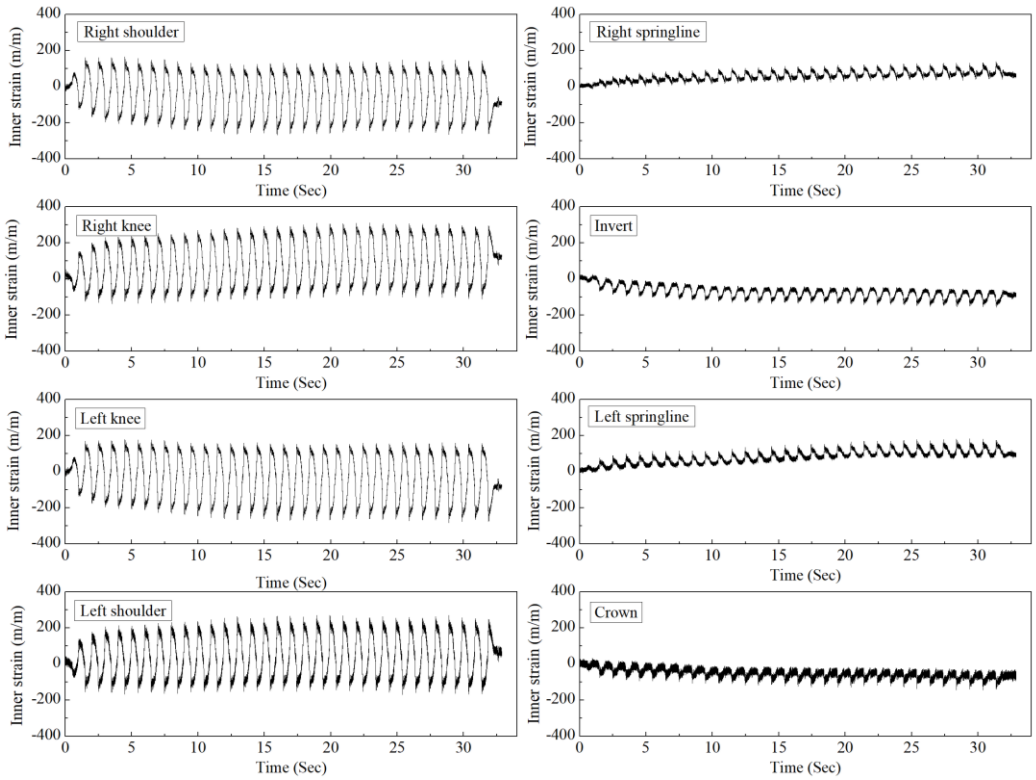

Figure 4-3. Initialized distribution of internal strain for no weak zone and overburden height 1D

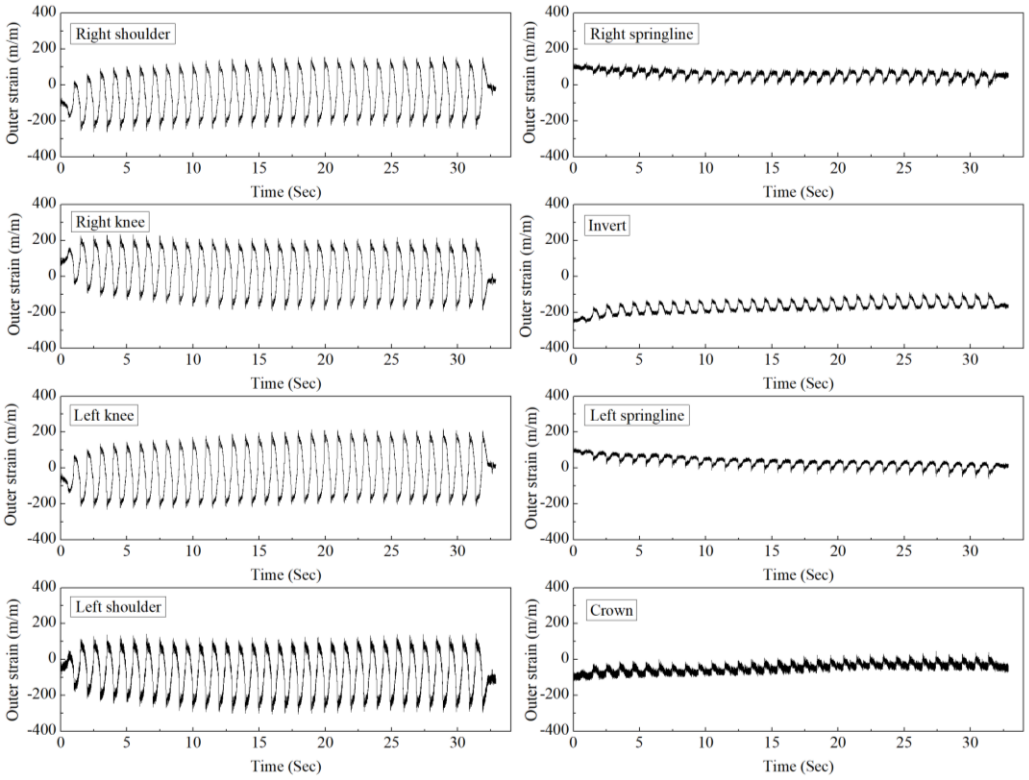

Figure 4-4. Distribution of outer strain for no weak zone and overburden height 1D

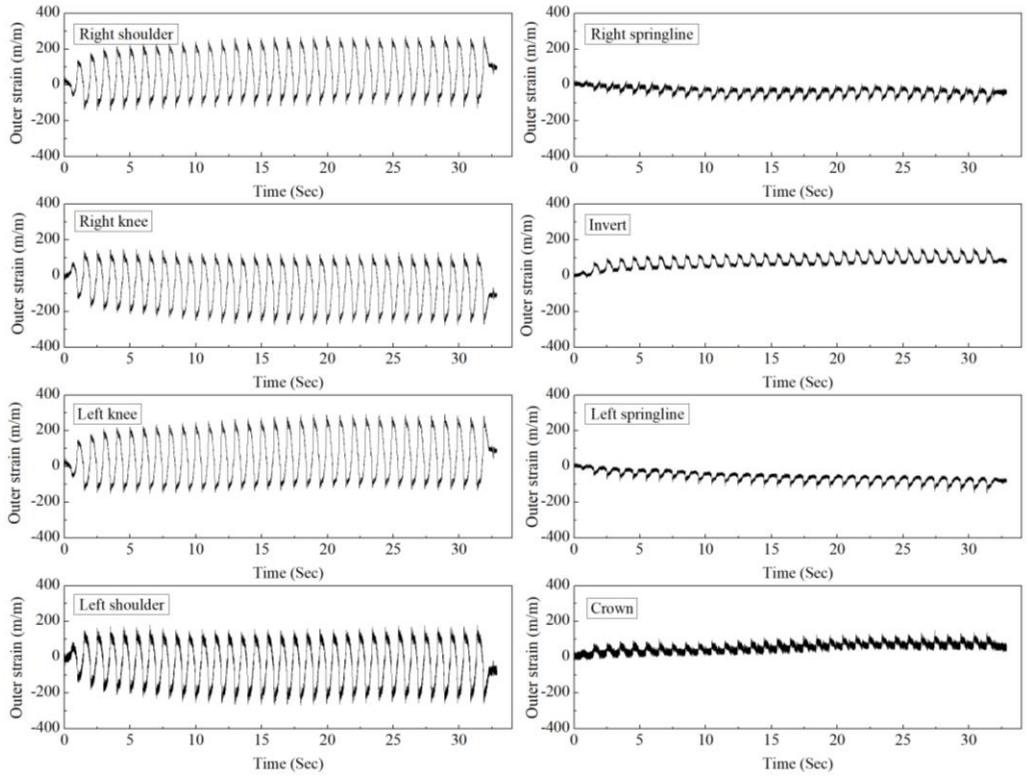

Figure 4-5. Initialized distribution of outer strain for no weak zone and overburden height 1D

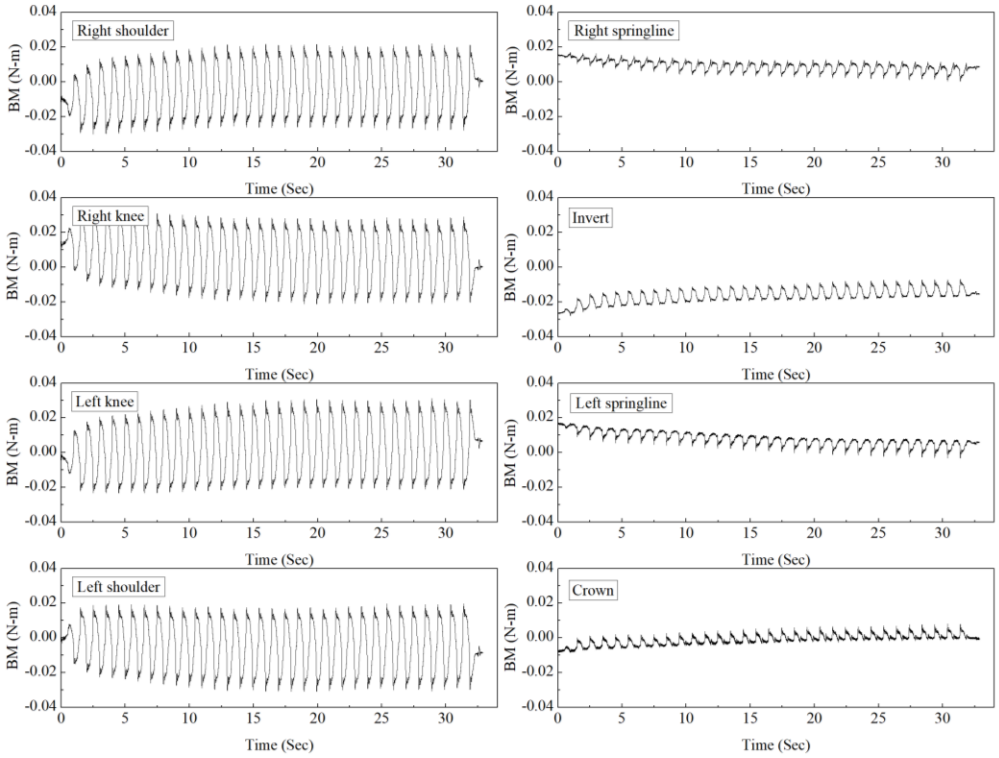

Figure 4-6. Distribution of bending moment for no weak zone and overburden height 1D

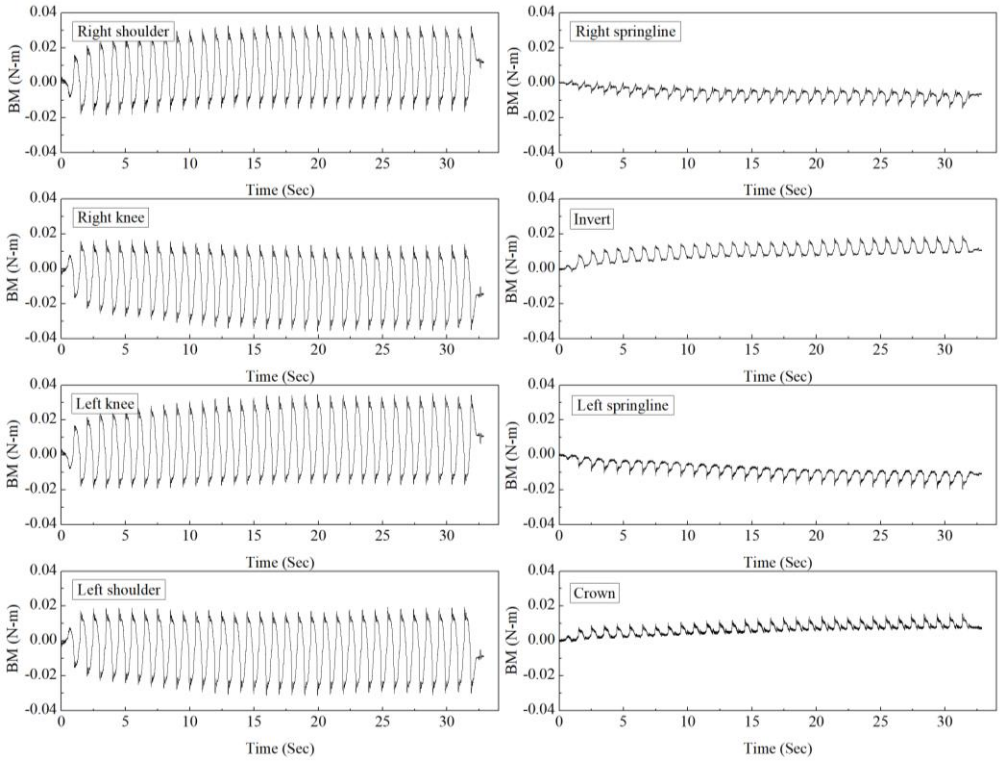

Figure 4-7. Distribution of initialized bending moment for no weak zone and overburden height 1D

The initialized strain distribution at the crown and invert show that the external strains are tensile and the internal is compressive. This phenomenon also indicates that during the shaking process the tunnel is squeezing inside about the vertical axis. Hence, the tunnel bending behavior is ovaling in nature along with the squeezing inside as illustrated by the initialized BM shown in Figure 4-7.

The horizontal and vertical points show different distributions as compared to the diagonal locations of the tunnel. For no weak zone case during the entire shaking activity, the inner strains at invert remain positive and at the crown, it is negative which means that the invert is experiencing an upward pressure from the bottom and tries to move upward. The springlines inner strains show that the internal fibers at springlines remain in compression. The outer and inner strains were used to calculate the bending moment distribution by the method explained in chapter 3. The bending moment distribution follows the distribution of the outer strain at each point around the periphery of the lining s shown in Figure 4-6.

The distributions of the strains and the bending moment shown above also include the effect of the overburden pressure. To check the effect of only shaking on the strain and BM distribution, these values have been initialized w.r.t., the first values. The results of initialized internal strain have been presented in Figure 4-3 while Figure 4-5 demonstrates the distribution of the initialized outer strain. Here, the direction of the inner and the outer strain at the diagonal locations remains similar to the not initialized strains. However, the initialized strains at the crown, springlines, and invert are different from the strains having the impact of dead weight. For only dynamic conditions, the internal strains at springline locations are always positive which means that the tunnel is squeezing along the horizontal axis and the springlines are in tension.

4.2 Ground Response

The ground response is an important aspect of seismic analysis of underground structures. Here the ground response is measured in terms of shear displacement, and ground internal strain e.g., volumetric strain and deviatoric strain.

4.2.1 Shear displacement

When a shear wave will strike any buried structure like tunnels, substations, etc., it causes the movement of the structure in the horizontal as well vertical plane depending upon the direction

of the excitation. The resulting shear displacement will impose the force on the tunnel structure which depends upon the magnitude of the shear displacement, type of structure, geometry of the structure, ground stiffness, and earthquake magnitude. The shear displacement has been recorded with the help of a laser transducer installed at the springline height of the tunnel. The measured displacement response was subtracted from the table displacement response (T) to get the values of shear displacement. It has been observed that by changing the location of the cavity the shear displacement changes significantly. The produced shear displacement can change the stress state of the material which is closely related to deformation behavior (Chen et al., 2010). Development of stresses and resulting strains in case of dynamic loading depends on the shaking direction and wave propagation e.g., for a typical horizontal shaking the strain behavior is shown in Figure 4-8. At the mean position, the soil element shows only the compressive/tensile strains as indicated by positions 1 and 3 while for the position of the table other than the mean position, along with the compressive/tensile strains the shear strain also starts developing as indicated by position 2 and 4.

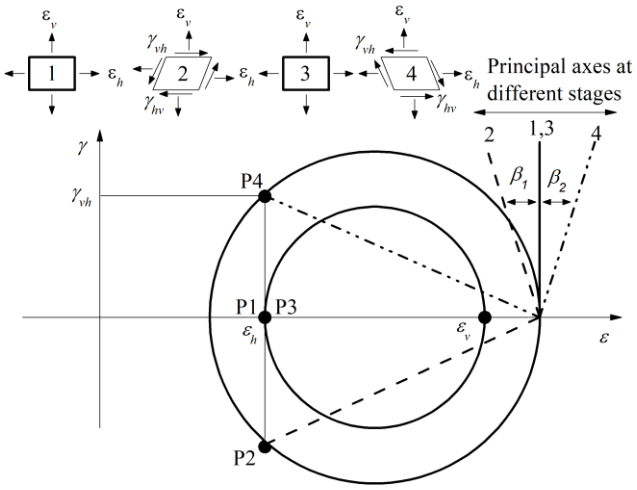

Figure 4-8. Strain behavior in cyclic loading

The positive values of shear strain represent the shearing of ground on the right side and vice versa. As illustrated in Figure 4-8, the shear strain at the mean position (denoted by positions 1 and 3) is zero and becomes maximum at extreme positions (denoted by positions 2 and 4) of the shaking table. When there is no weak zone the positive and negative shear displacements are approximately equal and exhibit a symmetrical distribution around the horizontal axis. This indicates that the ground is experiencing equal shearing on either side during the shaking process which is the result of homogenous ground preparation and uniform excitation on both sides. The

creation of a weak zone around the lining increases the ground shearing towards the right side. The reason for this increase in shear displacement is ground loosening which in turn loses its part of shear strength. Moreover, due to the weakness of the local part of the ground, the surrounding ground tries to move towards that weaker part. The incoming soil towards the weak zone pushes the soil further towards the right direction. As the weak zone was always placed on the right side that's why in each case the ground was sheared on the right side. To check the effect of the weak zone position on ground shearing, the highest value of the shearing strain for all cases having a void ratio of 0.45 has been noted and presented in Figure 4-11 and Figure 4-12 for overburden height 1D and 2D respectively. In the case of overburden height 1D, the graph indicates that with the introduction of the weak zone shear displacement increased and the highest value has occurred for the weak zone at springline position. However, for overburden height 2D the shear strain is lesser than shallow overburden height. Furthermore, the maximum shearing strain was observed when the weak zone was placed on the crown of the tunnel, and here, in this case, the weak zone at springline locations yielded the minimum value of the shear strain.

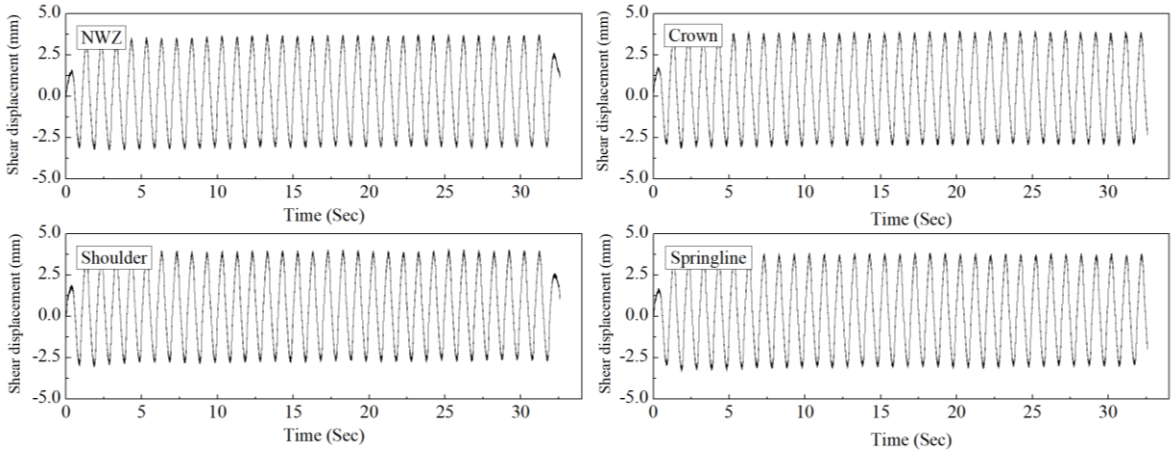

Figure 4-9. Shear displacement variation with time for different positions of the weak zone and overburden height 1D (e=0.45)

4.2.2 Time variation

While analyzing the seismic response, the effect of the shaking duration was investigated. To explore this phenomenon the photos were analyzed at different time intervals e.g., during 1st cycle, 5th cycle, 10th cycle, 20th cycle, and 30th cycle. For each cycle, eight photos were analyzed as shown in Figure 4-13 which illustrates that the photos were analyzed at maximum and minimum shear displacement, at zero shear displacement, at maximum and minimum table displacement,

and zero table displacement of each cycle. It is important to note that the maximum shear displacement occurs when the table is very close to its mean position and the shear displacement becomes zero when the table is at the extreme position during its shaking. Therefore, the time between zero displacement and maximum table displacement is very small, and a similar thing happens between the maximum shear displacement and zero table displacement. Figure 4-14 shows the outcomes of the development of the deviatoric strain for the ground-only case. The direction of the ground movement has been illustrated by arrows placed at the top of the figure. It can be seen that as the number of cycles increases the concentration of the deviatoric strain increases.

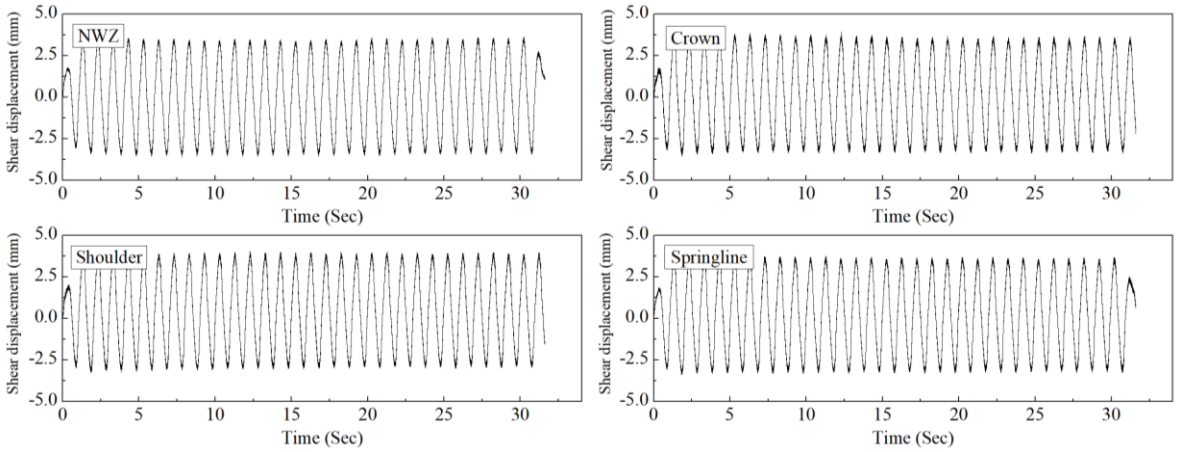

Figure 4-10. Shear displacement variation with time for different positions of the weak zone and overburden height 2D (e=0.45)

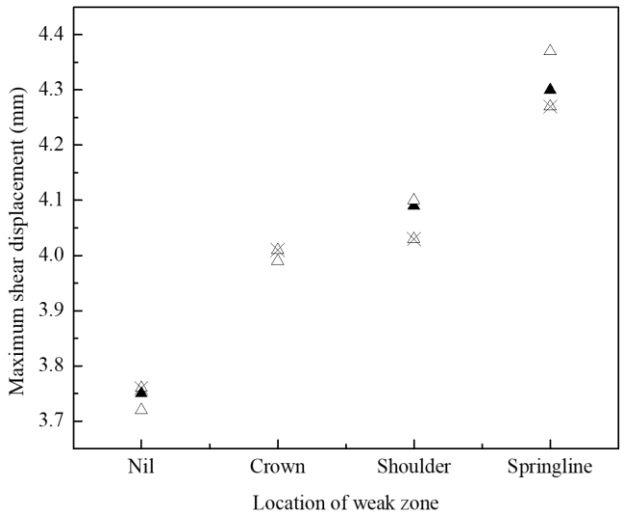

Figure 4-11. Effect of weak zone location on the shear displacement of the ground (Overburden height = 1D and e = 0.45)

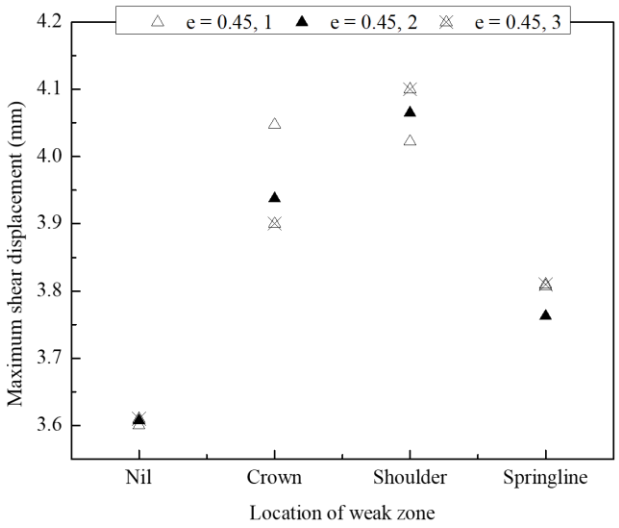

Figure 4-12. Effect of weak zone location on the shear displacement of the ground (Overburden height = 2D and e = 0.45)

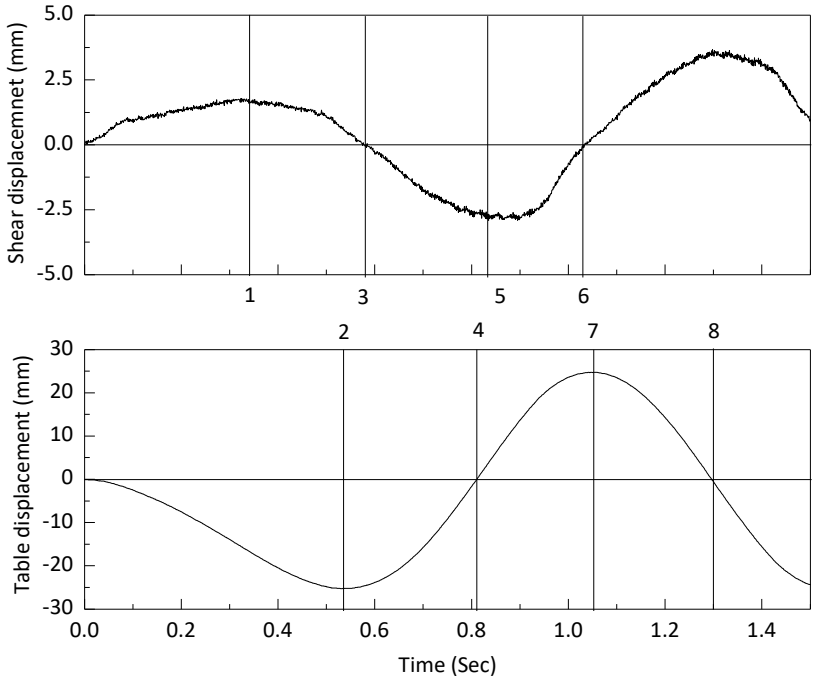

Figure 4-13. Positions of examined photos during each cycle

Due to shallow overburden height, the development of the shear band is not very clear however, it is evident that with the increase in the shear displacement the ground strain increases. For a specific cycle, when the photos were compared for shear displacement equal to zero, they show minimum development of the deviatoric strain. The ground strain at this stage is due to the residual strain which further increases with the increase in the shaking time. As compared to the

initial cycles during the 10th cycle significant deviatoric strain has been developed which shows that the 10th cycle can be the representative of the analysis to capture the average behavior of the ground. If we compare the development of the ground strain for the 20th and 30th cycles, it is not wrong to say that there is no significant difference between the 20th and the 30th cycles. This is because after completion of the 20th cycle maximum compaction has been occurred and the ground particles have been packed.

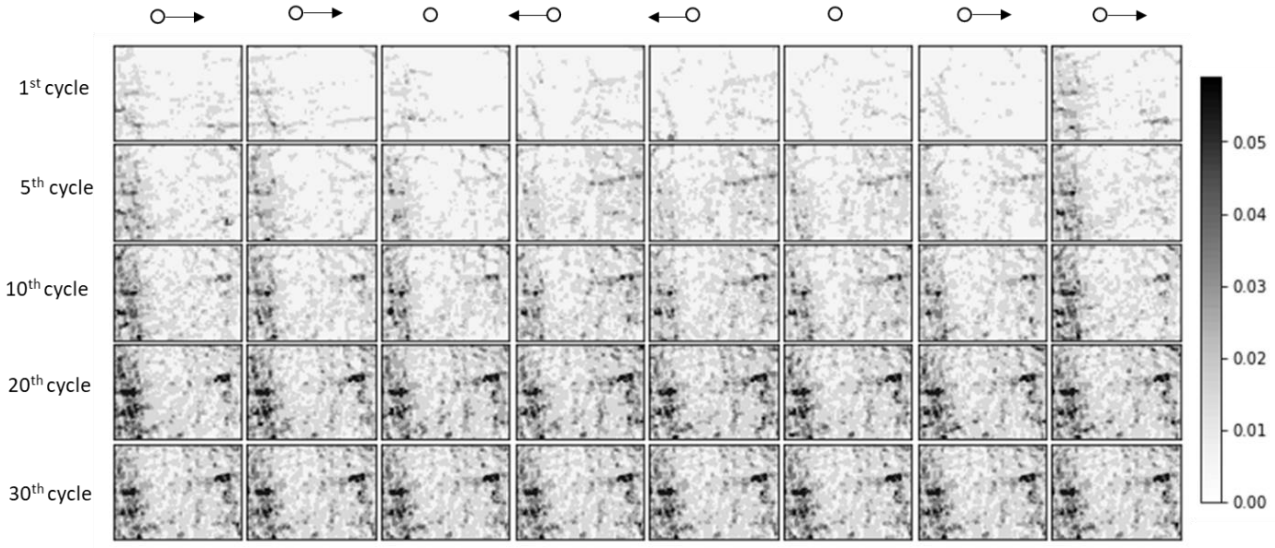

Figure 4-14. Effect of shaking time on the development of the deviatoric strain for ground only (Overburden height = 1D)

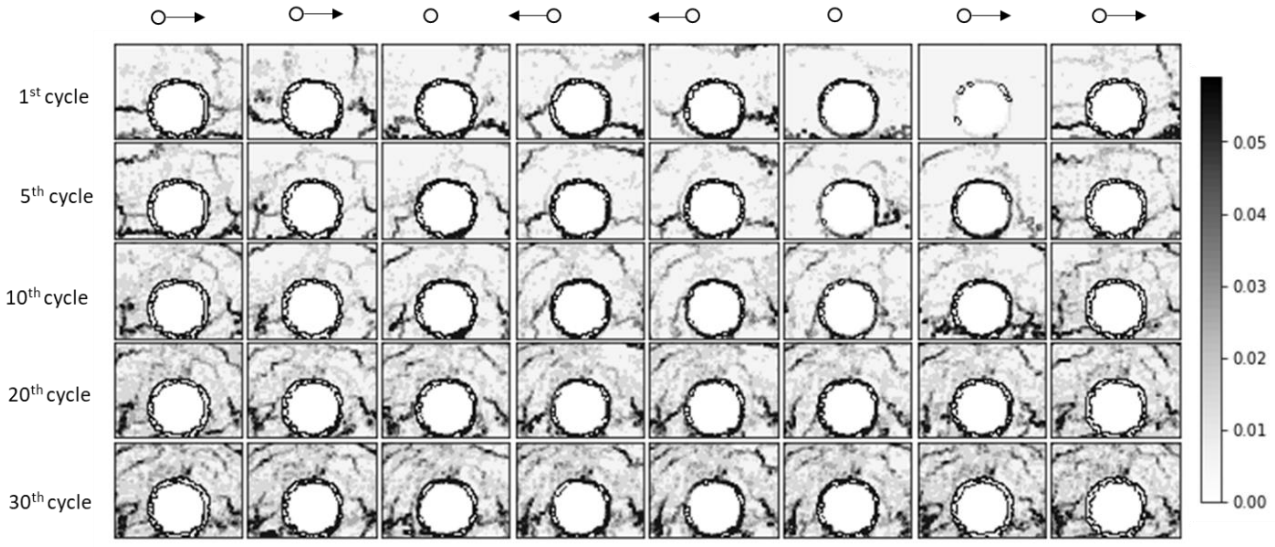

Figure 4-15. Effect of shaking time on the development of the deviatoric strain for no weak zone case (Overburden height = 1D)

After placing the tunnel inside the ground and before the creation of the weak zone the photos were analyzed, and the results have been presented in Figure 4-15. The placement of the tunnel inside the ground changed the ground response, especially around the tunnel boundary. The deviatoric strain can be seen from the very first cycle which in the case of only ground was very slim. The development of the ground strain is due to the flexible nature of the tunnel model as compared to the surrounding ground. As the tunnel is flexible than the model ground hence it bends more than the ground material when shaken. This means that the construction of a tunnel structure will change the ground behavior as for no tunnel case. With the increase in the number of the cycle, the ground strain starts multiplying for initial cycles. As the number of the cycles increased beyond the 20th cycle the change was not so significant. As in the previous case, the results of the 10th cycle can provide a reasonable average response of the ground material. Due to the placement of the tunnel in the model ground, the maximum shear strain was seen at the springline position of the tunnel. The development of the shear strain at the springline height is due to the squeezing of the tunnel along the vertical axis. This squeezing of the tunnel along the vertical axis will produce the ovaling phenomena while the table is in shaking conditions. It can also be seen that when the relative displacement of the ground w.r.t., the table is zero, there is the minimum shear strain for that particular cycle, and as the shear displacement increase (left or right) the shear strain increase accordingly.

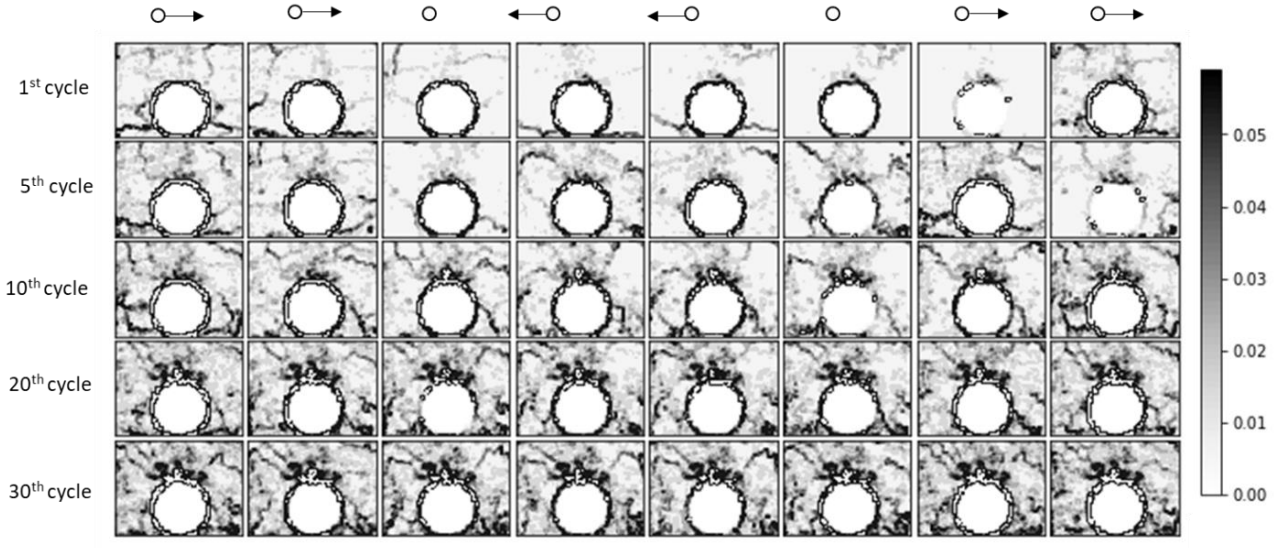

Figure 4-16. Effect of shaking time on the development of the deviatoric strain for the weak zone at the crown (Overburden height = 1D)

Figure 4-16 shows the results of the deviatoric strain when a weak zone was placed at the crown position. The plotted data shows that the presence of the weak zone has changed the ground response and here the strain accumulates primarily at the position of the weak zone. This accumulation of the strain is very critical for the lining structure as it will impose more stresses on the tunnel structure. The ground shearing happens along the line spreading by the size of the weak zone. It seems that if we project the lines further, they will intersect at the center of the tunnel. By comparing the shaking time, it was found that during initial cycles there is not so significant development of the deviatoric strain. However, as the number of cycles approached 10, the strain starts accumulating.

From the above discussion, it has been found that the results calculated at the 10^{th} cycle can represent reasonably well the average behavior of the lining structure and the ground material. As an increase in the number of the cycles increases the response, hence the results after the 30 cycles will provide the effect of the maximum shaking time. With the increase in the shear displacement, the response has increased therefore the results calculated at the maximum shear displacement will provide the maximum development of the ground strains.

4.2.3 Ground response in terms of volumetric strain

The ground response from photos has been recorded in terms of internal strains and here the effect of weak zones on volumetric strain (ε_v) will be discussed. Displacement vectors obtained from image analysis were employed to derive different strain fields following the process defined earlier. Photos were analyzed for three positions i.e., at maximum table displacement during 10^{th} cycle, at the completion of 30^{th} cycle, and the maximum shear displacement of the ground as indicated in Figure 4-17. The results obtained through different scenarios have been compared with the full contact case. For no weak zone condition, the results of volumetric strain have been presented in Figure 4-18. The negative values of volumetric strain are regarded as shrinkage while the positive values indicate the expansion. Shrinkage and expansion have been simultaneously observed around the tunnel with the former having a higher value. The plotted data shows that as the number of cycles increase, the development of the volumetric strain increases. The increase in the volumetric strain is due to more compaction that happened with more shaking of the ground. As the maximum shear displacement occurred before the 30^{th} cycle, therefore the values of the strain observed at the 30^{th} cycle are higher than those at the maximum shear displacement.

Furthermore, with the increase of overburden height the volumetric strain increases due to high gravitational stresses. The higher gravitational stresses will cause more ground settlement resulting in higher values of the volumetric strain.

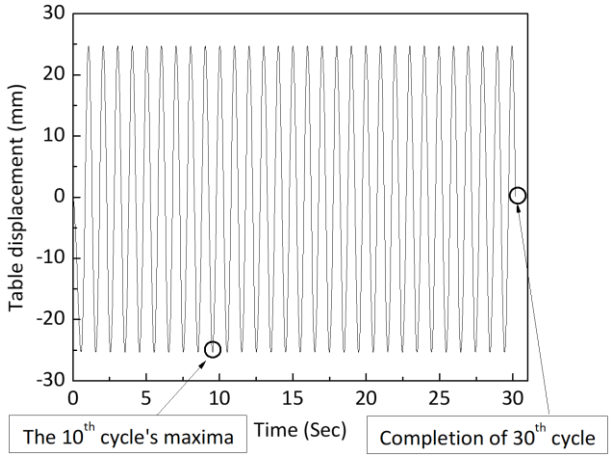

Figure 4-17. Indication of measurement positions

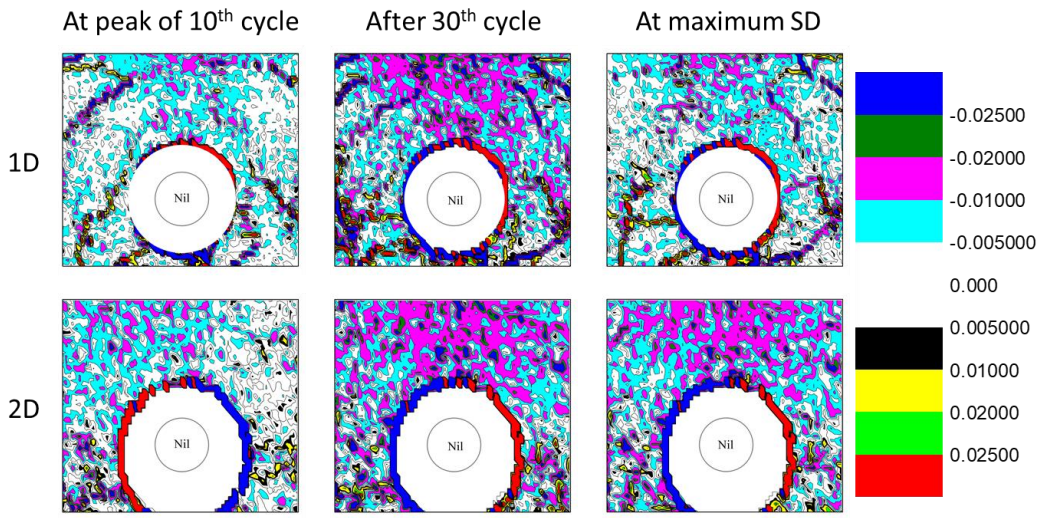

Figure 4-18. Distribution of volumetric strain for no weak zone case

A weak zone was introduced at the tunnel crown and the volumetric strains have been plotted in Figure 4-19. It can be seen that due to the weaker part there is strain localization happened around the crown position. With the increase in overburden height although the size and void ratio of the weak zone was the same the development of the volumetric strain has significantly increased. The increase in the volumetric strain due to high soil cover is due to the high gravitational stresses acting on the tunnel model. Figure 4-20 represents the distribution of the volumetric strain when the weak zone was placed at the shoulder position under an overburden

height of 1D and 2D. The graph represents that with the increase in overburden height more volumetric strain developed around the weak zone position.

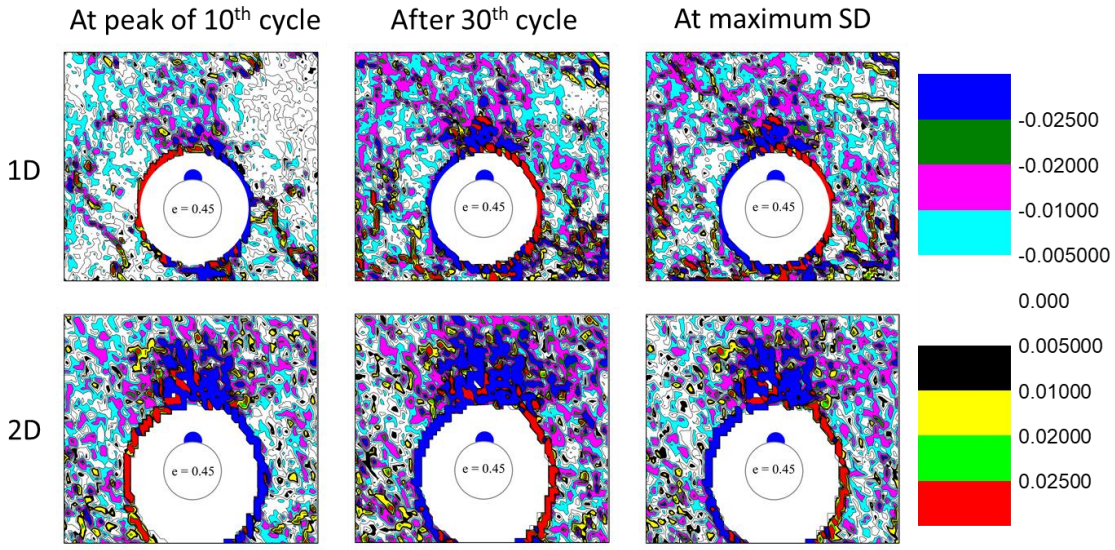

Figure 4-19. Distribution of volumetric strain for the weak zone at the crown

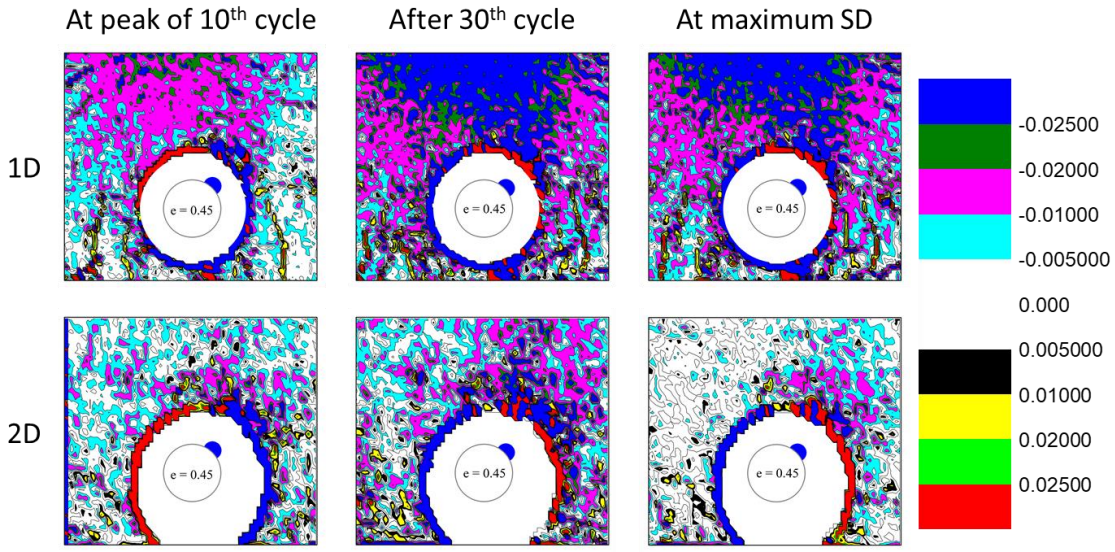

Figure 4-20. Distribution of volumetric strain for the weak zone at shoulder

The plotted data in Figure 4-21 shows that due to the presence of the weak zone at the springline of the tunnel there is a localized development of the volumetric strain around the weak zone. The localized volumetric strain can be attributed to the more groundmass movement towards the weaker part. Contour plots exhibit that the distribution of volumetric strain is symmetric around the central axis of the weak zone through the center of the tunnel. By comparing the time, it is

evident that as the time of shaking increases there is more and more development of the volumetric strains. The figures also reveal that the amount of shrinkage is higher than expansion because the ground is getting compacted during the shaking process. By assessing the effect of overburden height, it was found that with the increase in the overburden height the volumetric strains developed in the groundmass, increased when analyzed at different intervals. The increase in ground strain is due to high gravitational stresses in case of higher overburden height.

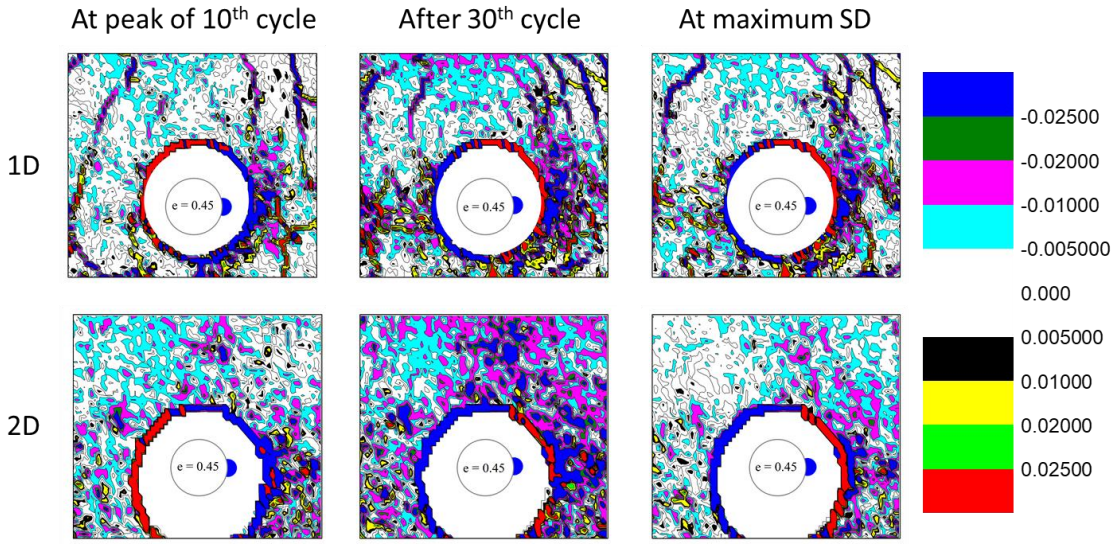

Figure 4-21. Distribution of volumetric strain for the weak zone at springline

4.2.4 Ground response in terms of deviatoric strain

Apart from the volumetric strain, the ground strains have also been estimated in terms of deviatoric strain. The deviatoric strain is very important as it represents the failure possibility of the groundmass. The distribution of deviatoric strain measured at different time intervals i.e., at the maximum displacement of the 10^{th} cycle, after the 30^{th} cycle, and the maximum shear displacement for no weak zone case has been presented in Figure 4-22. Moreover, the effect of the overburden height has been illustrated. It can be seen that there is the development of the deviatoric strain around the tunnel boundary which is due to the boundary effect. As the number of cycles increases, an increase in the deviatoric strain has been observed. By comparing the overburden height, it is found that there is no significant effect of overburden height for no weak zone case.

After analyzing the distribution of the deviatoric strain for no weak zone case, a weak zone was created at the tunnel crown and the results have been presented in Figure 4-23. The

introduction of the weak zone causes the strain at the crown position which accumulates further with the increasing number of cycles. The increase in the strain with the increasing number of cycles can be attributed to more compaction and more ground moving towards the weaker part. With the increase in the overburden height, the deviatoric strain has increased further. This increase is due to high gravitational stresses which have caused more ground settlement. Moving the weak zone at the shoulder location resulted in the accumulation of the deviatoric strain at the shoulder position as shown in Figure 4-24. The localized development of the deviatoric strain is due to the ground loosening caused by the creation of the weak zone. The more incoming ground will cause more strain as the number of cycles increased. The higher overburden height of the ground above the tunnel model intensifies the localized development of the deviatoric strain. The high values of the deviatoric will impose more strains on the tunnel structure. Moving the weak zone to the springline position, the deviatoric strain appears around the springline location as sown in Figure 4-25. The reason for the deviatoric strain is due to the ground loosening and loss of the shear strength. As the weak zone was placed at the right springline, therefore, the major deviatoric strain developed at the right side. However, along with the right springline, the left springline also shows the development of the deviatoric strain. Moreover, with the increase of the overburden height, the development of the deviatoric strain also intensifies as shown in Figure 4-25. Finally, as the number of the shaking cycles were increased the deviatoric and volumetric strains increased.

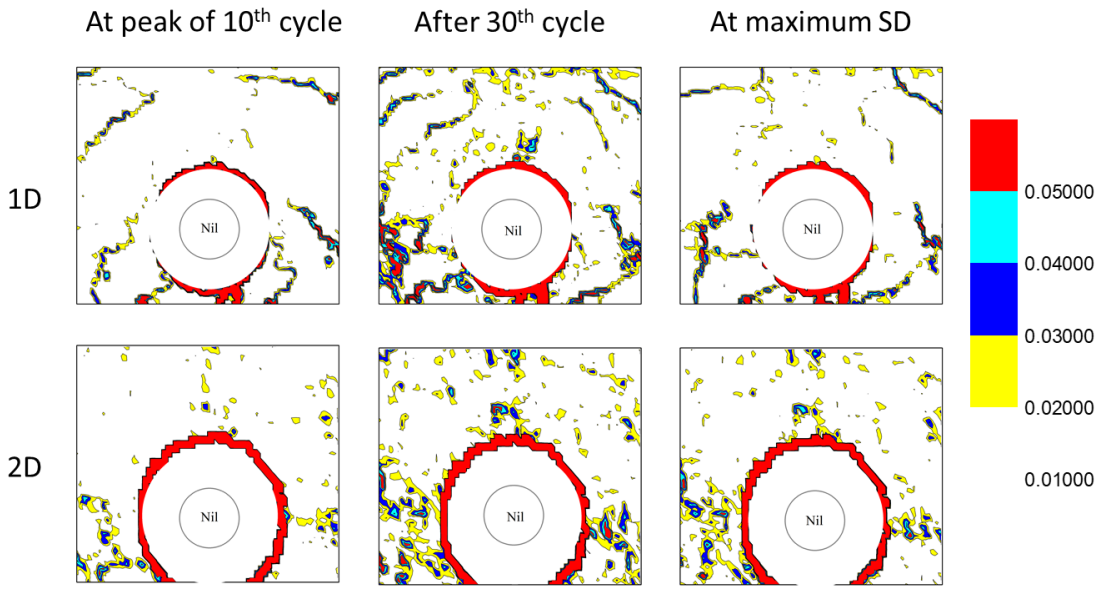

Figure 4-22. Distribution of deviatoric strain for no weak zone case

While analyzing the volumetric strain, the weak zone at the springline produced the volumetric strain at the springline location. With the increase of the overburden height, the volumetric strain also increased not only on the local position but also at the other positions around the tunnel as shown in which further intensifies with the increase of the shaking duration. The presence of the weak zone at the springline location attracts more ground towards the springline position. More ground moving toward the weak zone resulted in higher deviatoric strains. The higher overburden height has increased the spread as well as the values of the strain.

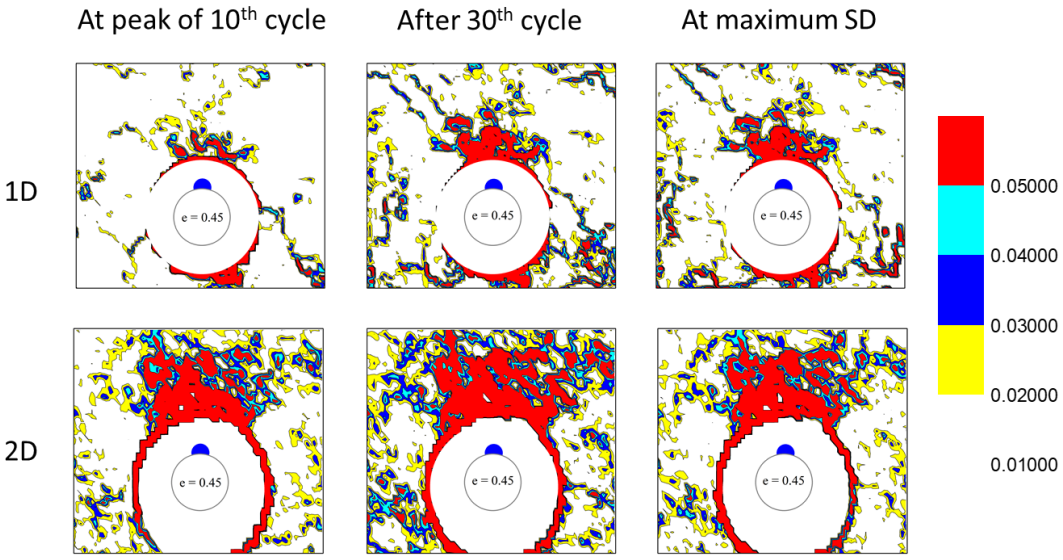

Figure 4-23. Distribution of deviatoric strain for the weak zone at the crown

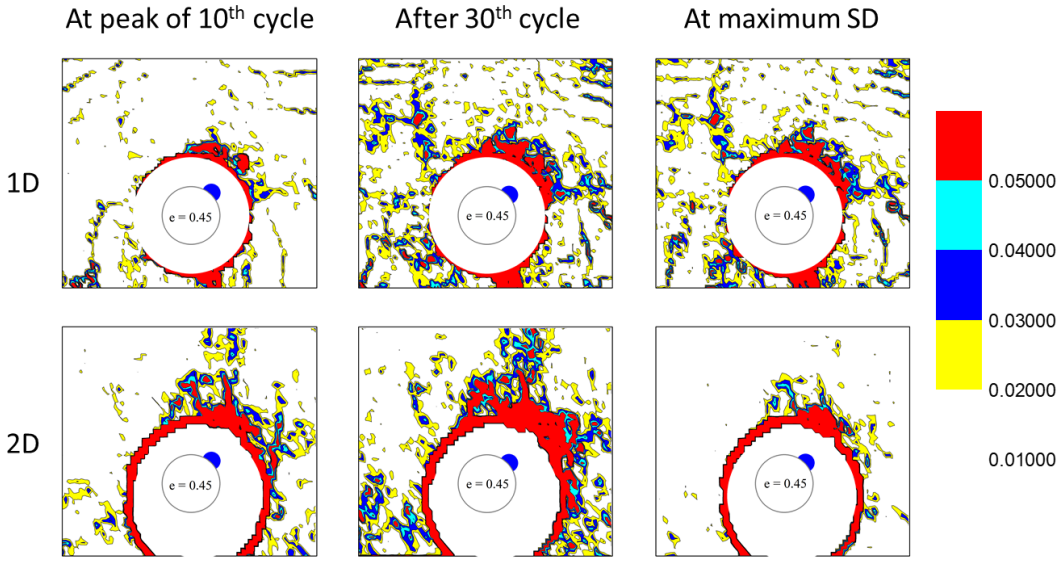

Figure 4-24. Distribution of deviatoric strain for the weak zone at shoulder

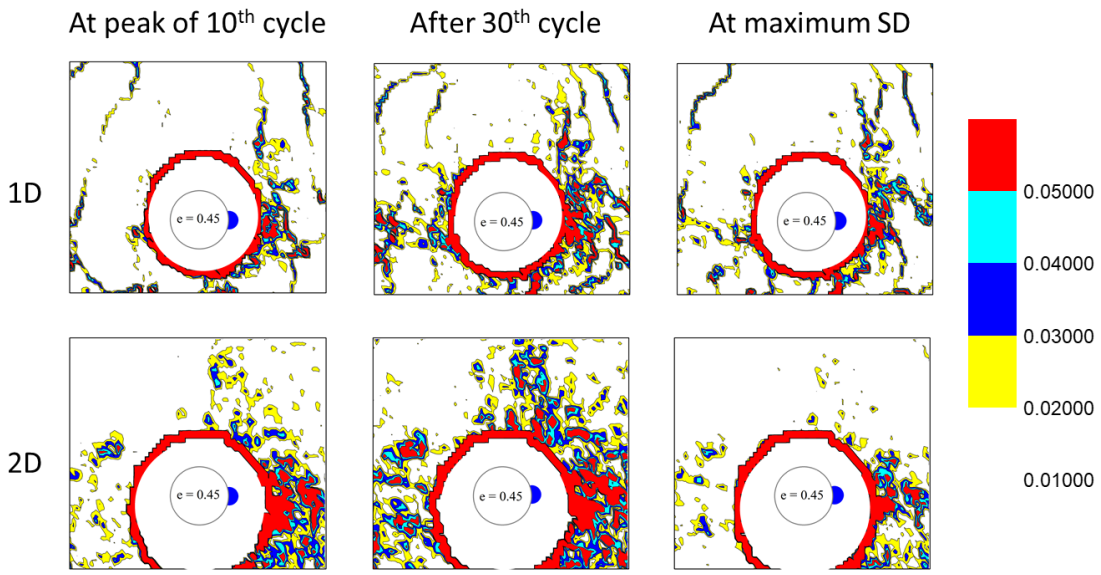

Figure 4-25. Distribution of deviatoric strain for the weak zone at springline

4.3 Tunnel Response

Tunnel response has been measured in terms of the internal strain, outer strain, and bending moment. Internal strain is a very important aspect used for health monitoring of the tunnels. It can easily be measure by installing the strain gauges at the desired locations. Internal strain can be used to estimate various other important parameters e.g., the axial stress, bending moment, and/or the shear force produced in the lining. However, the correct alignment of the strain gauges is very important to calculate the desired quantities. In this research, the strain gauges were installed specifically to measure bending moment. However, while writing this thesis, the internal strain has also been presented by keeping in view the field restrictions. The tunnel response measured in terms of internal stain and the bending moment has been presented for before shaking as well as for during shaking conditions.

4.3.1 Before shaking

4.3.1.1 Internal strain

The before shaking condition represents the rest state of the table. The measurement of internal strain under such conditions is made after placing the tunnel model in the model ground and after creating the weak zone at the desired location. The results of the internal strain of the tunnel tested under overburden height of 1D and 2D for no weak zone have been presented in

Figure 4-26. The graph presents that for no weak zone condition the distribution is almost symmetrical about the vertical axis. However, along the horizontal axis, the invert shows higher bending that is due to the fixed bottom boundary. Furthermore, the deflected shape represents that the crown and invert are under compression while the springline positions are in tension, however, the diagonal positions experience small strain. The increase in the overburden height increased the strains in the lining however, in the case of higher overburden height the crown of the tunnel more bending as compared to the less overburden height. The observed behavior, in this case, is similar to that observed in the biaxial compression test results.

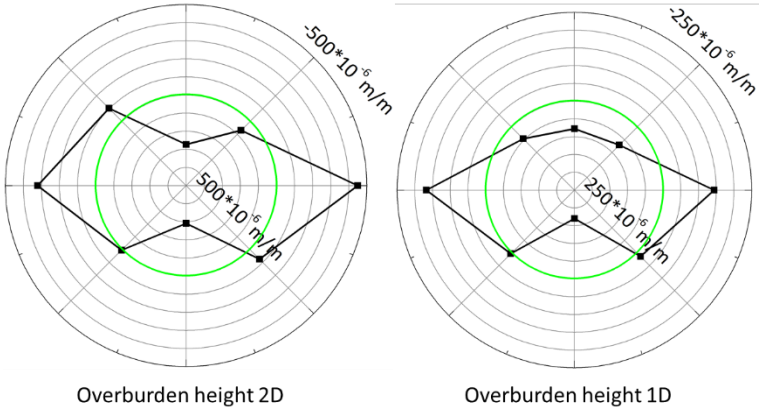

Figure 4-26. Distribution of internal strain for no weak zone

The bending behavior of a tunnel accompanying the weak zone is different as compared to the case of the full contact case. After placing the weak zone around the tunnel for overburden height 1D and 2D have been investigated. The introduction of a weak zone around the tunnel allows the tunnel to bend in the outward direction primarily at the point of the weak zone and slightly on the surrounding locations as illustrated in Figure 4-27. The bending of the tunnel towards the weaker zone is due to the space available for bending and for doing so the internals train changed itself from tension to compression which can cause concrete cracking or spalling. It can be seen that with the increase of the overburden height, the tunnel response multiplies. When the weak zone was placed at the crown, the tunnel extends towards the weak zone while compressed at the surrounding locations. Moving the weak zone to the shoulder extends the tunnel from the shoulder position and is compressed at surrounding positions. The changing of the weak zone to the springline positions follows a similar pattern as described earlier. The maximum response (in terms of internal strain) of the tunnel was recorded when the weak zone was stationed

at the shoulder position. The distribution behavior of the internal strain and tunnel bending behavior shows good correlations w.r.t. to the overburden height.

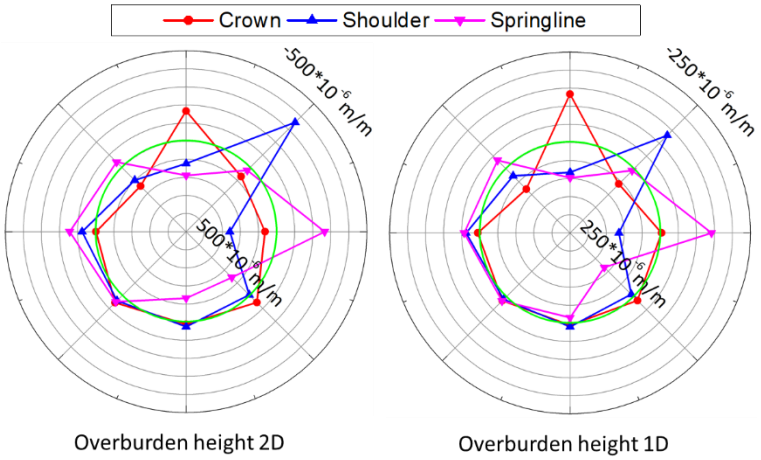

Figure 4-27. Effect of weak zone position on internal strain before shaking

4.3.1.2 Bending moment

The static bending moment is defined as the bending moment measured from strain values recorded at the rest state of the table. The strain values were recorded soon after fixing the tunnel and removing the required amount of material to achieve the specific void ratio. The values of static BMs around the tunnel periphery were drawn in where different charts for the outcomes obtained at the crown, shoulder, and springline are included. When there is no weak zone, the largest BM occurs at the tunnel invert as shown in Figure 4-28. The BMs at the springlines and knees are positive which implies that the internal fiber of the lining is experiencing the tensile stress, and at the crown, invert, and shoulders of the tunnel the BMs are negative, i.e., the internal fiber of the lining is under compression. When a cavity is made at the crown, the loosening contact between the ground and the lining produced the ground unpacking at the invert and crown while it imparts additional loads at the shoulders and springlines of the tunnel. Moreover, it changed its sign from negative to positive bending moment. Meguid and Dang, 2009 and Tan and Moore, 2007 also proved that the existence of weak zones behind the lining can lead to a change in the magnitude of BMs and reversal in the moment sign. Setting the weak zone to the right shoulder leads to an increase in the BMs at the shoulder, and invert, and decreases the BMs at crown and springline positions. When the weak zone is introduced at the springline, BM at the springlines increases coupled with a decrease in BMs at the crown, right knee, and invert of the tunnel. As the

contact loss between ground and lining at different positions increases, the lining BM tends to change substantially at the crown, springline, and invert but less significant changes observe at diagonal positions. Note that with no weak zone the BM distribution is symmetrical along the horizontal and vertical axis and the tunnel deforms slightly inwards at the crown and invert, and outward at springlines. As the weak zones are introduced, the movements of the lining are outwards in the direction of the cavities, while compressing the lining inward at the adjacent positions. This tendency is because of the interplay between the lining and the supportive material causing ovaling of the tunnel. As the weak zone at the crown unloads the lining at the crown and invert, the springlines take the additional loads and vice versa.

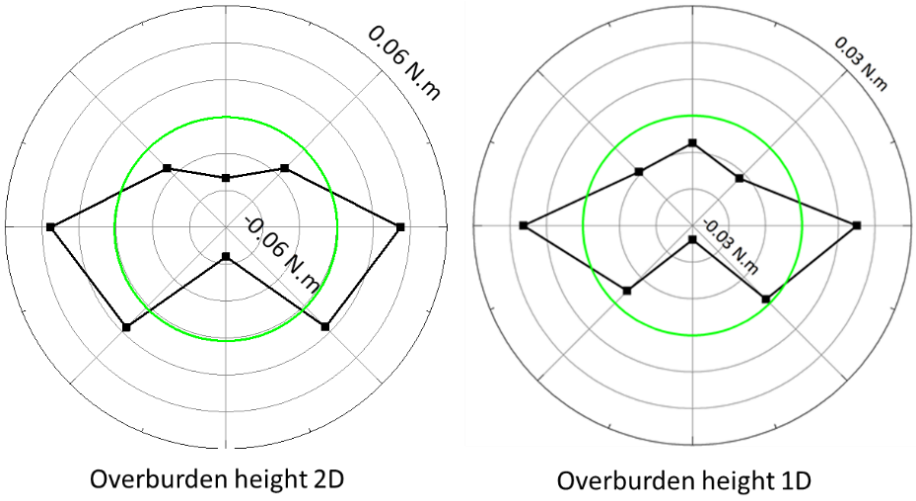

Figure 4-28. Distribution of bending moment for no weak zone

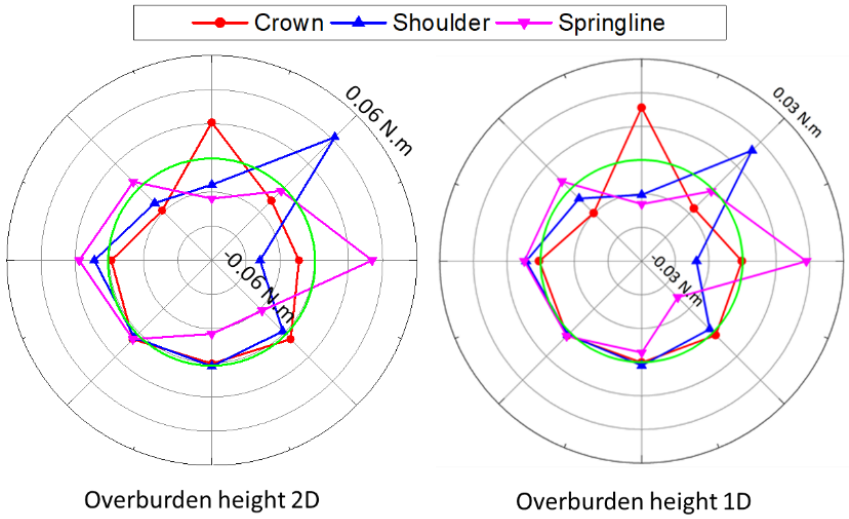

Figure 4-29. Effect of weak zone position on bending moment before shaking

4.3.2 During shaking

4.3.2.1 Internal strain

To check the seismic behavior of tunnels having weak zones behind the lining, the internal strains have been drawn at different time intervals. The values presented here are the incremental values over the static response. For a tunnel with full contact between the lining and the surrounding ground, under the application of the shear wavefront, theoretically, the tunnel bends along the diagonal position as illustrated in Figure 4-33. The introduction of a weak zone changes the bending behavior of the tunnel. Here in this section, the results have been plotted at the maximum displacement of the 10th cycle in Figure 4-30, after the 30th cycle illustrated in Figure 4-31, and at the maximum shear displacement of the ground in Figure 4-32. It is worthy to highlight that all values of internal and bending moment drawn to show the effect of the seismic effect are the incremental values over the static values. This means that the plotted data show the effect of shaking on the tunnel response and changes in its behavior due to the presence of a weak zone behind the lining.

When the weak zone was placed at the tunnel, the crown tends to bend the tunnel at the crown position due to the pressure of the incoming round. However, there are no significant changes occurred at other positions. When the weak zone has moved to shoulder and springline positions, the strain at the crown becomes higher because the incoming ground is not affecting it directly. The tunnel bending behavior at the maximum displacement of the 10th cycle is towards the left side which is because the table position was also on the extreme left side.

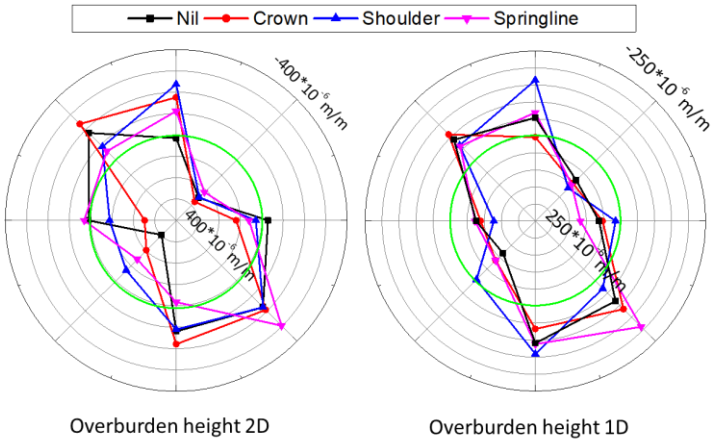

Figure 4-30. Effect of weak zone position on internal strain at maximum 10th cycle (e = 0.45)

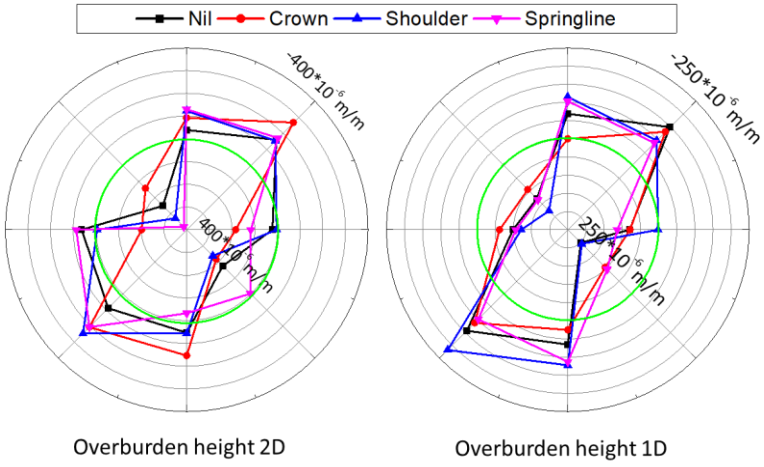

Figure 4-31. Effect of weak zone position on internal strain at the completion of 30th cycle (e = 0.45)

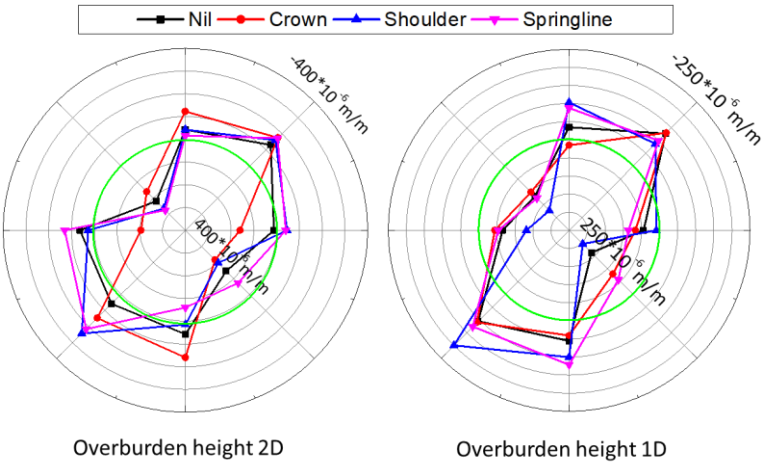

Figure 4-32. Effect of weak zone position on internal strain at maximum shear displacement (e = 0.45)

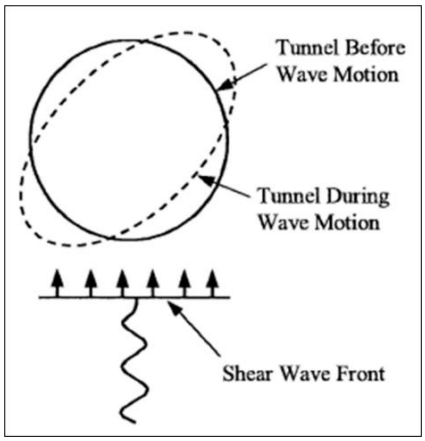

Figure 4-33. Tunnel ovaling (Owen and Scholl, 1981)

4.3.2.2 Bending moment

Dynamic bending moments around the tunnel lining are calculated from strain values recorded during the shaking process. As the dominant deformation for tunnels subjected to shear forces is the ovaling phenomena caused by the shear displacement of the ground. From the time histories of the bending moment, the values at the maximum displacement of the 10th cycle, at the completion of the 30th cycle, and maximum shear displacement were chosen and plotted to investigate the effect of the weak zone in Figure 4-34, Figure 4-35, and Figure 4-36 respectively. Here the results for the weak zone with a void ratio of 0.45 have been presented. In the case of tunnel response at maximum shear displacement, the tunnel behavior depends on the position of the weak zone.

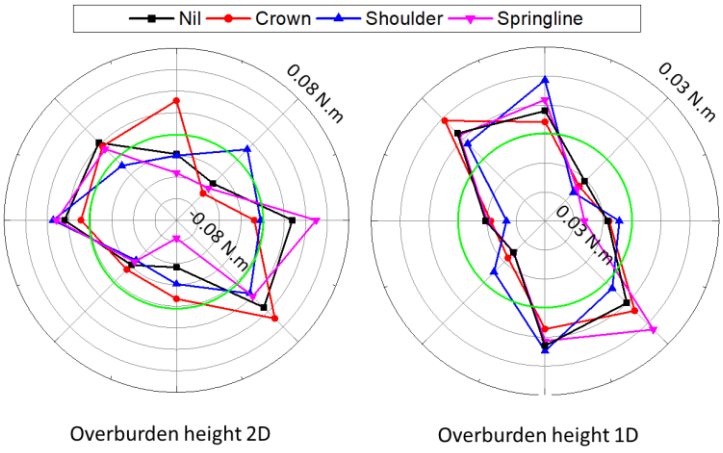

Figure 4-34. Effect of weak zone position on bending moment at maximum 10th cycle (e = 0.45)

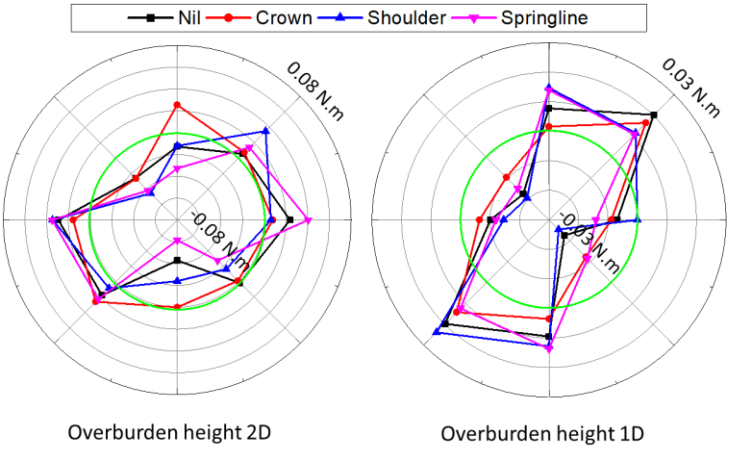

Figure 4-35. Effect of weak zone position on bending moment at the completion of 30th cycle (e = 0.45)

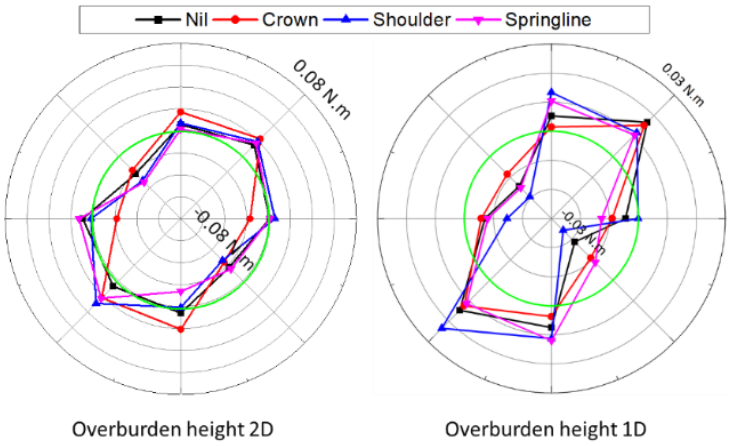

Figure 4-36. Effect of weak zone position on bending moment at maximum shear displacement

For example, when the weak zone was at the crown and the tunnel was shaken the surrounding ground moving directly towards the weak zone put extra pressure and the tunnel shows a downward bending here. In the case of the weak zone at the shoulder, due to more pressure of the incoming ground, the tunnel bends upward and in the opposite direction of the shoulder i.e., the left knee as indicated by the blue line. The tunnel is being pushed on the opposite side. Similar behavior has been observed for the weak zone at the springline.

4.4 Comparison of Bending Moment and Internal Strain

As mentioned earlier many researchers and designers are usually interested in calculating the bending moment at different locations. However, to measure the bending moment minimum of two strain gauges are needed to install i.e., one on the outer surface and the other on the inner face of the specimen. In the field, it is quite difficult to install the strain gauges on the outer surface of the tunnel due to the presence of overburdened soil. By paying close attention to the plotted diagrams, a comparison of the internal strain and the bending moment can be established. From the plotted graphs it is evident that the qualitative distribution of the internal strain and the bending moment is identical to each other. It means that by measuring the only internal strain it is possible to imagine the bending behavior and qualitative distribution of the bending moment around the tunnel lining. However, the exact value of the bending moment depends upon the inside as well as the outside strain in the lining. Therefore, the internal strain gives the idea of the bending behavior of the lining but not the quantitative amount of bending.

4.5 Conclusions

In this chapter, the effect of weak zone position has been explored and results have been presented in the form of ground response and tunnel response. The ground response has been measured in terms of volumetric strain and deviatoric strains while the tunnel response has been measured in terms of internal strain, outer strain, and the bending moment. From the assembled results the following results have been drawn.

- A weak zone around the tunnel acts like extra space and under static conditions, the tunnel tries to bend towards it and by doing so at the position of the weak zone the tunnel bends outward while slightly inside at the neighboring points.
- During the shaking process, due to the application of the shear wave, the tunnel bends along the diagonal axis. The reason for this phenomenon has been explored by the previous researchers and found that the lateral excitation is predominantly associated to the 45^0 isogonal conjugate bending of lining cross-section, for that reason the shoulders and knees would be the most vulnerable locations for BM (Sedarat et al., 2009). The shearing wave causes the ovalisation of the tunnel around the diagonal axis. The BMs change slowly in the beginning because of low-level excitations but later they start to wave around a mean value until the termination of the excitation.
- During excitation, the ground was sheared, and the response was measured in terms of the shear displacement which is symmetrical for no weak zone case. However, with the introduction of the weak zone, the shear displacement was increased due to the weakening of the groundmass. Weak zone-induced shear displacement can be very dangerous as it may result in more stresses in the lining.
- The effect of the weak zone on ovaling phenomena has been expressed in the form of ratios of vertical to horizontal lengths and the ratios of opposite diagonal lengths as illustrated in Figure 4-37. The more shearing displacement results in more ovalisation of the tunnel as the ratio of diagonal lengths are higher than vertical. Maximum ovalisation happened for the weak zone at the shoulder because the ovaling tunnel and weak zones are in the same direction as shown in Figure 4-38.
- A weak zone causes a high localized volumetric and deviatoric strain around the location of the weak zone. This increase in volumetric and deviatoric strain further intensifies with

the increase in the overburden height. The volumetric strain and deviatoric strain are qualitatively shown similar distribution for the weak zone at different positions around the lining. The percentage area under the volumetric strain shows that with the introduction of the weak zone the affected area under volumetric strain increases. It was also noted that the compression is higher than expansion.

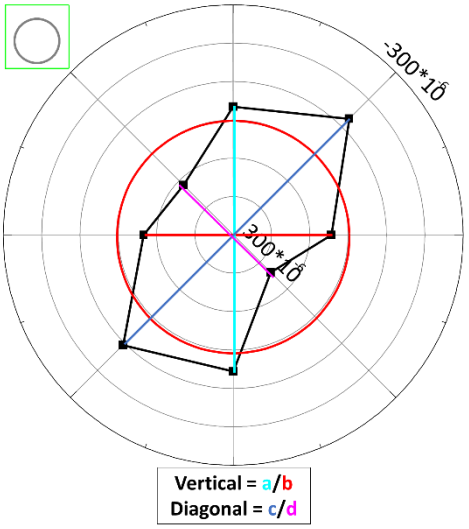

Figure 4-37. Illustration of the ratio between vertical and diagonal lengths of strain distribution

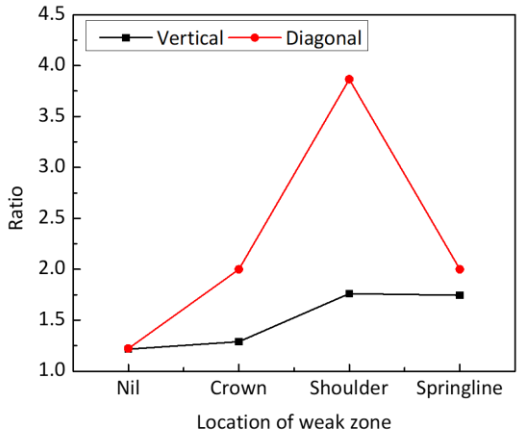

Figure 4-38. Distribution of the ratio of vertical lengths and diagonal lengths for different positions of the weak zone

- Before shaking, the weak zone increased the tunnel response measured in terms of internal strain, outer strain, and bending moment. The weak zone at the crown and shoulder has increased the internal strain two times as compared to the no weak zone case as shown in

Figure 4-39. Weak zone at springline position has increased the tunnel response at springline and crown location.

- During shaking, the maximum tunnel response has observed at the crown when the weak zone was located at the shoulder position. The response was found to increase almost three times as compared to the no weak zone case as shown in Figure 4-40. For the weak zone at the springline, the response of the tunnel was observed at the springline as well as the crown position.
- The distribution of internal strain and bending moment qualitatively show similar distribution. Therefore, the bending behavior of the tunnel can also be studied by measuring the internal strain only.

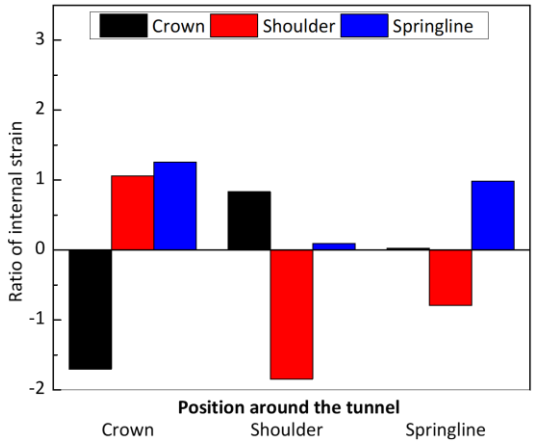

Figure 4-39. Increment of internal strain w.r.t. no weak zone before shaking

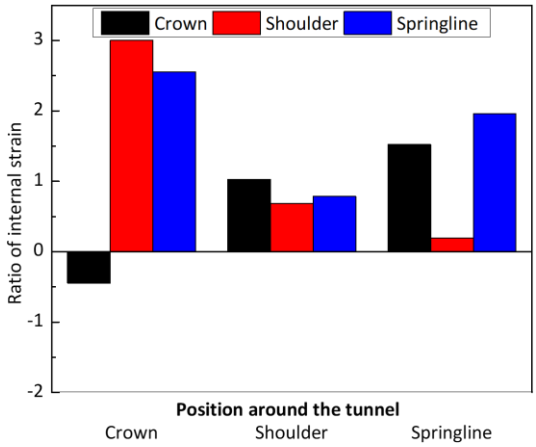

Figure 4-40. Increment of internal strain w.r.t. no weak zone during shaking

CHAPTER 5: EFFECT OF SIZE AND STIFFNESS OF WEAK ZONE

5.1 Size of Weak Zone

The development of a weak zone behind the tunnel can be attributed to many reasons including, poor workmanship, water erosion, slacking, swelling and shrinkage, and dynamic activities. The creation of a weak zone is a time-dependent phenomenon and with time, the size and geometry of the weak zone can be change. After the creation of the weak zone, if not filled properly it can extend to a larger size. The total length of the weak zone can be as large as half of the road tunnel length and ¾ of the railway tunnel length. In this study, two sizes of the weak zones have been tested. The size of the weak zone was defined with the help of the internal angle (θ) and the height (h) above the tunnel surface as shown in Figure 5-1. In this research work, two sizes of the weak zones have been explored in which the internal angles were 51^0 and 90^0 while the height was 20 mm in both cases. Both sizes have been investigated under the overburdened height of 1D and 2D.

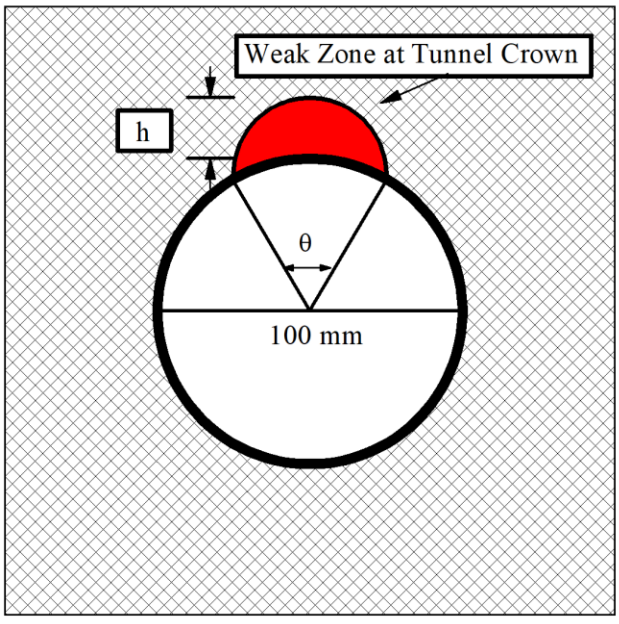

Figure 5-1. Definition of the size of weak zone

5.1.1 Ground response

5.1.1.1 Shear displacement

The effect of the size of the weak zone has been checked on the shear displacement of the ground and the results have been presented in Figure 5-2. The results exhibit that with the increase in the size of the weak zone the shear displacement has increased at each position of the weak zone. The increase in shear displacement is due to the loss of more shear strength as the bigger size weak zone will loosen the soil more as compared to the smaller size weak zone. Surprisingly, the shear displacement in the case of the higher weak zone when it was placed at the tunnel springline is lesser than the small size weak zone. This may be due to the collapse of the surrounding ground while preparing the weak zone, resulting in a ground that later acted as a stiffer ground as compared to the other cases.

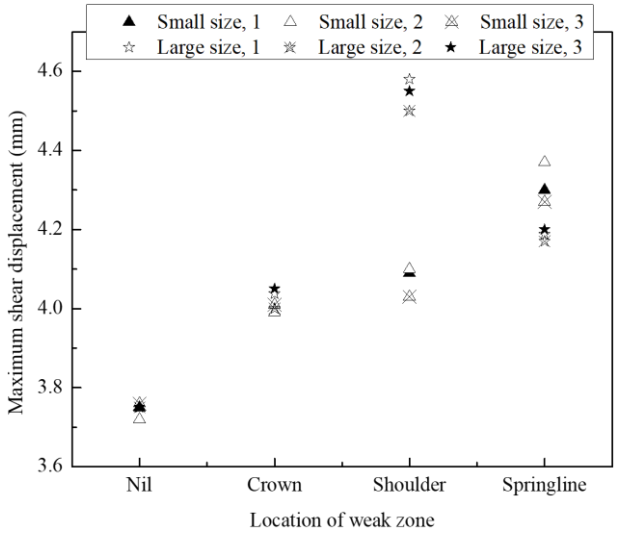

Figure 5-2. Effect of size of the weak zone on the shear displacement of the ground (Overburden height = 1D and e = 0.45)

5.1.1.2 Ground response in terms of volumetric strain

The ground response measured in terms of volumetric strain and the results for no weak zone have been illustrated in Figure 5-3. The negative values of the volumetric strain are termed shrinkage while positive values as expansion. The results of the volumetric strain are plotted at the maximum shear displacement of the ground. The results of the size of the weak zone have been plotted by keeping it at the crown, shoulder, and the springline position and the void ratio of all weak zone equal to 0.45 and overburden height 1D. The graphs plotted in Figure 5-4 shows that

due to the presence of the weak zone the localized volumetric strain was developed i.e. if the weak zone was at the crown the maximum change observed at the crown, similarly for the weak zone at the shoulder and springline the highest development of the volumetric strain occurred at the shoulder and springline respectively. As the size of the weak zone increases the increase in the volumetric strain has been observed at the position of the weak zone. Along with the increase in volumetric strain, the influenced area also increased. The shrinkage and the expansion area show that for the weak zone at different positions, the higher size of the weak zone has more shrinkage and expansion as compared to the small size as shown in Figure 5-3. Moreover, the shrinkage is higher than compression.

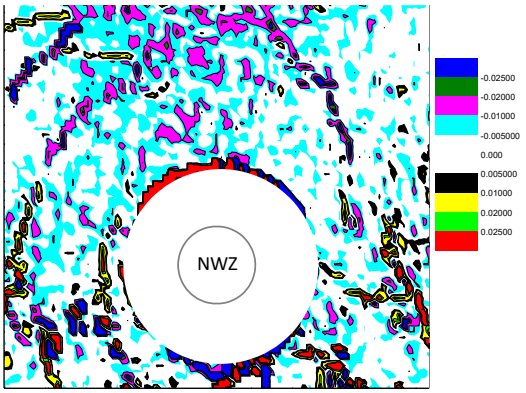

Figure 5-3. distribution of volumetric strain for 1D

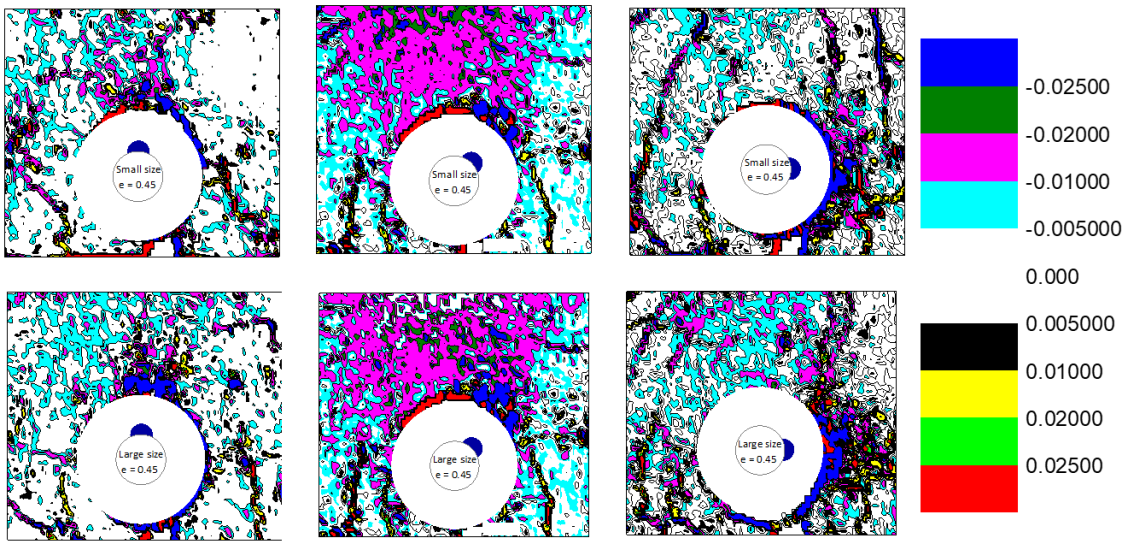

Figure 5-4. Effect of size of the weak zone on volumetric strain distribution at maximum shear displacement (overburden height = 1D & e = 0.45)

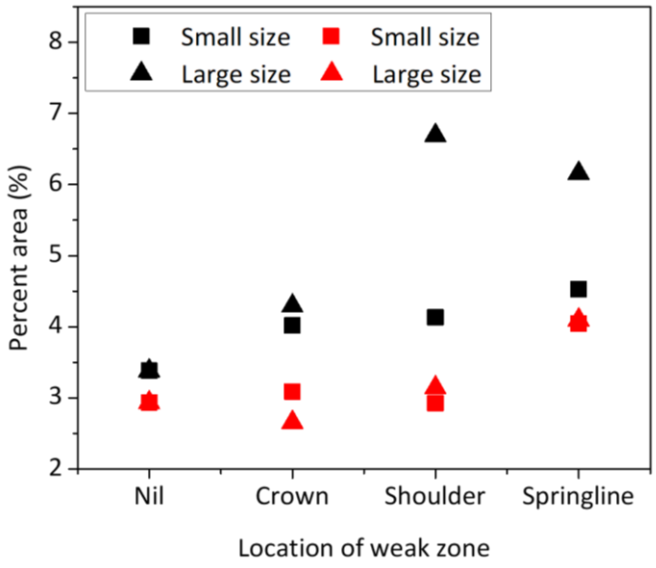

Figure 5-5. Summary of volumetric strain for small and large size of weak zone

The effect of weak zone size on the development of the volumetric strain has also been checked for overburden height 2D. Figure 5-6 shows the effect of weak zone size on the volumetric strain for the weak zone at the crown position and having the void ratio of 0.30, 0.45, and 0.60. It can be seen that for a particular value of the void ratio, with the increase of the weak zone size, the volumetric strain increase. Moreover, the spread area of the volumetric strain is also higher in the case of the higher weak zone as compared to the smaller size.

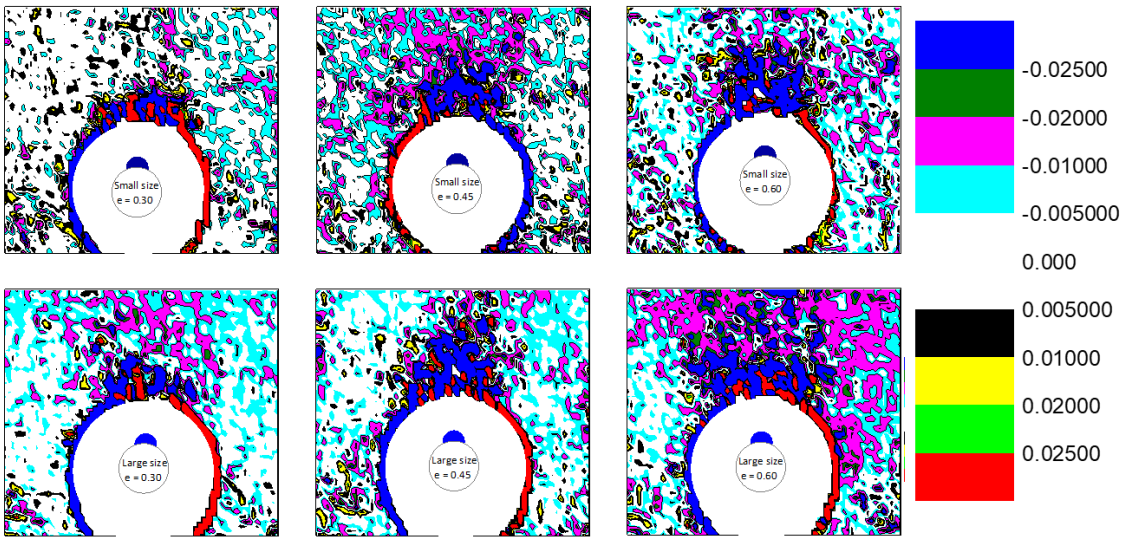

Figure 5-6. Effect of weak zone size on the distribution of volumetric strain for different values of the void ratio under overburden height 2D and weak zone at the crown

The effect of weak zone size for shoulder position under overburden height of 2D has shown in Figure 5-7. The plotted data shows that, the increase in the weak zone size results in a localized increase in volumetric strains round the shoulder location. This increase in volumetric strain is due to more ground loosening caused by the large size of the weak zone and the same trend has been observed in all cases of the void ratios. Figure 5-8 shows the results for the weak zone at the springline position which are showing a similar trend as observed for crown and shoulder cases.

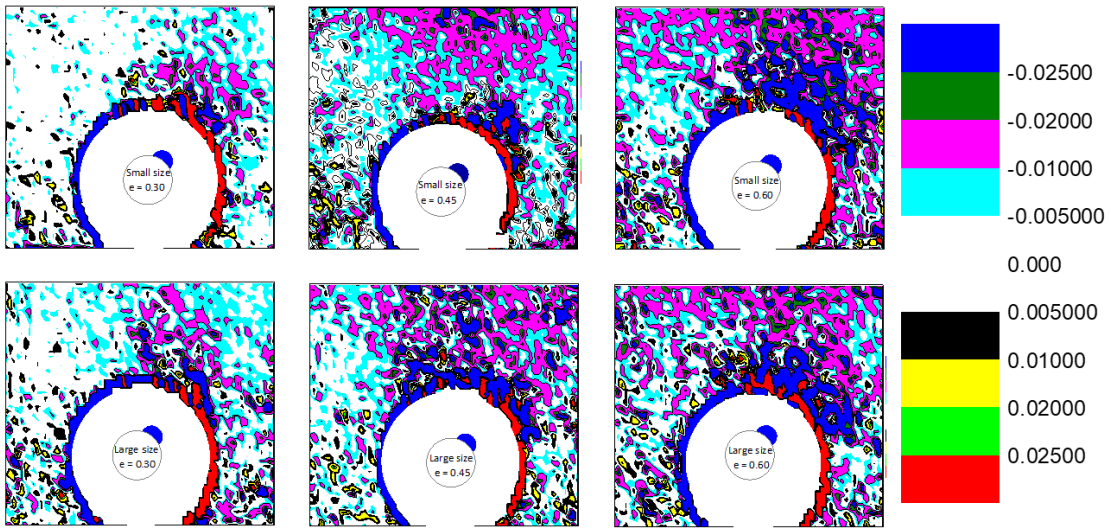

Figure 5-7. Effect of weak zone size on the distribution of volumetric strain for different values of the void ratio under overburden height 2D and weak zone at shoulder

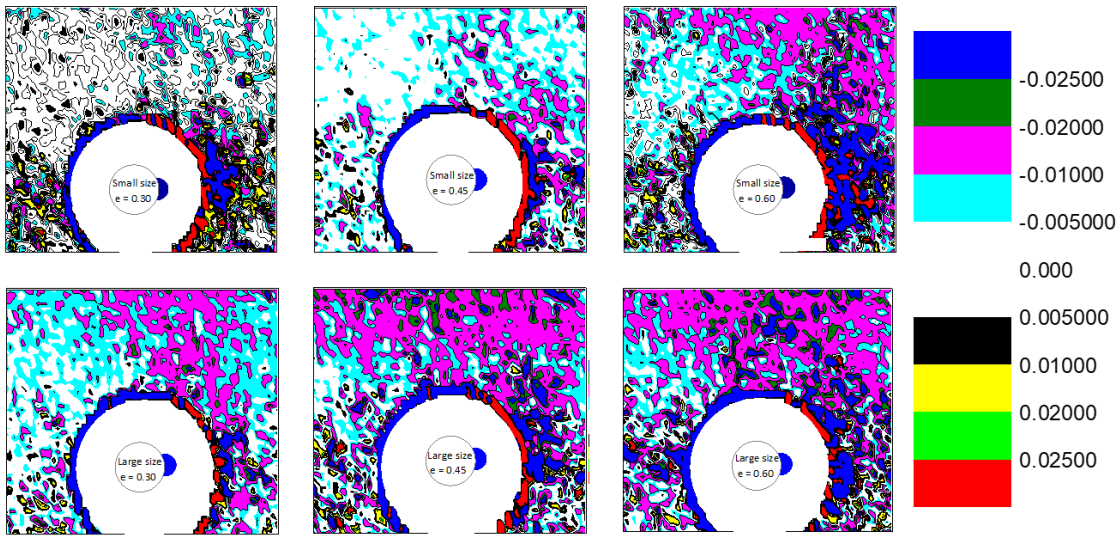

Figure 5-8. Effect of weak zone size on the distribution of volumetric strain for different values of the void ratio under overburden height 2D and weak zone at springline

5.1.1.3 Ground response in terms of deviatoric strain

This section will explain the effect of weak zone size on the deviatoric strain produce in the groundmass during the shaking process. Figure 5-9 shows the distribution of deviatoric strain for no weak zone case in which around the tunnel boundary and the springlines of the tunnel, there is the occurrence of the deviatoric strain. The deviatoric strain developed around the tunnel boundary is due to the tunnel-soil boundary effect.

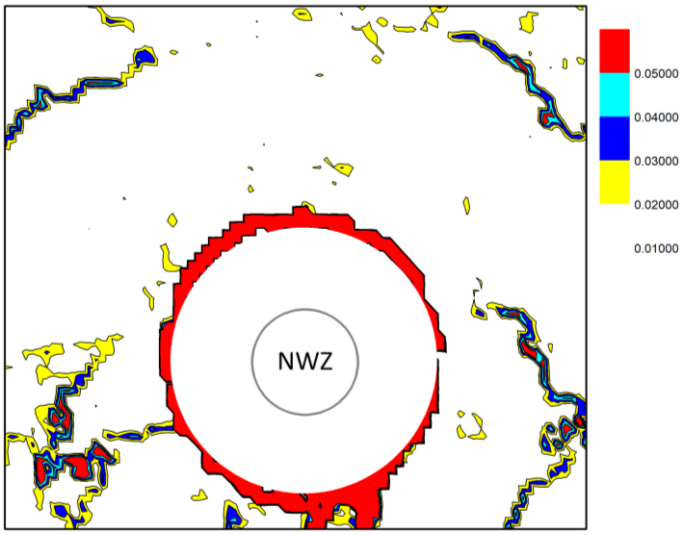

Figure 5-9. deviatoric strain for no weak zone and overburden height 1D

The effect of weak zone size has been checked after placing it on tunnel crown, shoulder, and springline position. For overburden height 1D the void ratio of 0.45 has been explored however, for overburden height 2D void ratios of 0.30, 0.45, and 0.60 have been examined. Figure 5-10 shows the results of weak zone size for overburden height 1D. They indicate that due to the presence of the weak zone deviatoric strain accumulates around the weak zone boundary. As the size of the weak zone was increased the deviatoric strain becomes higher. For three cases of the weak zone position i.e., crown, shoulder, and the springline position higher size of the weak zone yielded the deviatoric strain over the larger ground around the tunnel. This larger development of the deviatoric strain is associated with the shear strength loosening due to the removal of a greater number of particles.

The effect of weak zone size for overburden height 2D has been illustrated for void ratios 0.30, 0.45, and 0.60. Figure 5-11 shows the effect of size when the weak zone was placed at the crown position. It can be seen that for the void ratio of 0.30 as the size of the weak zone increases

the deviatoric strain increases. This increase in the deviatoric strain is due to more ground loosening due to the formation of the weak zone. As the void ratio of the weak zone increases from 0.30 to 0.60, the development of the deviatoric strain also increases with the maximum for the void ratio of 0.60. As the size of the weak zone increases the spread of the deviatoric strain increases over a larger area around the weak zone. As compared to the shallow overburden height (1D) the deviatoric strains for higher overburden pressure (2D) become higher.

When the weak zone was placed at the shoulder position the results are presented in Figure 5-12. Due to the weak zone at the shoulder position, a localized accumulation of the deviatoric strain has been observed and the size of the weak zone was increased the deviatoric strain distribution becomes higher. This increase in the ground strain is due to the ground loosening that happened by the more ground removal. The maximum change has been seen for higher size with the void ratio of 0.60 as in this case the maximum loosening has happened. The obtained results of deviatoric strain are the function of the weak size as well as its void ratio. At a small void ratio, the increase in weak size intensifies the development of the deviatoric strain and a similar happens with the weak zone with higher void ratios. These obtained results are in perfect agreement with those obtained through simulations as documented in the literature.

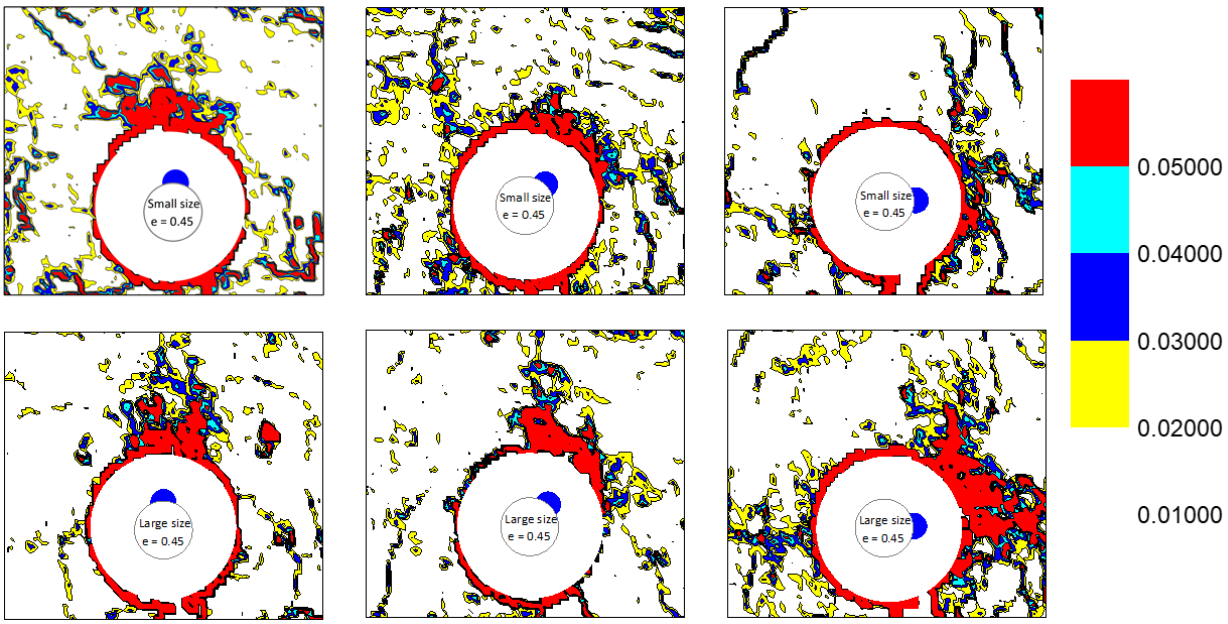

Figure 5-10. Effect of weak zone size on the distribution of deviatoric strain for a weak zone at different locations under overburden height 1D

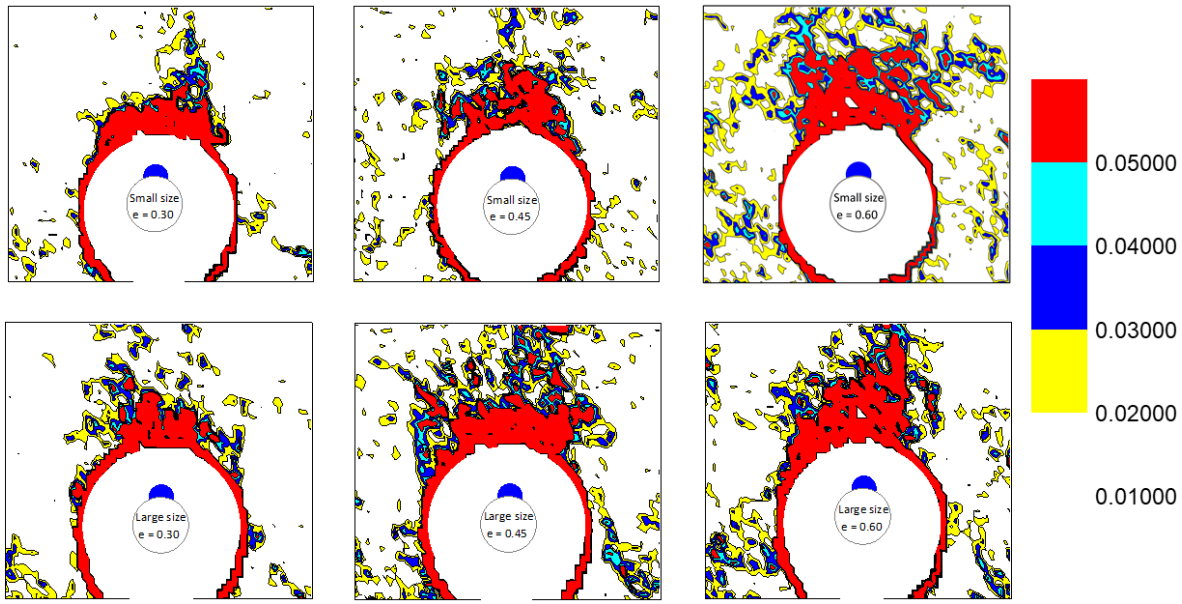

Figure 5-11. Effect of weak zone size on the distribution of deviatoric strain for different values of the void ratio under overburden height 2D and weak zone at the crown

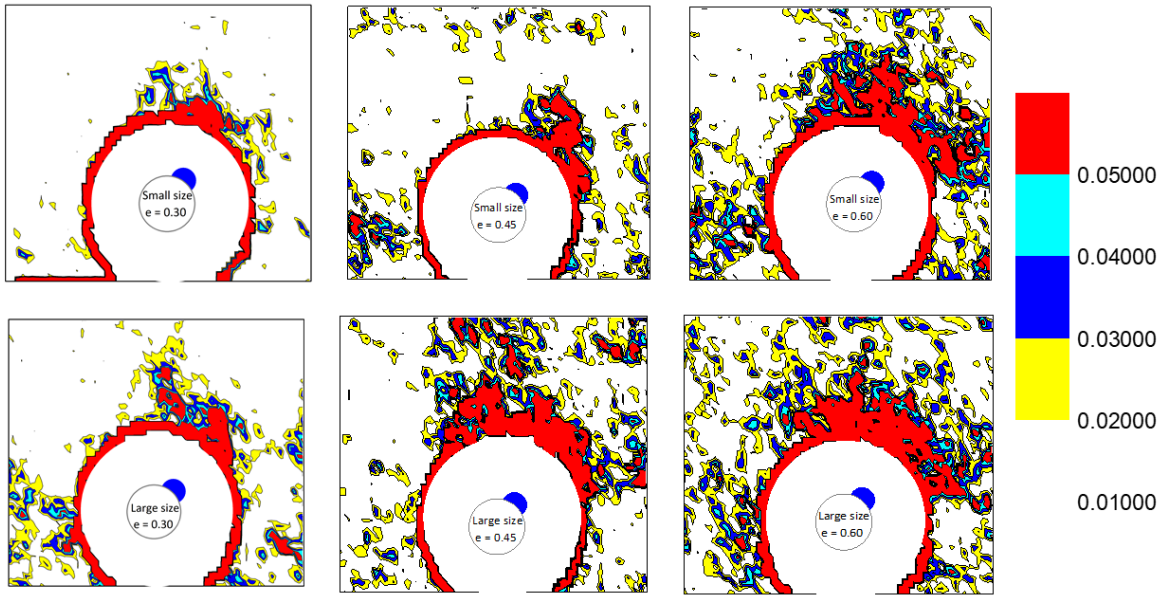

Figure 5-12. Effect of weak zone size on the distribution of deviatoric strain for different values of the void ratio under overburden height 2D and weak zone at shoulder

The results of deviatoric strain after placing the weak zone at the springline position have been presented in Figure 5-13. The plotted data showed that the behavior of the strain development is identical as of crown and shoulder cases i.e., with the increase of the weak zone size the deviatoric strain increases, and this phenomenon intensifies with the increase in the void ratio.

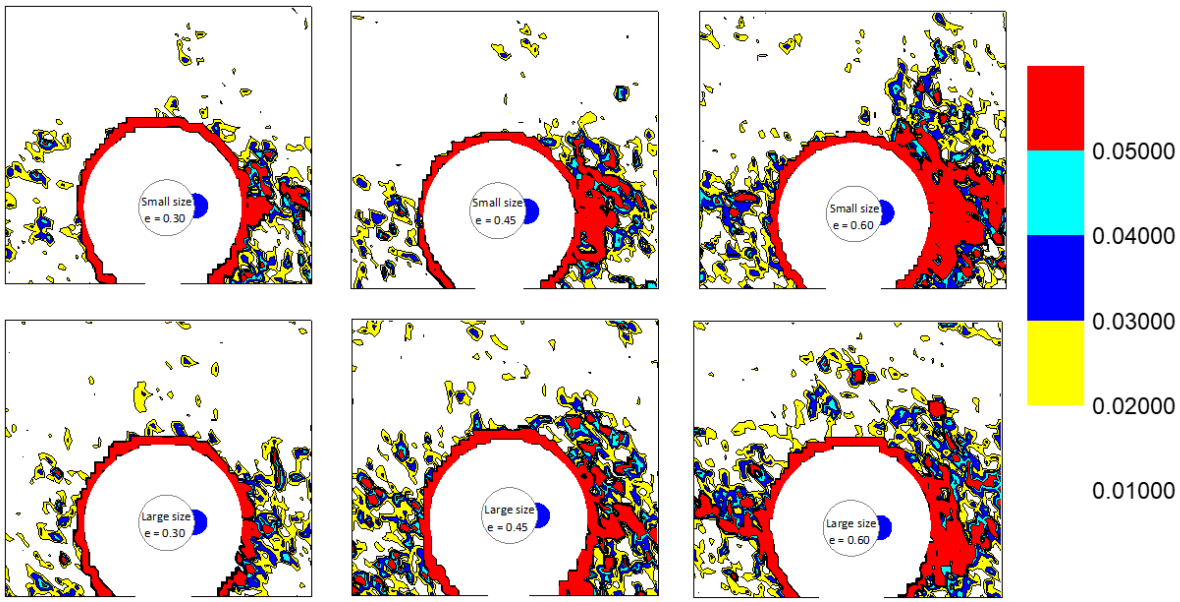

Figure 5-13. Effect of weak zone size on the distribution of deviatoric strain for different values of the void ratio under overburden height 2D and weak zone at springline

5.1.2 Tunnel response

The effect of the weak zone size has a significant effect on the internal strain of the tunnel. By increasing the size of the weak zone, the internal strain changed significantly.

5.1.2.1 Before shaking

The effect of weak zone size on the internal strain under static conditions and for overburden height 1D has illustrated in Figure 5-14. The plotted data shows that with the increase in the size the internal strain increases for the position of the weak zone at all points. The increase in internal strain is due to the availability of extra space.

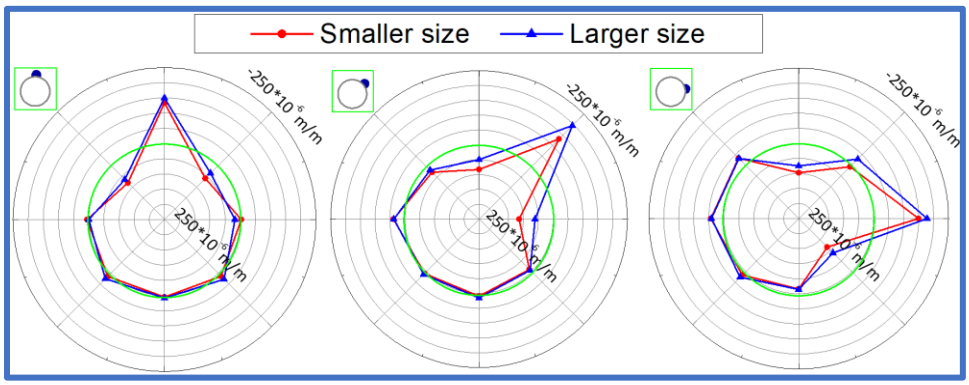

Figure 5-14. Effect of size of the weak zone on the static response of tunnel (overburden height = 1D & e = 0.45)

As the size of the weak zone was increased the more portion of the ground around the tunnel was loosened which will act as an extra space for the tunnel to bend in that direction. Therefore, for any specific position of the weak zone with the increase in size the localized strain was uplifted, and this phenomenon has been observed for all positions of the weak zone. As the plotted values are the incremental values over the ground strain, that is why only the position of the weak zone shows a substantial change in the strain and other points don't exhibit any appreciable changes in the internal strain. Here in this section, for overburden height of 1D only one value of the void ratio i.e., 0.45 has been explored and for this void ratio, the size of the weak zone was checked after placing it at the crown, shoulder, and springline positions.

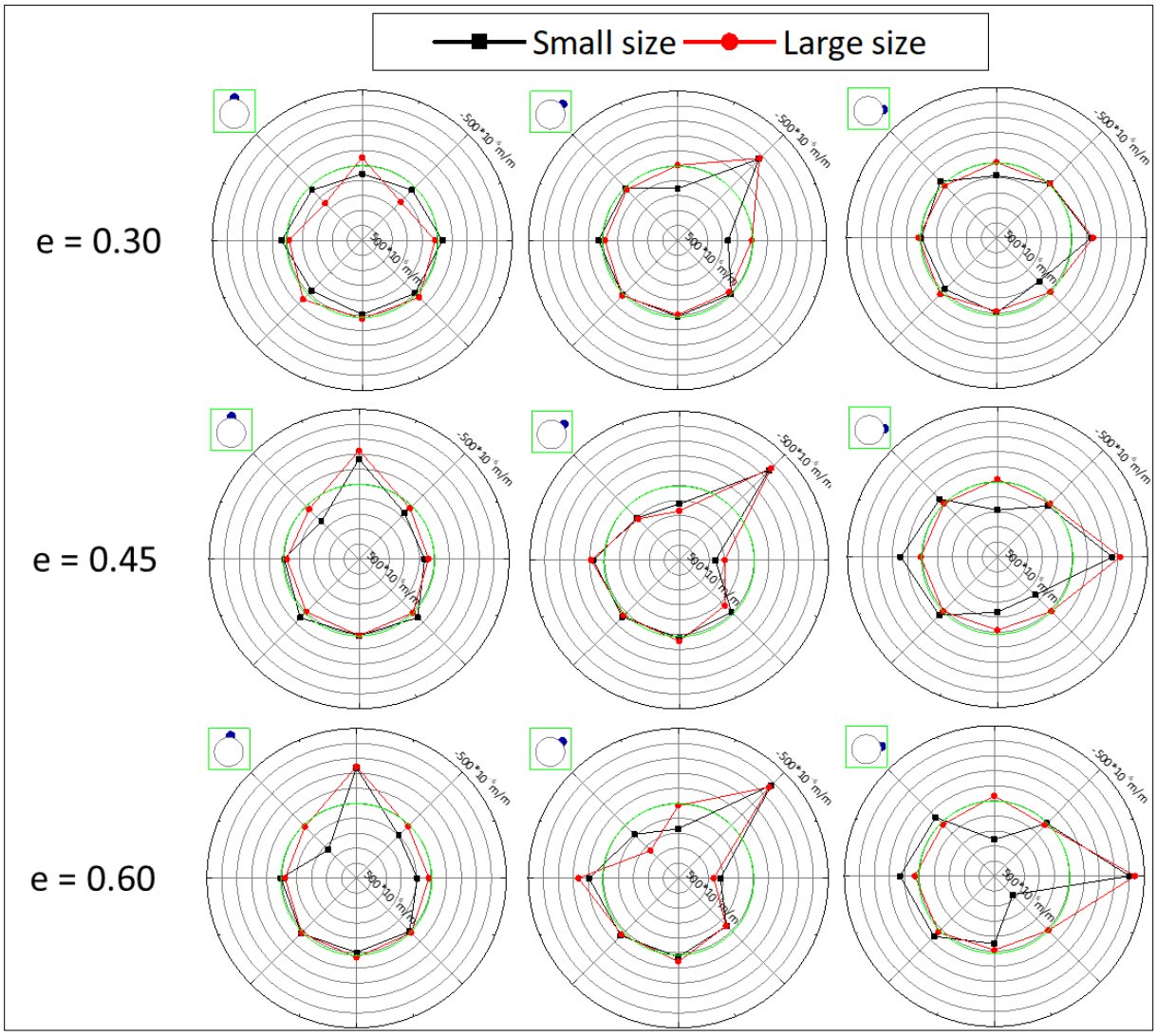

Figure 5-15. Effect of size of the weak zone on the static response of tunnel for different values of the void ratios (overburden height = 1D)

For overburden height of 2D, the effect of size of the weak zone has been investigated for three different values of the void ratios i.e., 0.30, 0.45, and 0.60 and the results have been presented in Figure 5-15. The first row shows the results of weak zone size for void ratio 0.30 and placing it at the crown, shoulder, and springline positions. Similarly, the 2nd and 3rd rows show the results for void ratios of 0.45 and 0.60 respectively. It can be seen that for a specific value of void ratio and position of the weak zone, as the size of the weak zone was increased there is an increase in internal strain was observed. It is also important to note that with the increase in the size of the weak zone the spread of change of internal strain also increases because the higher size of the weak zone occupies more area around the tunnel as compared to the smaller size. The effect of the size of the weak zone is very consistent because even by changing the stiffness of the ground the pattern of change in the values of the strain remains the same.

5.1.2.2 During shaking

The internal strain at maximum shear has been plotted in Figure 5-16. It shows that with the increase in the size of the weak zone the response of the tunnel changed significantly. For example, for the weak zone at the crown, the higher size weak zone will push the tunnel more on the right side as compared with the small size weak zone, as indicated by the blue line on the shoulder position. Moving the weak zone to the shoulder position, the tunnel shows outward bending at the crown location. Finally, for the springline case, the large size weak zones force the lining to the opposite side however, the change is relatively small.

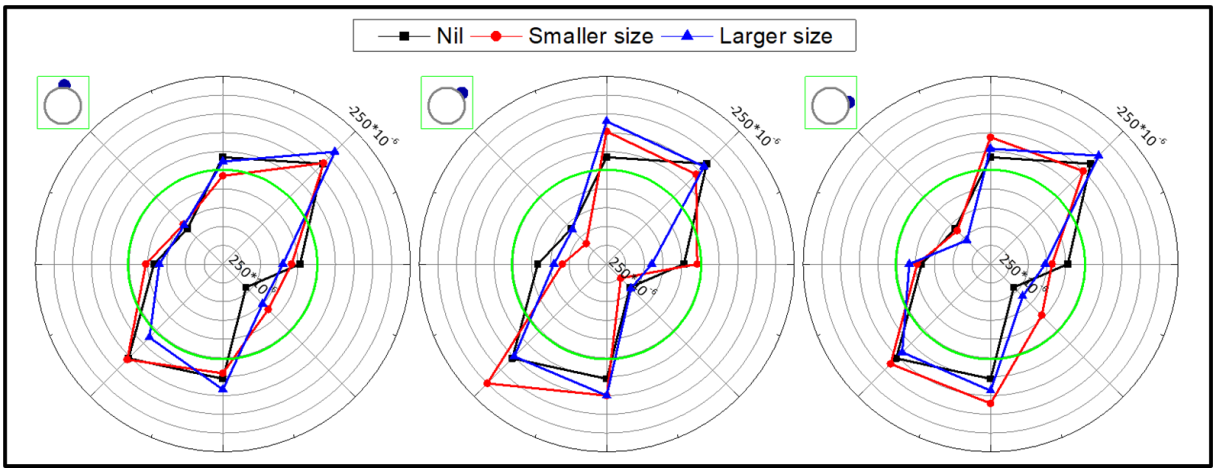

Figure 5-16. Effect of size of the weak zone on the response of tunnel at maximum shear displacement (overburden height = 1D & e = 0.45)

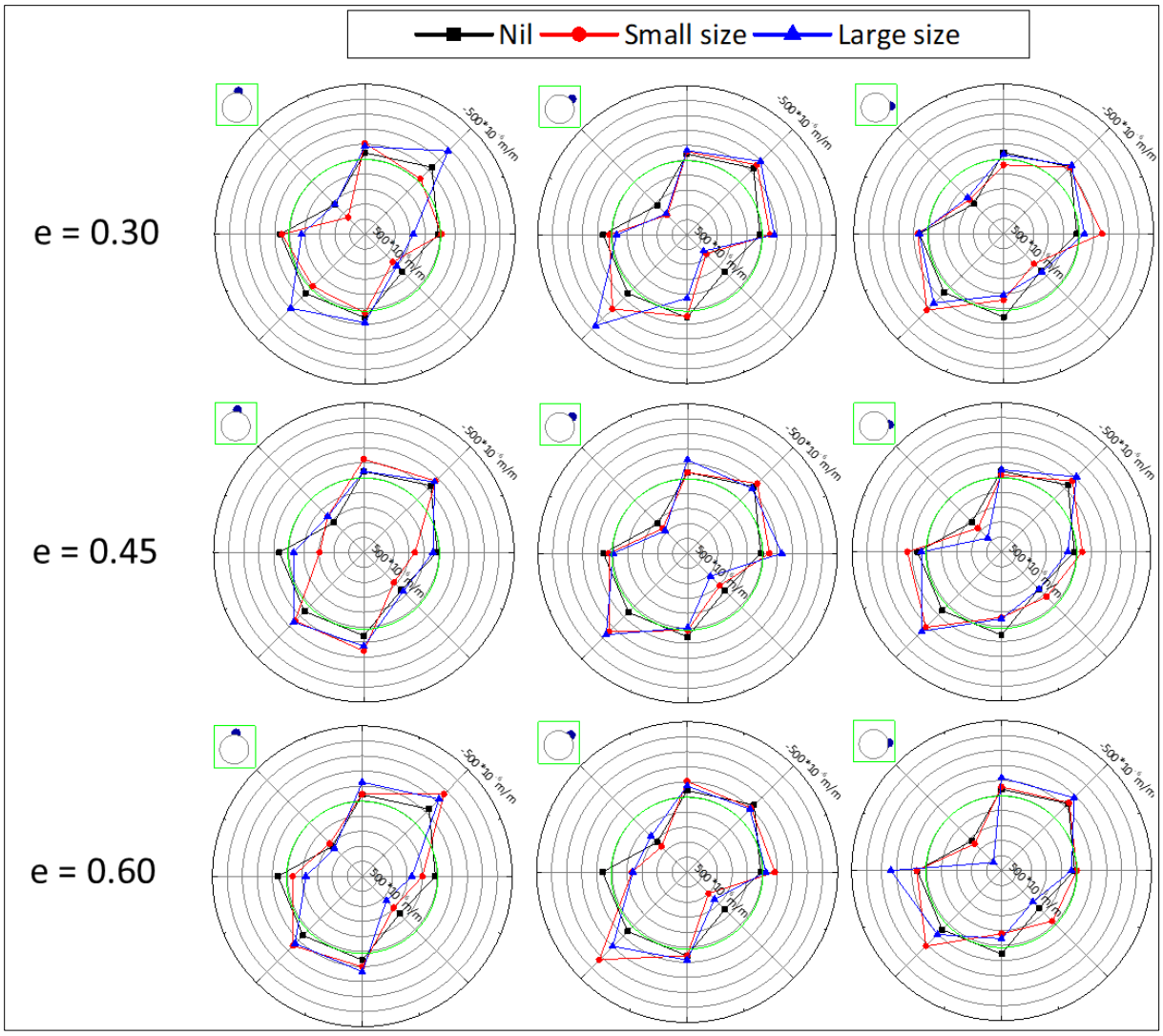

Figure 5-17. Effect of size of the weak zone on the response of tunnel at maximum shear displacement for different values of void ratio (overburden height = 2D)

For overburden height 2D the effect of weak zone size for three values of the void ratios i.e., 0.30, 0.45, and 0.60 has been illustrated in Figure 5-17. The effect of size has been explored after placing the weak zone at the crown, shoulder, and springline locations. When the weak zone was placed at the crown position and for the void ratio of 0.30, when the size of the weak zone has increased the tunnel bending along the diagonal axis as the strain at the right shoulder becomes higher as compared to the smaller size weak zone. When the void ratio was increased to 0.45 shows more bending at the crown position due to the higher ground pressure exerted by the soil moving towards the weak zone position. Finally, the weak zone with a void ratio of 0.60, shows more inward bending of the tunnel at the right knee location due to more pressure from the top.

Moving the weak zone at the shoulder position and creating a weak zone with a void ratio of 0.30 shows that the tunnel bends more along the diagonal axis on the left side. The reason is the ground moving towards the right shoulder where the weak zone was positioned. By increasing the size of the weak zone, the bending was noted to increase further. When the void ratio was increased to 0.45 and the size was increased there is upward bulging as been observed at the crown position. This upward bulging can be attributed to the higher soil pressure coming along the diagonal axis in the case of the higher size of the weak zone. The tunnel response accompanying the weak zone with a void ratio of 0.60 shows different behavior in which the tunnel shows more ovalisation in the case of a small size weak zone. This may be due to the reason that while preparing the weak zone the stiffness and size were slightly disturbed.

When a weak zone having a void ratio of 0.30, was located at the springline position and its size was varied it shows that the more soil moving towards the weak zone location push the tunnel in the horizontal direction. Due to this pushing force as a reaction, the tunnel bends from the upper left side. Increasing the void ratio of the weak zone to 0.45 and 0.60, a similar trend was observed in which the more ground moving towards the weak zone in case of higher size weak zone force the tunnel more at the springline location. As mentioned earlier due to rection the ground on the left upside forces the tunnel bending.

5.2 Stiffness of Weak Zone

Stiffness is an important property of soil that affects the mechanical and strength properties. The stiffness is usually measured in terms of the elastic modulus of the ground. However, the void ratio of the soil also affects the elastic properties of the soil.

5.2.1 Ground response

5.2.1.1 Shear displacement

The shear displacement measured at the springline height was converted to shear strain by dividing them by the vertical height as shown in Figure 5-18. The plotted values indicate that as the stiffness of the ground decreases (i.e., the void ratio increases) the shear strain of the ground increases. This increase is due to the loss of ground shear strength as a result of weakening in the soil. Moreover, the springline position shows a higher shear strain as compared to the shoulder and the crown position.

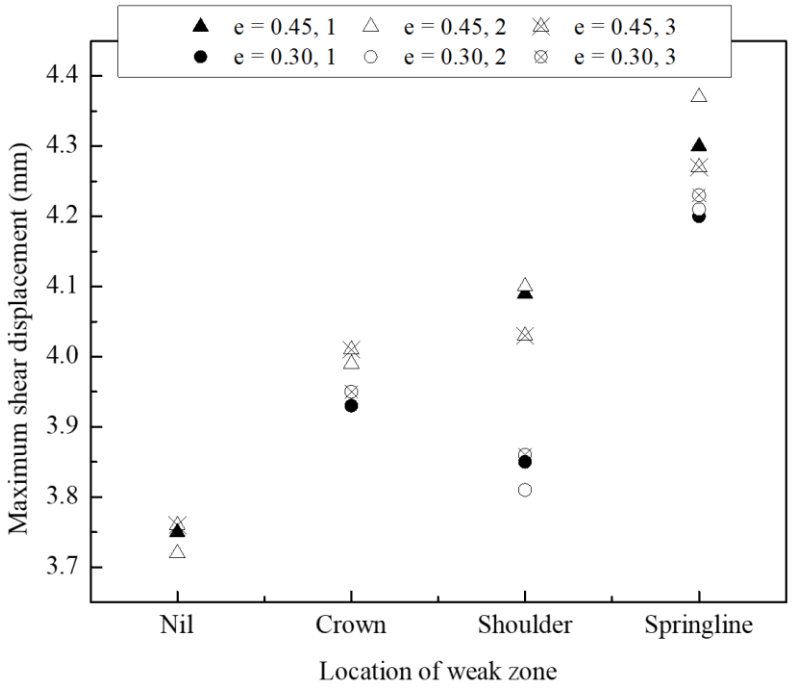

Figure 5-18. Effect of void ratio of the weak zone on the shear displacement of the ground (Overburden height = 1D and $\theta = 51°$)

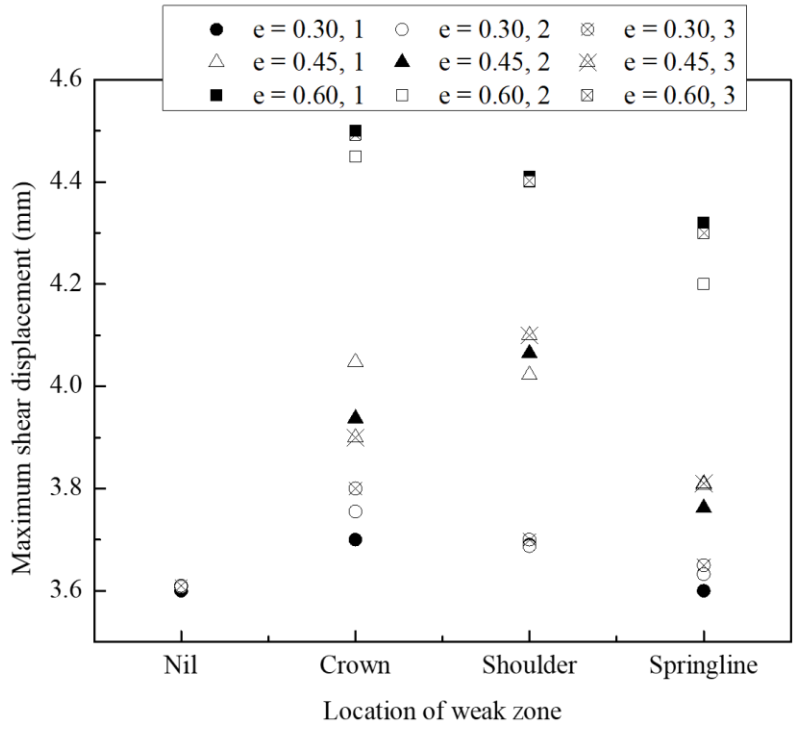

Figure 5-19. Effect of void ratio of the weak zone on the shear displacement of the ground (Overburden height = 2D and θ= 51°)

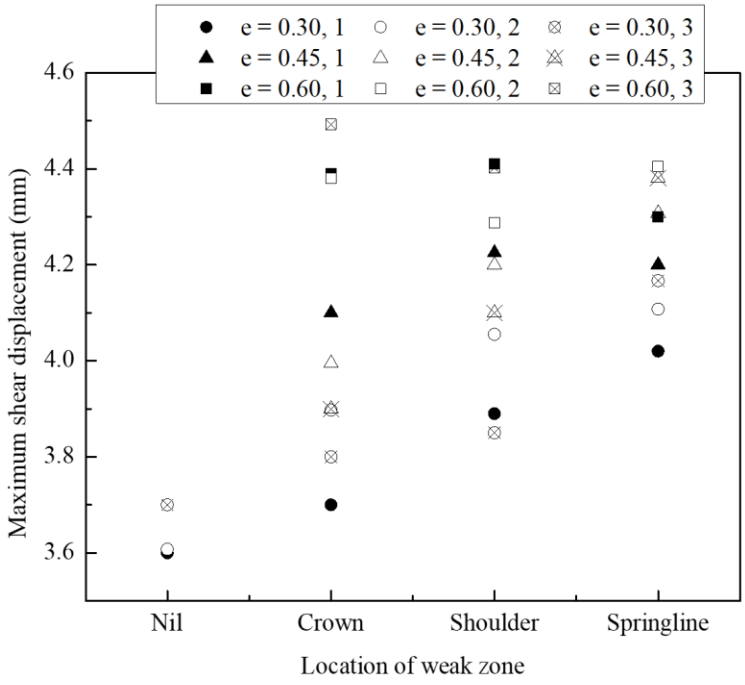

Figure 5-20. Effect of void ratio of the weak zone on the shear displacement of the ground (Overburden height = 2D and θ= 90°)

5.2.1.2 Ground response in terms of volumetric strain

The ground response for different void ratios at different overburden heights has been discussed here. For overburden height, 1 D, two values of the void ratios i.e., 0.30 and 0.45 have been compared. The plotted data indicate that the 0.45 void ratio yields more volumetric strain as compared to the 0.30 value for weak zones at different positions around the tunnel. The higher volumetric strain in the case of void ratio 0.45 is that the ground with a higher void ratio is softer than the ground with a void ratio of 0.30. It is worthy to note that with the increase in void ratio the volumetric strain increase, however, the affected area around the tunnel (spread of the volumetric strain) is almost the same. The percentage area under compression and expansion is summed up and shown in Figure 5-22. The summary of volumetric strain shown in Figure 5-22 reveals that for each location of the weak zone the softer ground imposes higher volumetric strain.

For overburden height 2D the volumetric strain has been plotted for two different sizes. Figure 5-23 shows the effect for size in which the internal angle was 51° while Figure 5-24 represents the results of size with an internal angle of 90°. Within one size of the weak

zone, three void ratios i.e., 0.30, 0.45, and 0.60 have been explored after placing them at the crown, shoulder, and springline locations.

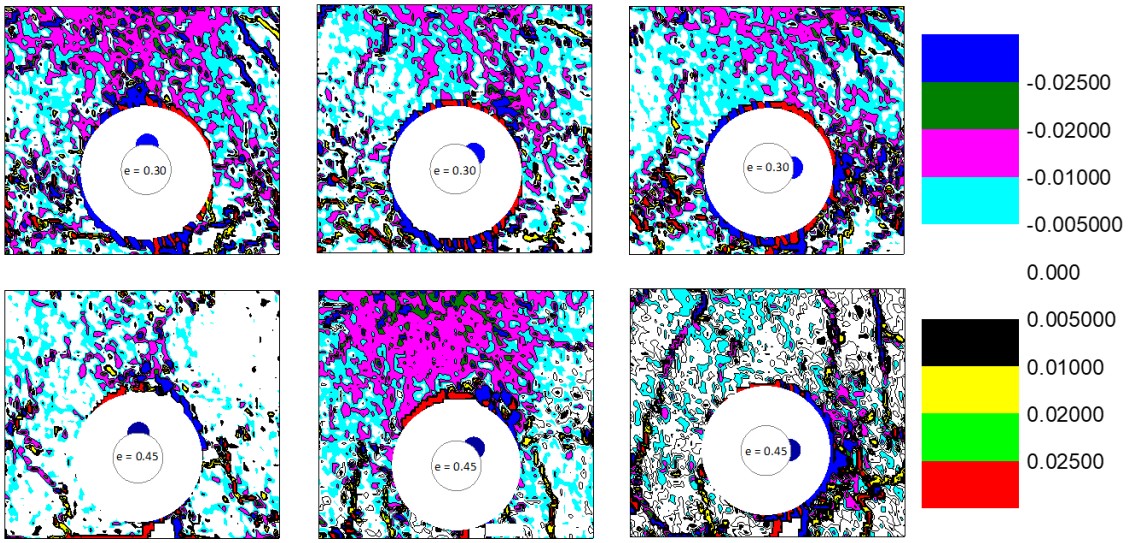

Figure 5-21. Effect of stiffness on volumetric strain distribution at maximum shear displacement (Overburden height 1 D)

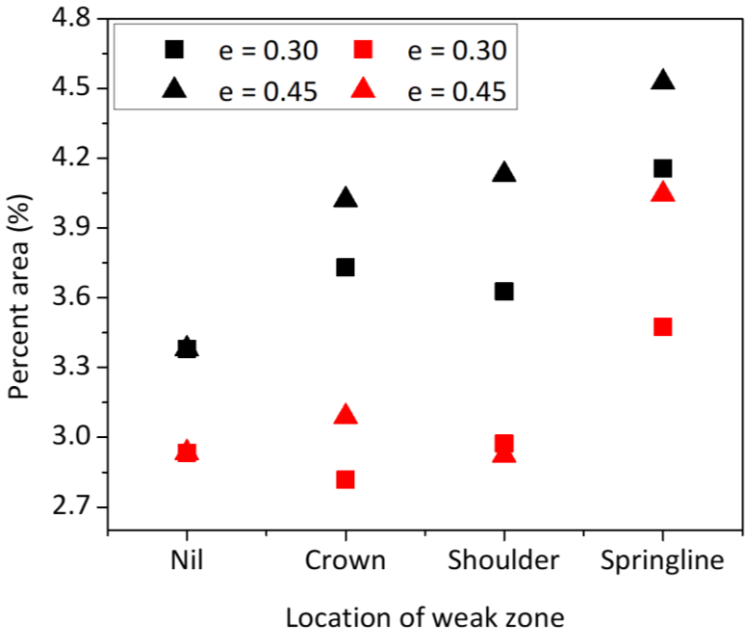

Figure 5-22. Summary of volumetric strain for different stiffness of the weak zone (overburden height 1 D)

For weak zone with an internal angle of 51°, the effect of stiffness on the volumetric strain has shown in Figure 5-23. The plotted data represents that when the weak zone at the

crown position, as the void ratio of the weak zone was increased from 0.30 to 0.60, the volumetric strain increases. This increase in ground response is associated with the reduced shear strength of the ground and will exert more stresses on the lining structure. Moving the weak zone to the shoulder position and increasing the void ratio resulted in higher volumetric strain. It is important to note that when the void ratio increased from 0.45 to 0.60, the increase in the volumetric strain is higher as compared to the increase in volumetric strain when increased from 0.30 to 0.45. Finally, the weak zone at the springline position yielded the localized volumetric strain around the springline position which increased further with the increase in the void ratio of the weak zone.

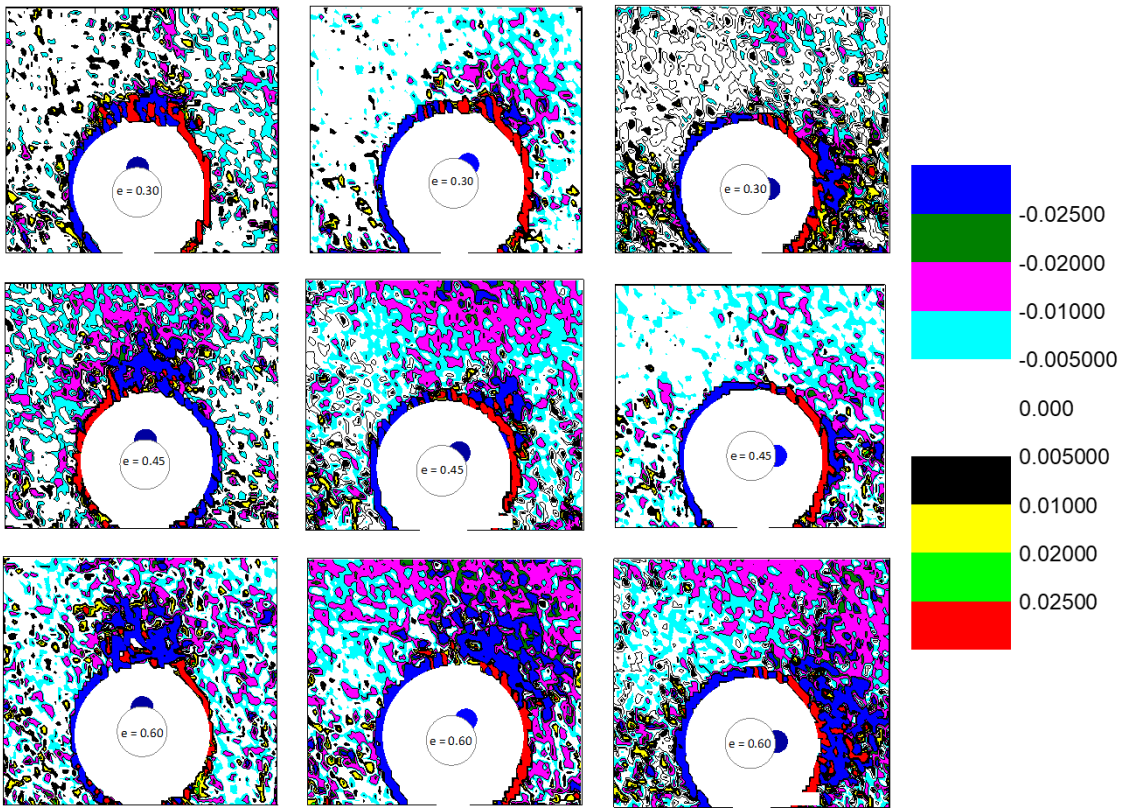

Figure 5-23. Effect of stiffness of weak zone on volumetric strain distribution for overburden height 2D and $\theta = 51°$

Figure 5-24 represents the effect of weak zone stiffness on the volumetric strain in the groundmass for the weak zone with an internal angle of $90°$. The results indicate that for the weak zone at a specific location and the void ratio was increased, the outcomes of the volumetric strain increase. The effect of stiffness on the volumetric strain for large size weak size is similar to the

small size however, the spread of the volumetric strain is higher in the case of the larger size weak zone. The increase in the volumetric strain due to the increase in the void ratio is due to ground weakening occurred by the removal of the ground particle. In the case of larger weak zone size, the reason for the more spread is that as the size is larger covers more area around the tunnel that's why the spread of the volumetric strain is higher.

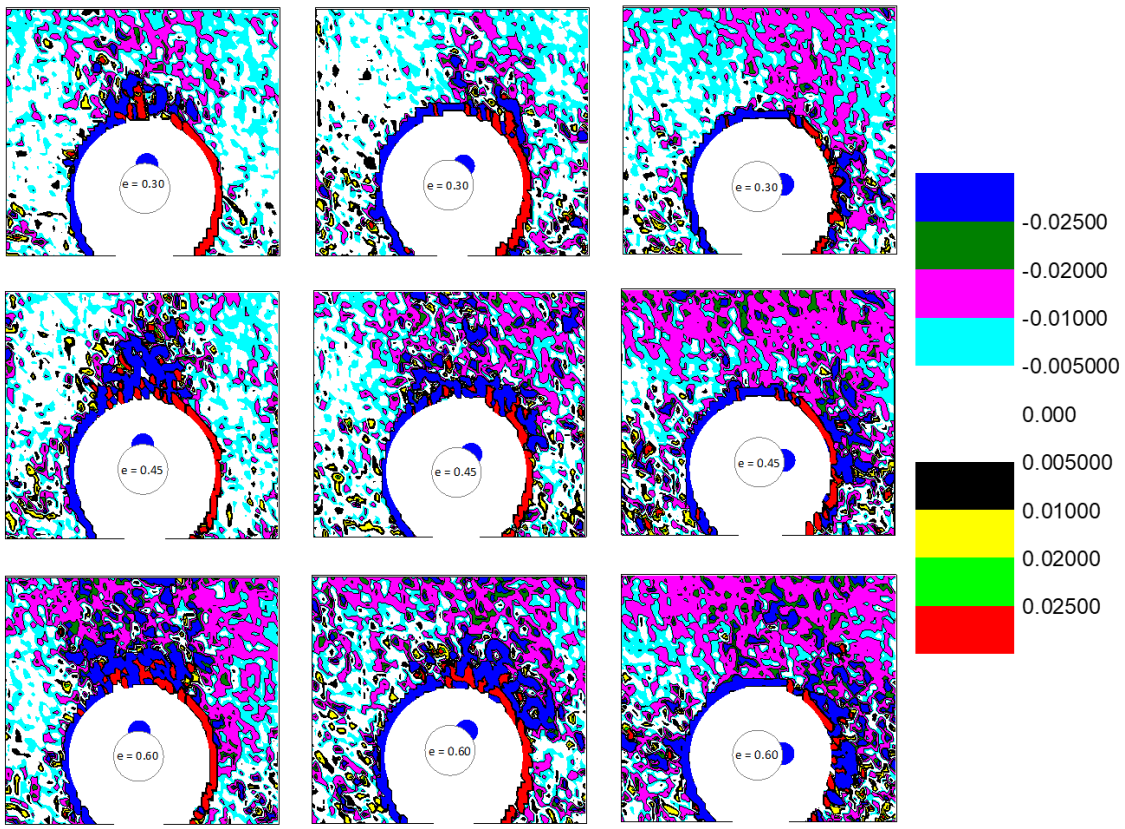

Figure 5-24. Effect of stiffness of weak zone on volumetric strain distribution for overburden height 2D and $\theta = 90°$

5.2.1.3 Ground response in terms of deviatoric strain

This section will explain the effect of weak zone stiffness on the deviatoric strain for overburden heights of 1D and 2D. Figure 5-25 illustrates the effect of stiffness on the deviatoric strain for overburden height of 1D and here two void ratios of 0.30 and 0.45 have been explored. When the weak zone was placed at the crown position and the void ratio was increased the deviatoric strain intensified. This intensification of the deviatoric strain is due to ground loosening that happened while making the weak zone. Placing the weak zone at the shoulder position and increasing the void ratio increased the localized deviatoric strain around the shoulder location.

Similarly, the weak zone at the springline position yielded the deviatoric strain at the springline location which intensifies with the higher void ratio.

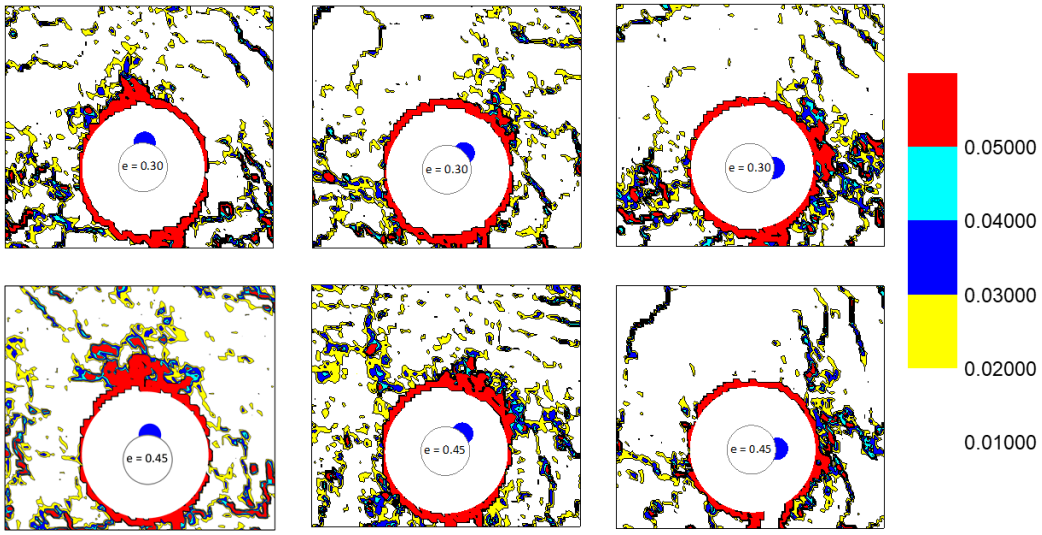

Figure 5-25. Effect of stiffness of weak zone on deviatoric strain distribution for overburden height 1D and θ=51°

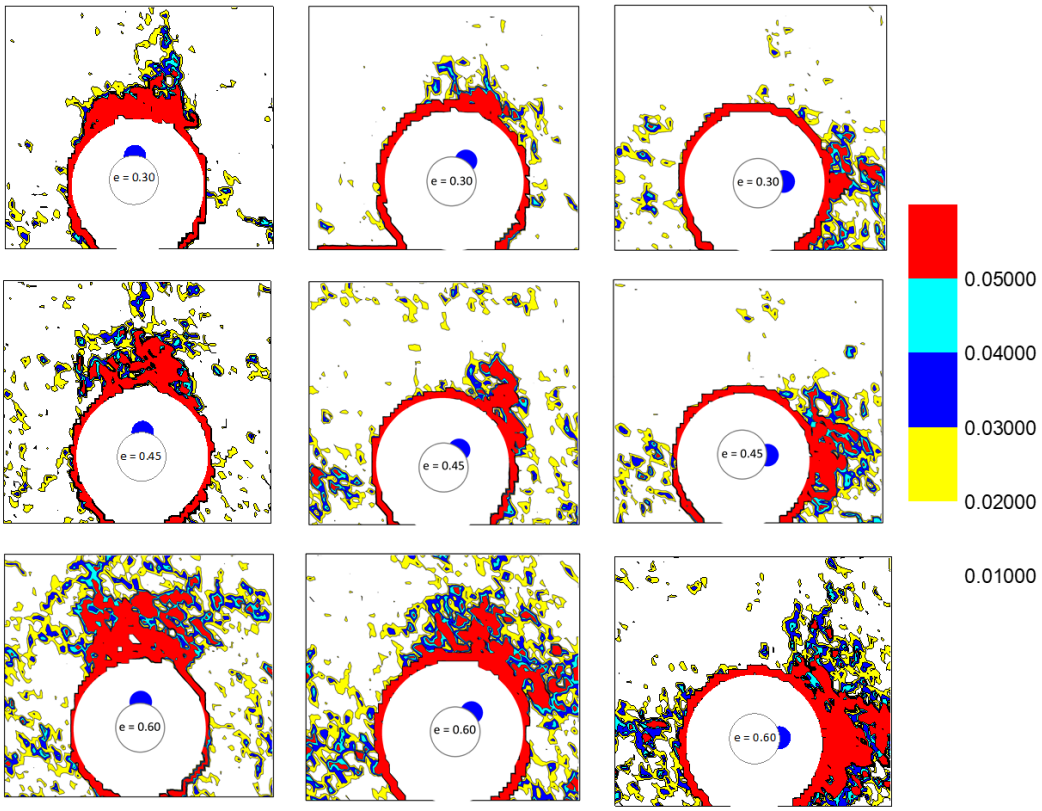

Figure 5-26. Effect of stiffness of weak zone on deviatoric strain distribution for overburden height 2D and $\theta = 51°$

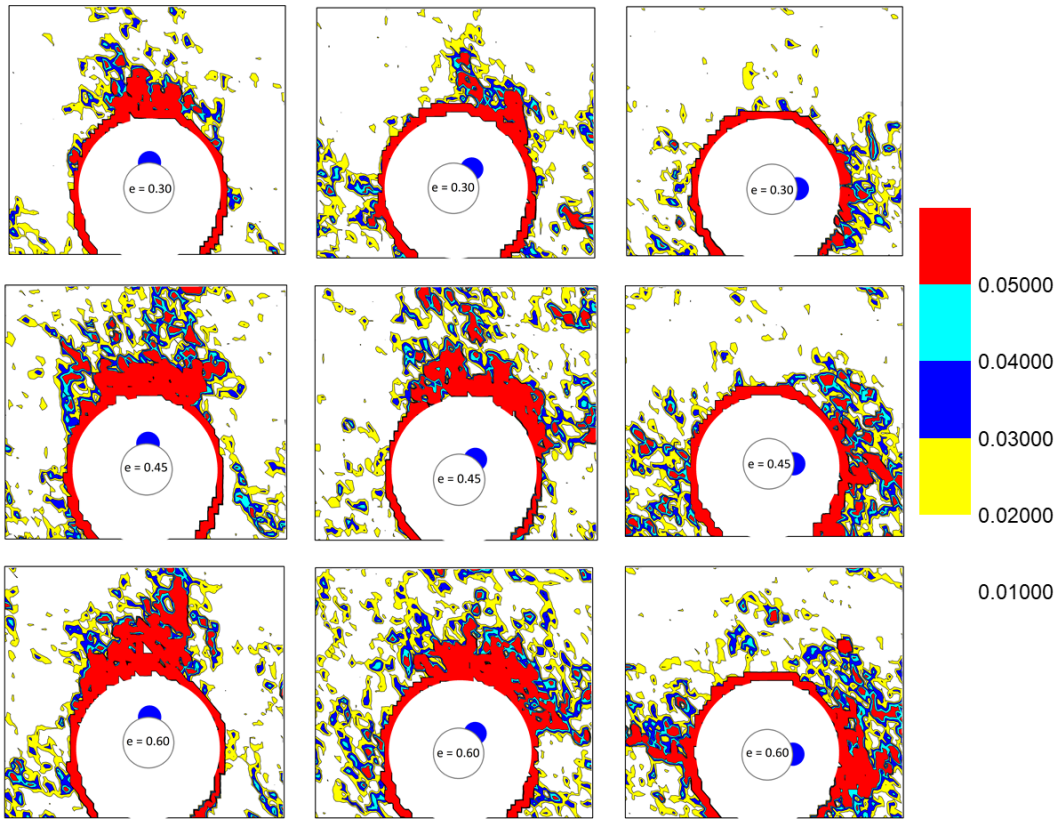

Figure 5-27. Effect of stiffness of weak zone on deviatoric strain distribution for overburden height 2D and $\theta = 90°$

The deviatoric strain for overburden height 2D has been plotted for two different sizes of the weak zones. Figure 5-26 shows the results of the deviatoric strain for different values of the void ratio for the smaller size of the weak zone. It can be seen that with the increase in the void ratio the deviatoric strain increases. This increase is attributed to the loss in ground shear strength resulted from the ground loosening. Similarly, for the higher size of the weak zone the localized deviatoric strain increase with the reduction in the ground stiffness as shown in Figure 5-27. By comparing the results of the small overburden height with higher overburden height it was found that the case of high overburden height yielded higher deviatoric strain in the groundmass.

5.2.2 Tunnel response

5.2.2.1 Before shaking

This section will discuss the effect of the void ratio on the tunnel response before the shaking begins. Figure 5-28 shows the effect of the void ratio on the tunnel response for overburden height 1D.

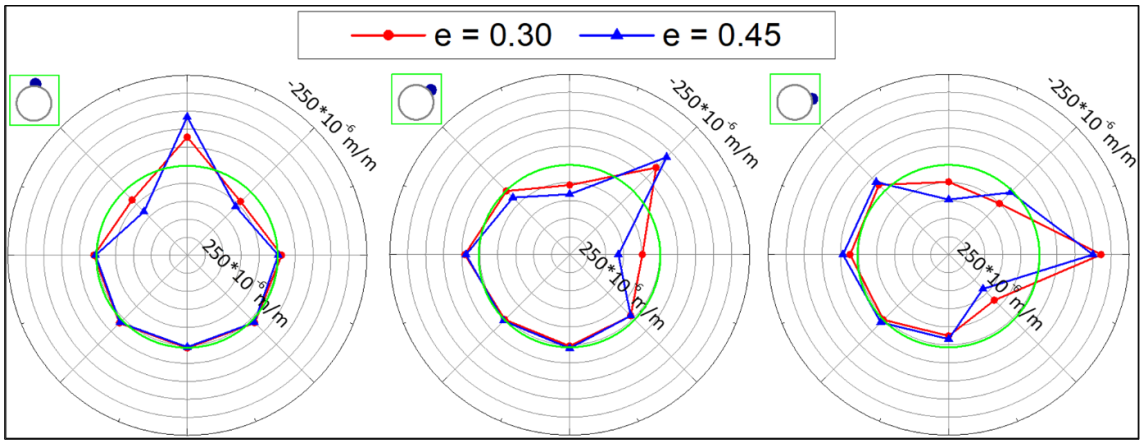

Figure 5-28. Effect of stiffness of the weak zone on the static response of tunnel (overburden height = 1D)

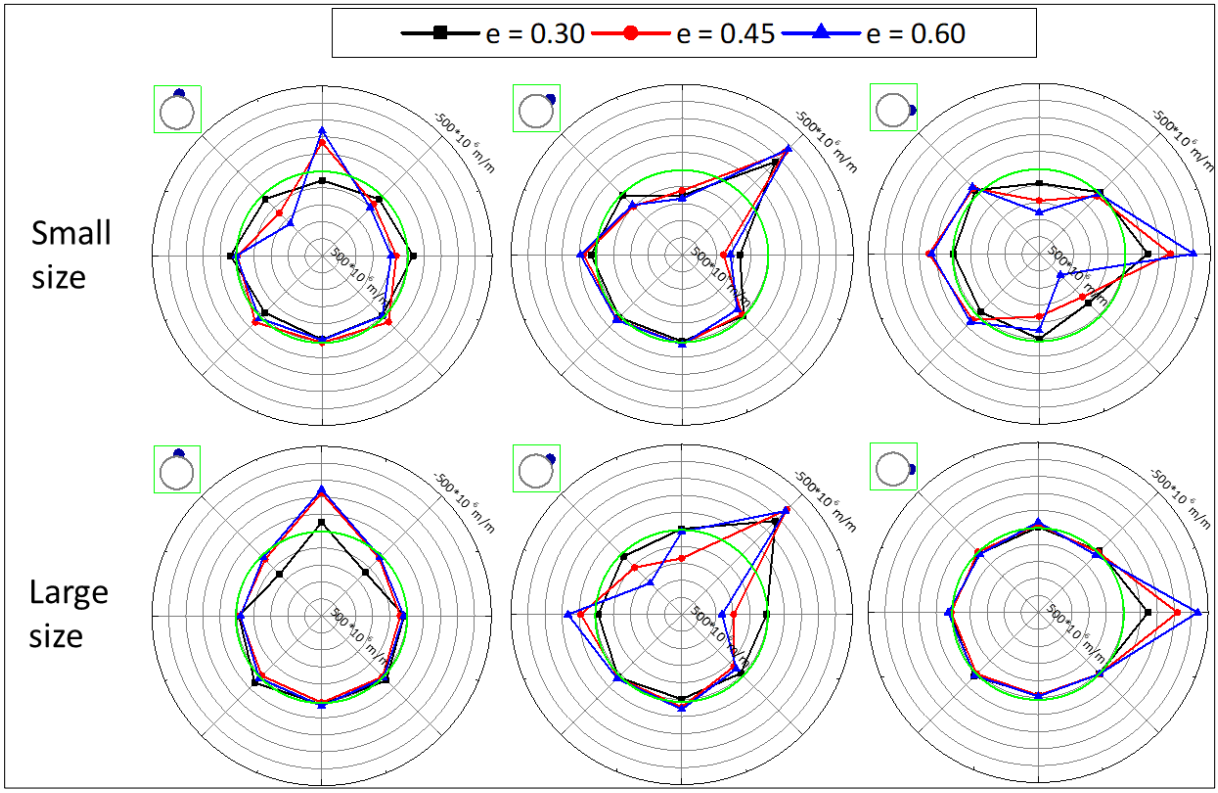

Figure 5-29. Effect of stiffness of the weak zone on the static response of tunnel for small and large size of the weak zone (overburden height = 2D)

The plotted data shows that if the size of the weak zone remains the same and the void ratio is increased the tunnel response changes. When the weak zone was placed at the crown position and the void ratio was increased from 0.30 to 0.45 the localized internal strain increased due to more ground loosening. As the size of the weak zone was the same therefore the changes at the

other points around the tunnel are not so significant. Moving the weak zone to the shoulder location shows that with the increase of void ratio the strain at the shoulder position increased. It is important to mention that as the tunnel tries to bend towards the weak zone, the points very next to the weak zone on either side show reduction in an internal strain which means the point of weak zone location bending more inside as compared to the case of lesser void ratio. The creation of the weak zone at the springline of the tunnel shows that the weak zone with a higher void ratio caused more outward bending at the springline position and inward at the neighboring position.

Figure 5-29 illustrates the results showing the effect of void ratio on the tunnel response for overburden height 2D. In the case of higher overburden height, three values of the void ratios i.e.,0.30, 0.45, and 0.60 have been explored. Along with the void ratios the two sizes have been also examined and will be discussed here. It is evident that for the small size of the weak zone and position at the tunnel crown, with the increase in the void ratio the internal strain increased at the location of the weak zone. This increase in the tunnel response is due to the ground weakening caused by the removal of more particles in case of higher void ratios. Moving the weak zone to the shoulder and the springline positions have shown similar results as in the case of the weak zone at the crown position. It is surprising to note that the void ratio of the weak zone and the tunnel response are in perfect alignment with each other.

5.2.2.2 During shaking

The effect of weak zone stiffness under the seismic conditions for overburden height 1D and 2D will be discussed here. Figure 5-30 shows the results for overburden height 1D in which the effect of two void ratios i.e., 0.30 and 0.45 has been checked. The plots show that when the weak zone was placed at the tunnel crown the softer ground will deflect the tunnel more downward at the crown position as compared to the stiffer ground which is highlighted by the downward bending of the tunnel at the crown position. The introduction of a weak zone at the shoulder position forces the tunnel to deflect at the crown is almost the same because the size of the weak zone is the same, however, the softer ground will deflect the tunnel more along the diagonal axis which is due to the pressure exerted by the more ground moving towards the shoulder position. For the springline case, the internal strain shows that for stiffer soil due to more ground coming towards the weaker zone the tunnel tries to bulge from the crown position and this bulging of the tunnel is higher than softer soil.

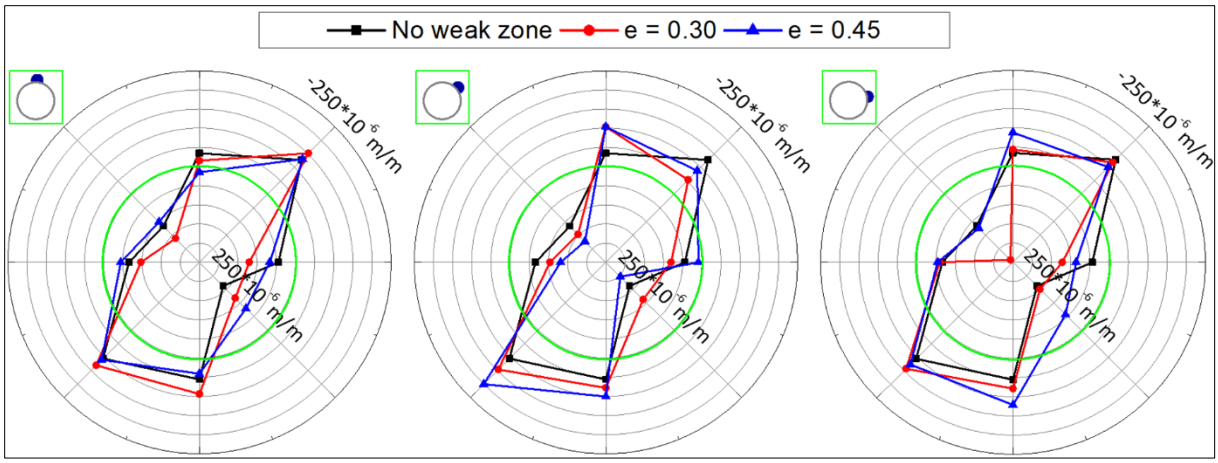

Figure 5-30. Effect of stiffness of the weak zone on the response of tunnel at maximum shear displacement (overburden height = 1D)

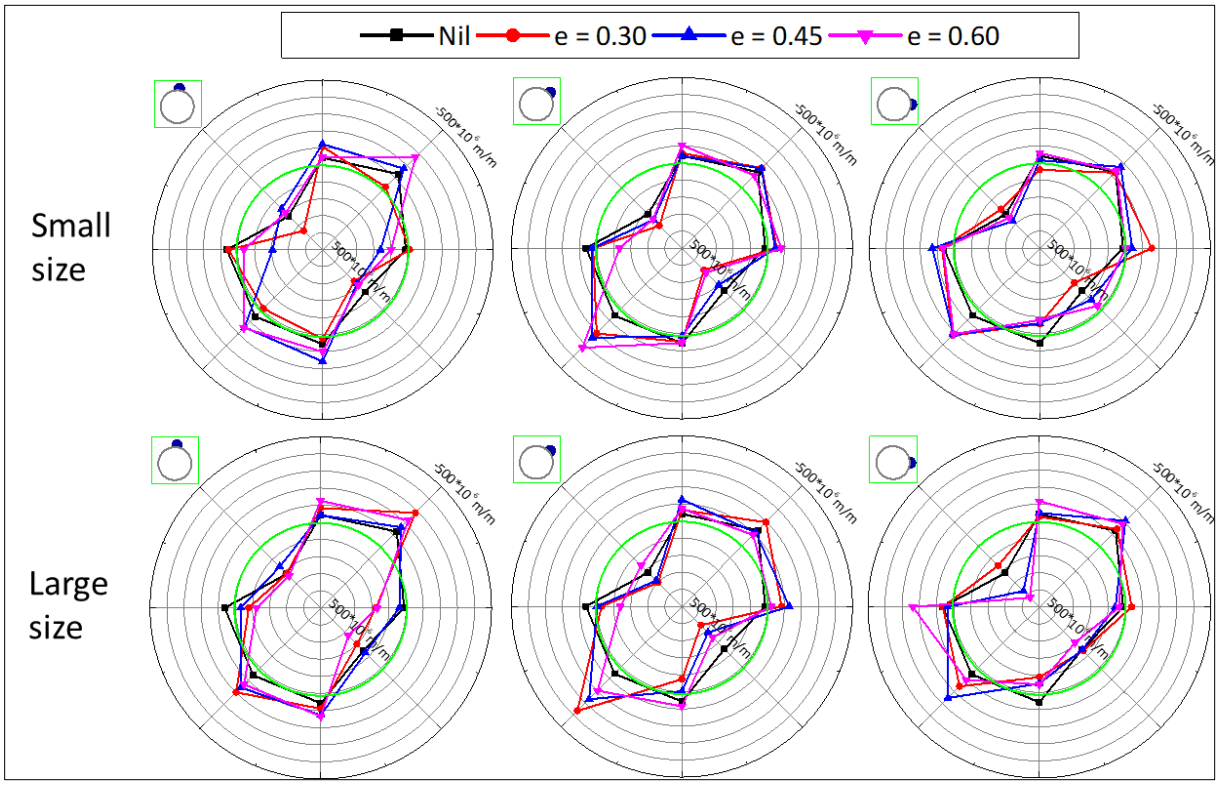

Figure 5-31. Effect of stiffness of the weak zone on the response of tunnel at maximum shear displacement for different sizes of the weak zone (overburden height = 2D)

The effect of ground stiffness on the tunnel response for overburden height has been shown in Figure 5-31. For higher overburden height effect of three void ratios along with the two sizes has been explored and results have been presented here. For the small size of the weak zone when it was located at the crown position with the increase in the void ratio of the weak zone the internal

strain changes around the tunnel. The maximum change was recorded at the shoulder position where the tunnel bends more for higher void ratios. The higher bending of the tunnel can be explained by considering the ground movement which is in the downward direction and along with the shaking, it will force the tunnel to bend along the diagonal axis. In the case of the weak zones with a higher void ratio more ground is moving because when the arching effect finishes the ground collapse and moves towards the weaker part. Moving the weak zone to the shoulder position the higher void ratio bends the lining more as depicted at the left knee position. Similarly, when the weak zone was created at the springline position the more ground moving towards the cavity has caused the higher bending of the tunnel at the springline position.

By increasing the size of the weak zone, the effect of the void ratio was again explored. It can be seen that with the increase in the size of the weak zone the overall trend of the tunnel bending remains the same however, the effect has been multiplied. For example, for the weak zone at the crown position, with the increase in the void ratio, the tunnel bending at the shoulder position has significantly increased. Similarly, when the weak zone was located at the shoulder and the springline positions and the void ratio of the weak zone were raised it shows bending at the left knee and the left shoulder but with higher magnitude. In conclusion, the effect of the void ratio is somewhat similar to the size but in the latter case, more points show changes in the tunnel response.

5.3 Conclusions

The effect of the size of the weak zone and stiffness has been explored in this chapter. Two sizes of the weak zone for two different overburden heights have been investigated. To explore the effect of the stiffness of the weak zone, for overburden height 1D two values of the void ratios 0.30 and 0.45 have been compared however, for overburden height 2D three values of the void ratios i.e., 0.30, 0.45, and 0.60 have been checked. The results have been presented in the form of ground response and tunnel response. From the presented data the following conclusions have been drawn.

- Shear displacement measured for larger and softer weak zones are higher than the smaller and stiffer size which is due to more ground weakening. Due to round loosening, the ground has lost some fraction of the shear strength, and the shear displacement was found to be increased. With the increase in the size of the weak zone, the shear displacement increased.

A similar trend has been observed with the increase in the values of the void ratio of the weak zone.

- The volumetric and deviatoric strains are higher in the case of large weak zones which caused more stresses to the lining. Similarly weak zones with a higher void ratio yielded more strains in the ground. By increasing the size of the weak zone along with the values of the ground strains the affected area around the weak zone also has increased in contrast to the increase in void ratio in which only values were increased but the affected area remains the same. Moreover, higher overburden height yields higher volumetric strains in the surrounding ground.
- The tunnel response measured through internal strains shows that by increasing the size and void ratio of the weak zone the tunnel response increased. Before shaking the maximum was observed when the weak zone was placed at the shoulder position as shown in Figure 5-32. During shaking the maximum response was noted at the crown position when the weak zone was positioned at the shoulder position as illustrated in Figure 5-33.

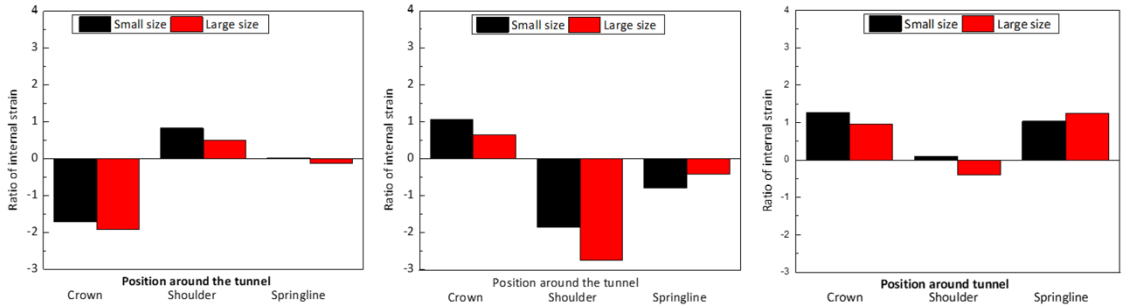

Figure 5-32. The incremental ratio of internal strain w.r.t. no weak zone to check the effect of size before shaking

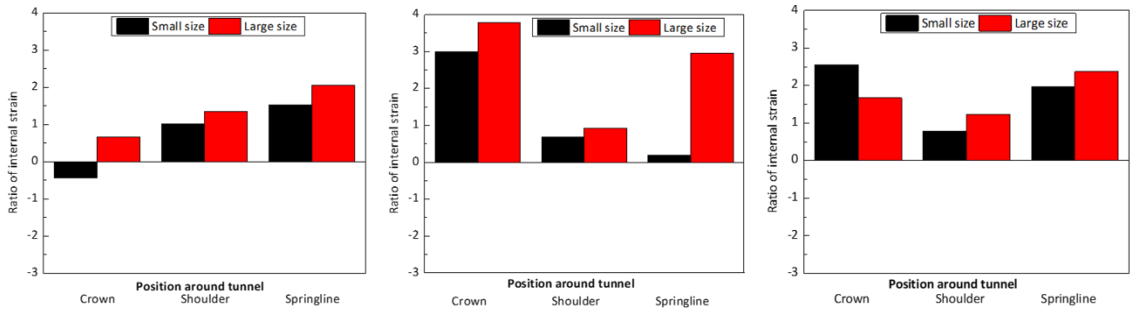

Figure 5-33. The incremental ratio of internal strain w.r.t. no weak zone to check the effect of size during shaking

- Increasing the void ratio of the weak zone has increased the response of the tunnel as shown in Figure 5-34. It can be seen that before shaking the maximum response always occur at the position of the weak zone.

- During the shaking process, the increase in the void ratio increased in the tunnel response. The maximum response has been recorded when the weak zone was located at the shoulder position however the response was observed at the crown position as shown in Figure 5-35. The higher response at the crown position is due to the bulging of the tunnel in the upward direction caused by the incoming ground.

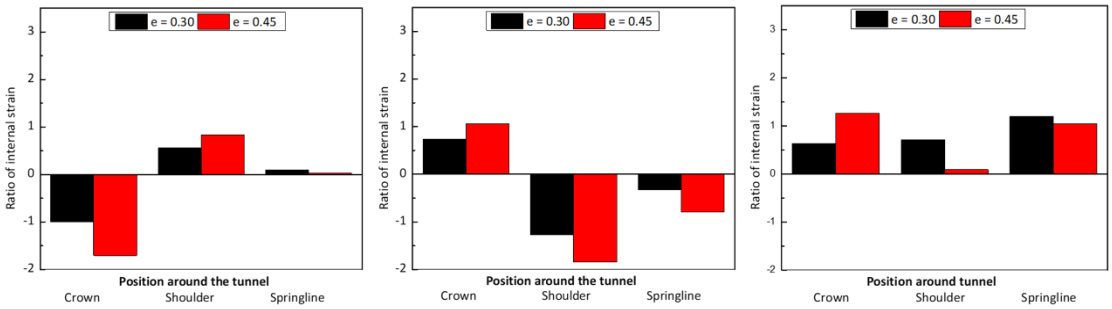

Figure 5-34. The incremental ratio of internal strain w.r.t. no weak zone to check the effect of stiffness before shaking

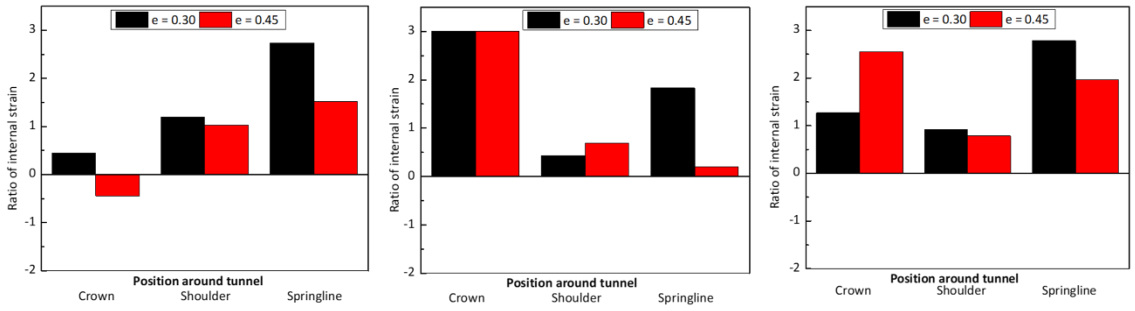

Figure 5-35. The incremental ratio of internal strain w.r.t. no weak zone to check the effect of stiffness during shaking

CHAPTER 6: COMBINED EFFECT OF CRACK AND WEAK ZONE

6.1 Position of Crack

To check the seismic performance of a crack tunnel, a crack along the longitudinal direction was introduced in the model tunnel. The crack represents the section of a complete separation of a segment as shown in Figure 6-1. The position of the crack along with the weak zone was varied around the tunnel and different observations were made.

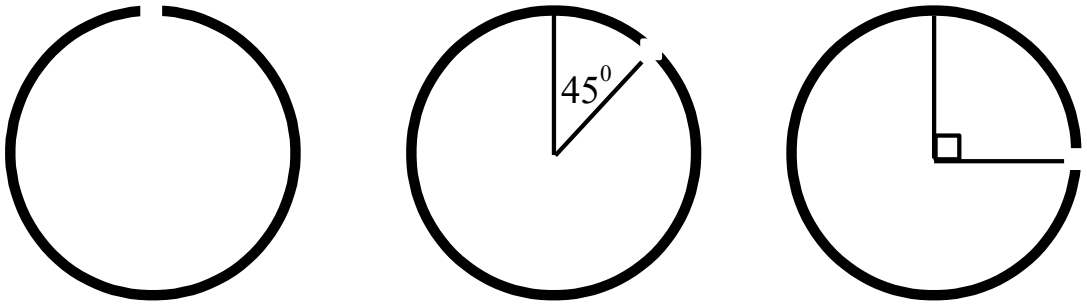

Figure 6-1. Position of crack around the tunnel

6.2 Effect of Crack

6.2.1 Ground response

6.2.1.1 Shear displacement

After investigating the effect of the weak zone, a comparison has been drawn between the weak zone and crack. The values of the shear displacement observed for the weak zone are higher than the crack in the tunnel as illustrated in Figure 6-2. The higher values observed for the weak zone are due to the ground weakening caused by the removal of the particles. However, in the case of a crack, the ground is not removed, and the crack might have an interlock. The shear strain variation for weak zone and crack is the same for crown and shoulder position. However, in the case of crack at the springline, the shear displacement is even lesser than the full contact case

which is because of ground moving on the left side instead of moving on the right side. For cracked tunnels, the values of the maximum shear displacement are slightly less as the ground is fully compact.

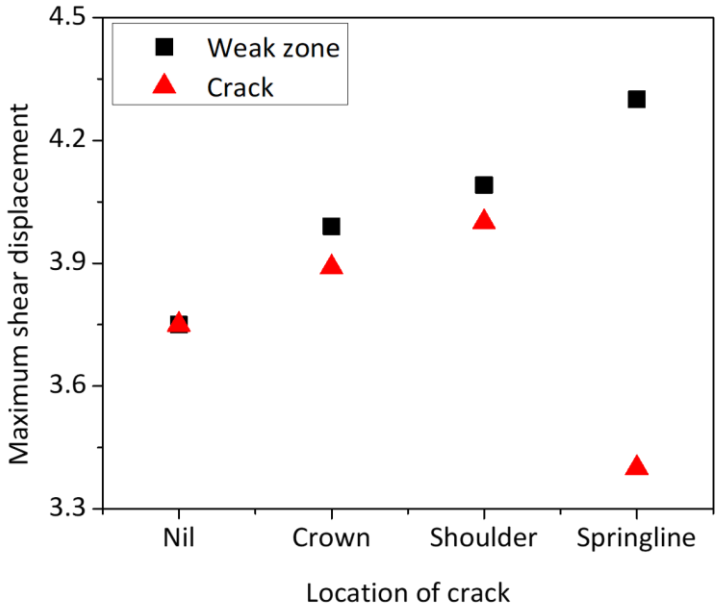

Figure 6-2. Comparison of the weak zone and crack in terms of maximum shear displacement

6.2.1.2 Ground response in terms of volumetric strain

The volumetric strain distribution due to a crack measured at maximum shear displacement is shown in Figure 6-3. As the ground was fully compact the crack other than the crown show lesser changes in volumetric strain. In case of crack at crown due to overburden pressure, the crack has just slipped resulting in a settlement of the ground.

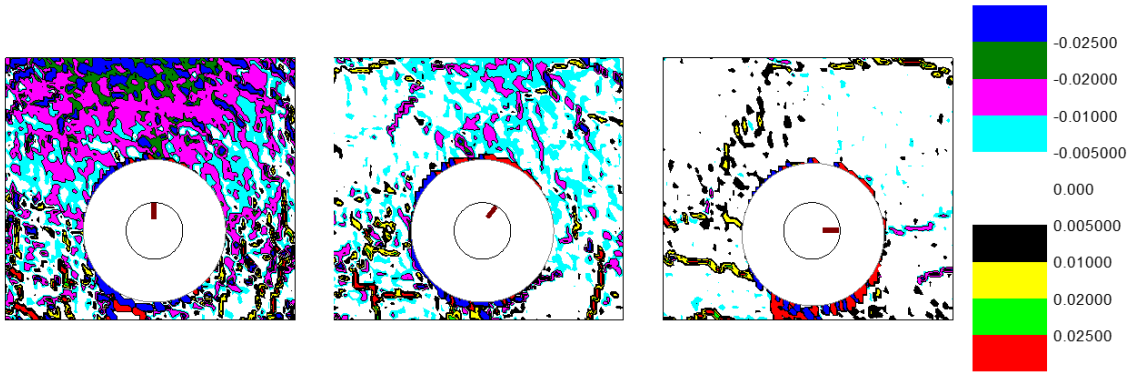

Figure 6-3. Volumetric strain distribution for the weak zone at the crown, shoulder, and springline position

The summary of shrinkage and expansion for cracks at different positions has been plotted in Figure 6-4. It can be seen that the maximum ground response has been shown for a crack at the crown position. The highest response is attributed to the slippage of the crack which is also seen in terms of internal strain. The shrinkage and expansion of ground for a crack at the shoulder and springline are similar to the full contact case as the crack doesn't have any weakness as in the case of the weak zone.

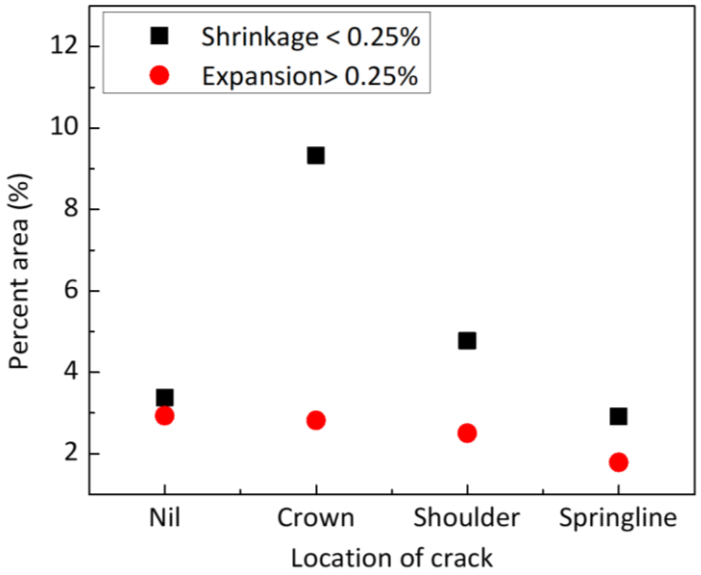

Figure 6-4. Summary of volumetric strain distribution for different positions of the crack

6.2.1.3 Ground response in terms of deviatoric strain

The effect of crack has been checked on the ground behavior in terms of deviatoric strain. In the case of crack, as the ground remains fully compact therefore no significant development of the deviatoric strain as shown in Figure 6-5. The effect of crack has been investigated after placing it on crown, shoulder, and springline position. When crack was placed at the crown there was a settlement at the top which shows the ground settlement, however, in the case of the deviatoric strain, there is no significant effect. This means that it is only the settlement and not ground failure.

6.2.2 Tunnel Response

The tunnel response has been measured in terms of the internal strain. To explore the effect of the crack on tunnel response has been discussed under static conditions and at maximum shear displacement. To draw a comparison between crack and weak zone the results have also been compared.

6.2.2.1 Before shaking

The effect of a crack along with the weak zone under static conditions has been shown in Figure 6-6. The plotted data shows that in the case of the weak zone the tunnel bends towards the location of the weak zone but in the case of a crack the tunnel behavior is different. When the crack was introduced, the tunnel always bends on the upward side. The upside bending of the tunnel is because of the separation of two parts of the tunnel structure. Due to the complete separation, the bending moment cannot be transferred to the next part and the lateral pressure force the tunnel to bend on the upward side.

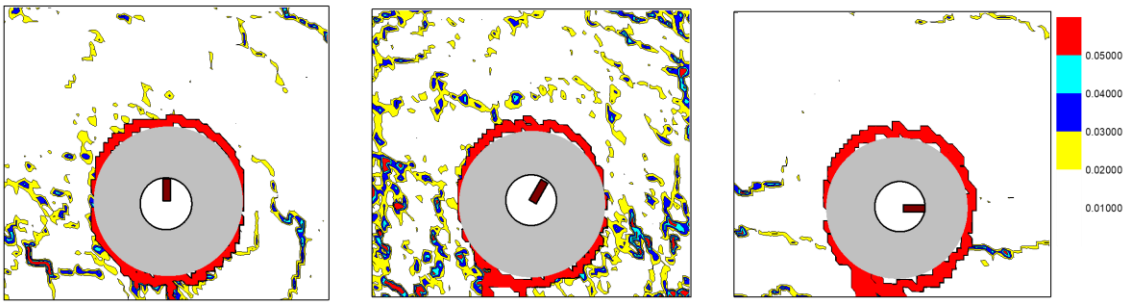

Figure 6-5. Summary of deviatoric strain distribution for different positions of the crack

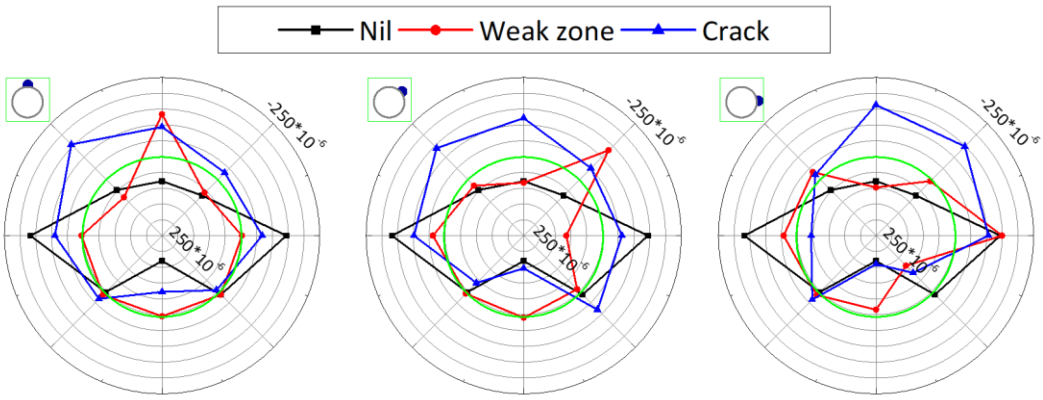

Figure 6-6. Effect of crack position on the static response of the tunnel

6.2.2.2 During shaking

The tunnel response by introducing the weak zone and crack at crown, shoulder, and springline positions under maximum shear displacement condition has been presented in Figure 6-7. The pots show that the presence of a weak zone intensifies the ovaling of the tunnel due to local weakening of the ground. However, when crack was introduced the tunnel bends in the inward direction. The maximum response has been recorded when the crack was placed at the

crown where the tunnel bends excessively. This inward bending is due to the crack slippage forced by the overburdened load.

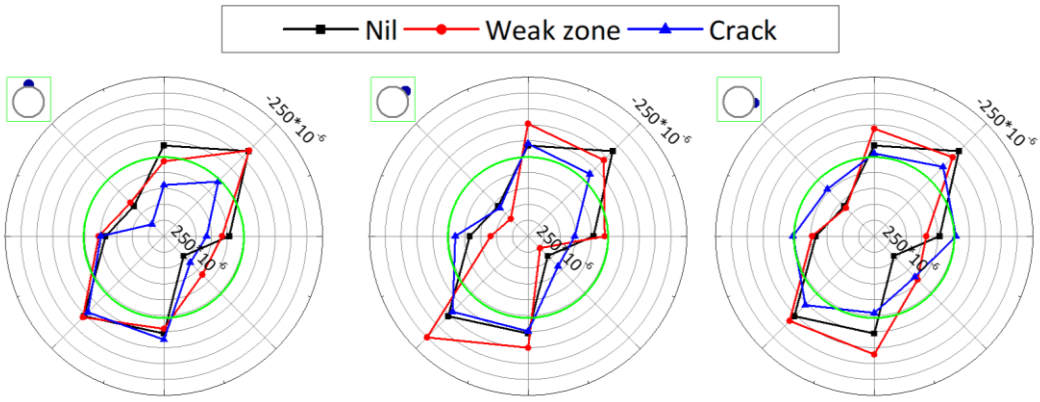

Figure 6-7. Effect of crack position on the response of tunnel at maximum shear displacement

6.3 Combined Effect of the Weak Zone and Crack on Ground Response

The combined effect of the weak zone and crack on-ground response has been measured in terms of shear displacement and ground volumetric strain.

6.3.1 Ground response

6.3.1.1 Shear displacement

After discussing the weak zone and crack effect separately, both parameters were varied together to check the effect on tunnel and ground response. The combined effect of the weak zone and crack on shear displacement has shown in Figure 6-8. The plotted values illustrate that by fixing the weak zone at a specific position and rotating the location of the crack, the maximum shear displacement has occurred when the crack was positioned at the shoulder position.

6.3.1.2 Volumetric strain

The combined effect of the weak zone and crack on the volumetric strain of the ground has shown in Figure 6-9 while the area under compression and expansion has been presented in Figure 6-10 and Figure 6-11 respectively. The volumetric strain distribution shows that the highest response has been recorded as follows:

- When the weak zone was positioned at the crown and the location of the crack was varied, the maximum response was recorded for a crack at the crown position while the other

locations show relatively fewer values. This is because the weak zone was created after placing the tunnel inside the ground and the formation of the weak zone is very controlled and uniform in nature. However, the crack was made before the placement of the tunnel in the ground hence the effect was less as compared to the weak zone case.

- The introduction of a weak zone at the shoulder yields an almost similar response for a crack at crown and springline position.
- The weak zone at springline positions shows maximum volumetric strain when the crack appears at the crown location. The crack at the crown is the main reason as in this case it usually slipped in the downward direction causing the maximum response.

In conclusion, the plotted data shows that the position of the weak zone has more effect when it comes to the ground strains. However, in the case of maximum shear displacement, it occurred when the crack was at the shoulder position. This is due to the reason that when the crack is at the shoulder position, maximum ovalisation occurs in the tunnel structure as it tries to elongate maximum along the diagonal direction. It is also worthy to note that similar to the only weak zone case the shrinkage is always higher than expansion. This is due to the compaction of the ground and inward movement of the tunnel model caused by the presence of the crack.

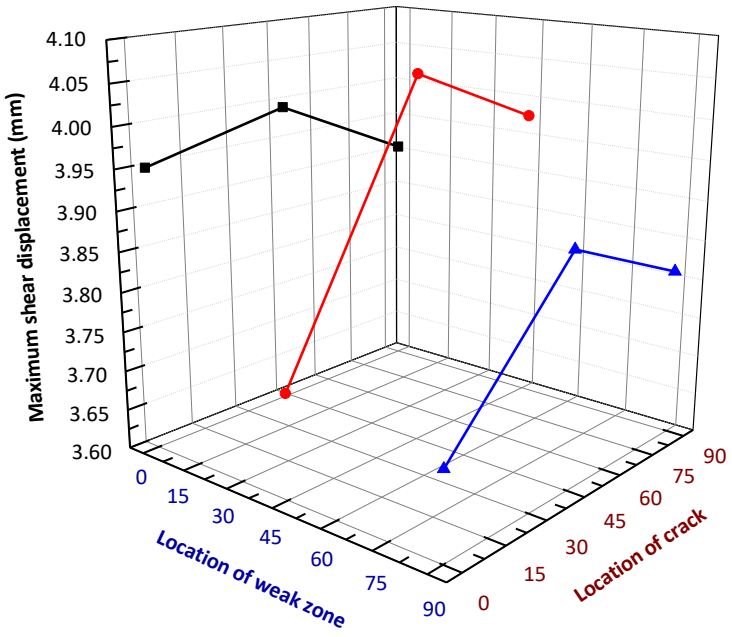

Figure 6-8. The combined effect of the weak zone and crack on maximum shear displacement

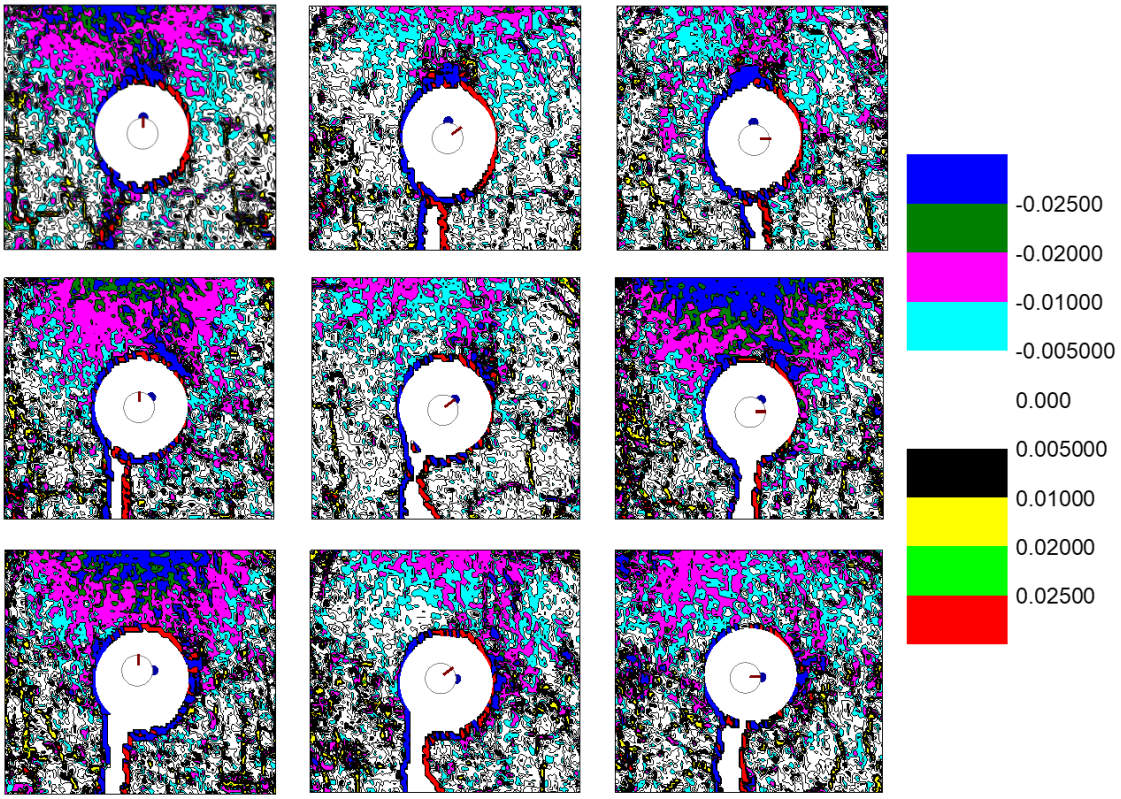

Figure 6-9. The combined effect of the weak zone and crack on volumetric strain distribution (Overburden height 1 D)

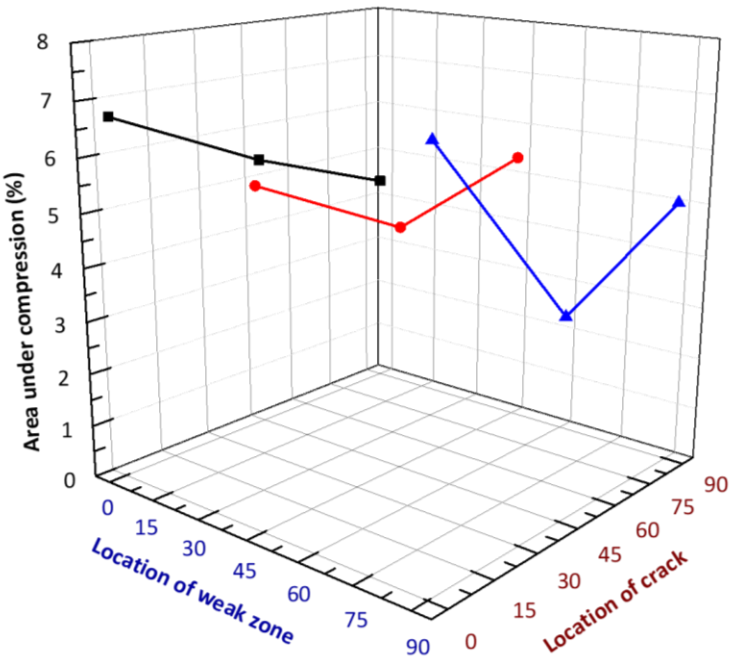

Figure 6-10. The combined effect of the weak zone and crack on ground shrinkage

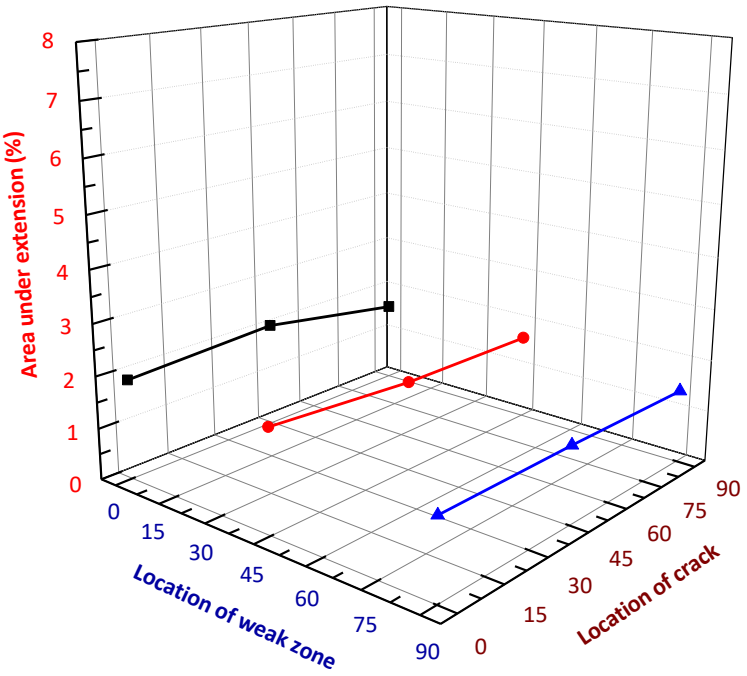

Figure 6-11. The combined effect of the weak zone and crack on-ground expansion

6.3.1.3 Ground response in terms of deviatoric strain

This section will explain the combined effect of the crack and weak zone. The position of the weak zone was varied by keeping the position of a crack at a specific point and the ground strains were analyzed. The photos were analyzed at maximum shear displacement position and the results have been presented in Figure 6-12. By keeping the crack at the crown and moving the weak zone from crown to springline through the shoulder indicate that the development of the deviatoric strain follows the position of the weak zone. It was found that the maximum deviatoric strain occurred at the location of the weak zone position. By comparing the effect of the crack, it was found that the maximum change has been observed when the crack was placed at the crown location. The reason is that for a crack at the crown position, the vertical force acting on the tunnel may be higher than the frictional force which holds the broken parts together. As the vertical force is higher than the frictional force it will cause the slippage of the crack in the downward direction causing a high concentration of the deviatoric strain. However, in case of a crack at the shoulder and the springline position, the confining pressure will compress the tunnel increasing the frictional resistance at the broken parts. During shaking the frictional resistance was found enough to hold the tunnel together that's why the ground response with the cracked tunnel is closer to the intact tunnel. For a fixed position of the weak zone, the maximum response was observed for a

crack at the crown position which is due to slipping of the crack inside. While for the crack at the shoulder and springline relatively lesser response has been recorded.

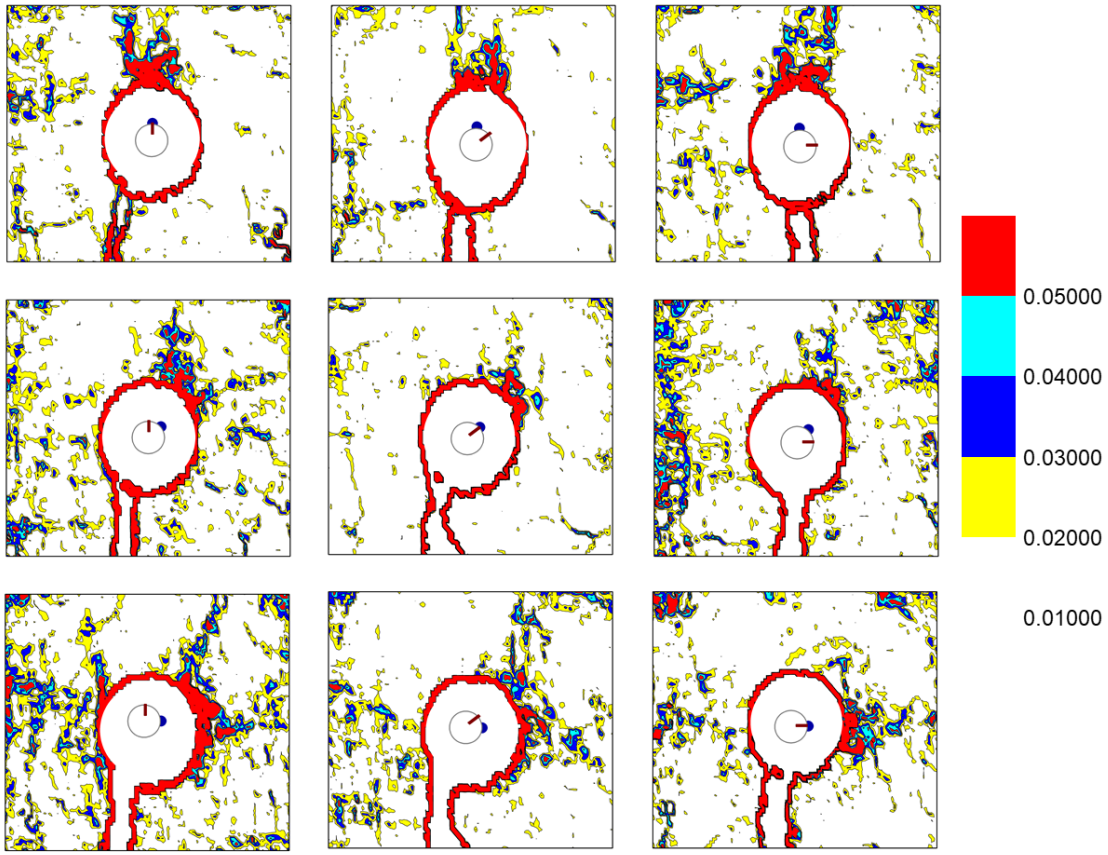

Figure 6-12. The combined effect of the weak zone and crack on deviatoric strain distribution (Overburden height 1 D)

6.3.2 Tunnel response

As mentioned earlier the tunnel response has been measured under static conditions and maximum displacement conditions.

6.3.2.1 Before shaking

The combined effect of the weak zone and crack on the static response of the tunnel is shown in Figure 6-13. The graphs indicate that for the weak zone at the crown, the maximum response was recorded when there was no crack as indicated by the red line. When crack was positioned at the crown position the minimum response was recorded and for other locations of the crack, the lines are in between the no crack and crack at the crown case. Moving the weak zone to shoulder position similar behavior has been observed in which the maximum changes were

observed for no crack while the minimum was observed for weak zone and crack at shoulder position.

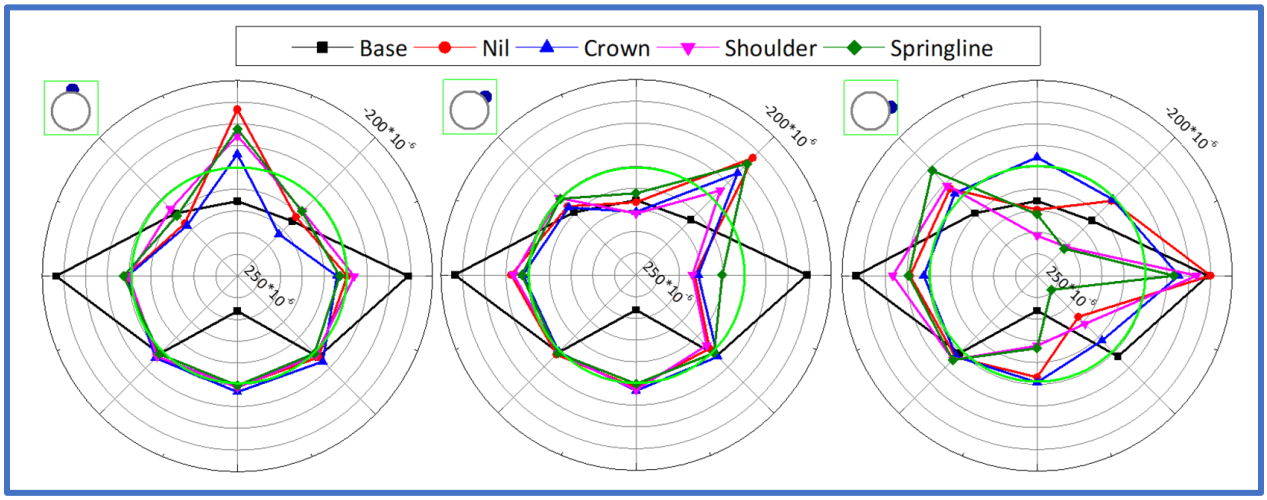

Figure 6-13. The combined effect of the weak zone and crack on the static response of the tunnel

6.3.2.2 During shaking

Figure 6-14 shows the combined effect of the weak zone and crack on tunnel response at maximum shear displacement condition. When the weak zone was placed at the crown position and the crack was varied around the tunnel large changes have been observed in the internal strain. When the crack and the weak zone were at the crown position the results have been shown by the blue line in the left figure and indicate maximum deflection at the tunnel crown which is the result of crack slippage in the downward direction. However, the downward slippage in the case of crack and weak zone at the crown is less than that of the only crack at the crown position. The reason is that due to the weak zone effect tunnel tries to bend outside while the only crack it bends inside and for combined effect the bending level is in between of them. For crack position at shoulder, there is no significant effect on the tunnel bending behavior at shoulder location, however, due to incoming ground from the top, bending at the crown has been observed. Moving the crack to the springline position shows the tunnel bending towards the right side (the side where the crack was stationed) the reason is that the incoming ground from the tunnel crown will push from the top and as there is a discontinuity at the springline position, and the overburden height is very small, so the upper part of the tunnel tries to move towards the right side.

When the weak zone was introduced at the shoulder position and the position of the crack was varied the results have been shown in the central figure. The figure indicates that when there

was no crack and the weak zone was placed at the shoulder position, the incoming ground from the shoulder side will force the tunnel to deflect outward at the crown position. When the crack was located at the crown position, the incoming ground from the shoulder side will try to deflect the tunnel at the crown however, as the crack at the crown moves downward, therefore, no upward movement has been seen. By keeping the crack and the weak zone at the shoulder position shows that incoming ground from the shoulder side will push the tunnel inward at the shoulder position as the crack is also positioned over there so the pressure of the ground will push the tunnel much higher at the crown and invert positions. This high bulging of the tunnel can be explained from the mechanism of the incoming ground towards the crack tunnel which response by bulging from the top and bottom parts of the tunnel. Shifting the crack to the springline position reveals that the tunnel has inside at the springline position, and no upward deflection has been observed at the crown part.

Introducing the weak zone at the springline position and moving of the crack around the tunnel has been illustrated in the right figure. The graph shows that for no crack case the incoming ground towards the springline position will push the tunnel inside at the springline position and due to this effect, the tunnel has moved in the upward direction at the tunnel crown i.e., the squeezing of the tunnel in the horizontal direction. Along with the weak zone at the springline position when a crack was introduced at the crown location, the tunnel in the downward direction, and in this case the downward bending is higher than the previous case. The reason is that when the tunnel was bending from the crown position there is space available for it to expand in the horizontal direction. Moving the crack to the shoulder location showed that there is a very significant bulging of the tunnel at the crown position. This is because the incoming ground from the side will push the tunnel inside and bulging from the top as in this case there is a discontinuity at the shoulder position so the tunnel was freer to ovalisation and because the gravitational stresses are less so the tunnel bulging was seen at the crown location but the effect at the invert is less significant due to fix boundary at the bottom side. Finally, when the crack and the weak zone location are at the springline location, the top part of the tunnel has shown very large bending towards the right side. The reason for this bending can be explained by considering the direction of the ground movement. As the result has been gathered at the maximum shear displacement and the ground is moving towards the right side. When the ground will exert force from the left side the tunnel will be pushed towards the right side and due to the presence of the weak zone and the

discontinuity at the springline, the tunnel bends very significantly towards the right side. It is also interesting to note that the major deflection has occurred on the top side as the bottom boundary is fixed and the tunnel can not go in the downward direction.

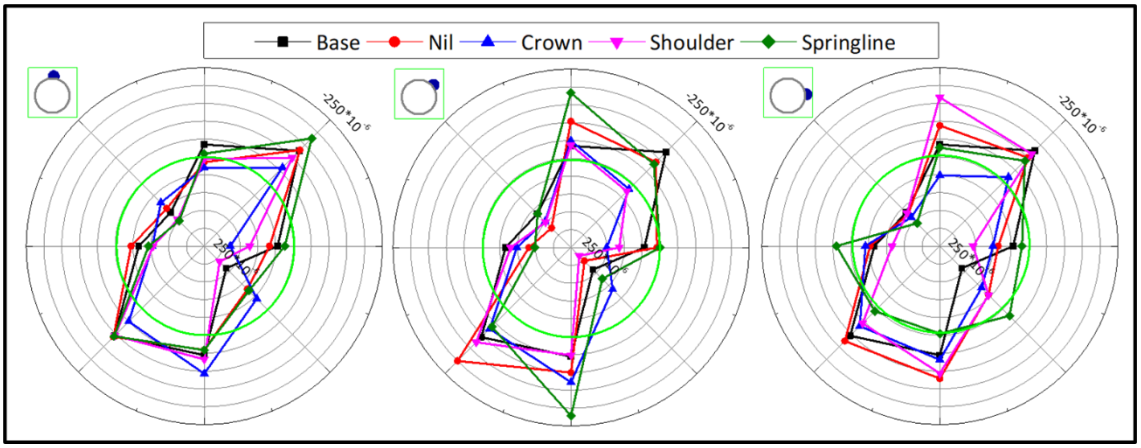

Figure 6-14. The combined effect of the weak zone and crack on the response of tunnel at maximum shear displacement

6.4 Conclusions

The effect of a crack in the lining has been checked and the results have been compared with the effect of the weak zone. The compared results include the ground response measured in terms of volumetric strain and deviatoric strain and the tunnel response measured in terms of internal strain measured at different locations around the lining. The behavior of the tunnel accompanying a crack and a weak zone is very different. Based on the results gathered from the current research the following conclusions have been drawn.

- The location of the weak zone and crack are the key parameters affecting the ground and tunnel response.
- The maximum ground response was observed according to the position of the weak zone and the highest values of the volumetric and deviatoric strains occurred at the location of the weak zone.
- The appearance of a weaker part lowers the seismic capacity and may change the failure pattern of the lining structure due to the insufficiency of counterforces from adjacent soil/rock. The bending behavior of the tunnel during shaking depends upon the position of the weak zone and crack. The tunnel with a crack at the crown position tends to slip during

shaking hence causing a downward deflection at the crown position. However, the crack at the shoulder position caused the bulging from the topmost part of the lining.

- The results gathered from the tunnel response are in alignment with the results from the ground response. The direction of the incoming ground plays a prime role in the bending direction of the tunnel.
- The maximum ground response in terms of the shear displacement has been observed when the weak zone was placed at the shoulder position.
- The tunnel bending under static condition for full contact case is symmetrical, however, the introduction of weak zone act as a free space, and the tunnel tends to move towards it while the presence of crack breaks the transfer of stresses and tunnel bends in the upward direction as illustrated in Figure 6-15. Under shaking conditions, tunnels with weak zone ovalize while cracked tunnels are compressed inside as compared to the uncracked tunnel.

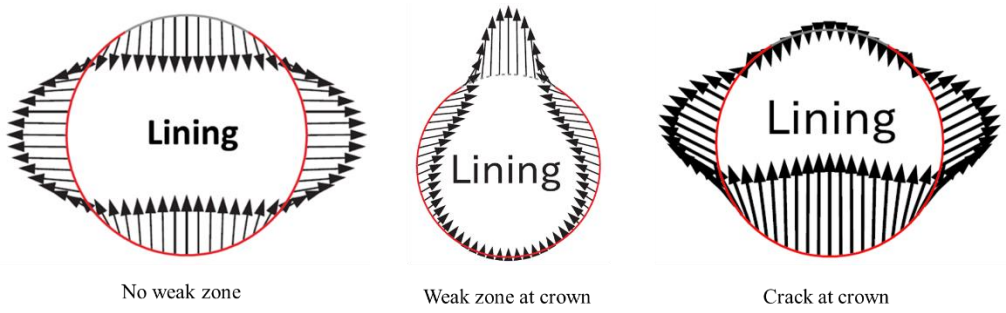

Figure 6-15. Tunnel bending behavior under different scenarios

CHAPTER 7: CONCLUSIONS AND RECOMMENDATIONS

7.1 Conclusions

In this paper, two-dimensional shaking table tests have been performed to evaluate the influence of weak zone and crack on the seismic response of circular tunnels. Particular attention has been paid to the preparation of weak zones and data analysis. Effects of weak zone position, weak zone stiffness, size of the weak zone, and overburden height have been explored and the results were compared with no weak zone case. A comparison between the effect of a weak zone and a crack has also been made. Results have been presented in the form of the ground response and the tunnel response. The ground response has been measured in terms of ground shearing displacement and strains in the groundmass e.g., volumetric strains and deviatoric strains. However, the tunnel response has been checked in terms of internal strain, outer strain, and bending moment. The following conclusions can be drawn from the results.

- Strain gauges can be used to detect the weak zone behind the lining by installing them on the inner face of the tunnel. If the internal strain recorded by strain gauges starts increasing, it will indicate the possible presence of the weak zone.
- The soil type is an important factor as the deformation behavior of the groundmass depends upon the soil type.
- In the actual field as there is high overburden pressure, if the weak zone starts developing, due to the arching effect the ground can sustain itself under static conditions. However, during seismic activity, the ground will fall exerting pressure on the lining. Therefore, timely detection and repair are essential.
- The pore water pressure will play an important role in the field as under static conditions the water will exert pressure to prevent the outward bending and can mislead the size and stiffness of the weak zone. However, during an earthquake, the deformations can be much more than the expected ones. Similarly, the ground strains will not be the same as the moisture will play an important role and the behavior of wet soil is entirely different as compared to the dry soil.

- PIV has proven a good tool to estimate the surface strain. The strain obtained through PIV analysis and that recorded with the help of strain gauges corresponded well with similar distribution patterns.
- The location, size, and stiffness of the weak zone are the key parameters affecting the ground and tunnel responses. The increasing size and decreasing stiffness of the weak zone can cause the internal strain and BM to alter the signs to result in cracking or even a complete breakdown of the lining.
- The lining follows with an outward deformation from the point where the weak zone is positioned and an inward displacement at the points farther from the weak zone. This phenomenon ends in a rise of the bending moments of the lining at all points around the lining. However, the maximum increase appears to occur where the weak zone is placed.
- A weak zone induces redistribution of the ground strain around the lining. A weak zone at the crown leads to yield more strain, compared to the ground without a weak zone. The higher the void ratio of the weak zone is, the higher the shifting of strain to neighboring parts of the ground nearby the tunnel and also the ground beyond the tunnel.
- The collective results of a seismic excitation and weak zone are more in control of compounding the deformation and stress states of the lining. The bending moment increases at the position of the weak zone and decreases at the neighboring points around the tunnel. The appearance of a weaker part lowers the seismic capacity and may change the failure pattern of the lining structure due to the insufficiency of counterforces from adjacent soil/rock. To identify the potentially vulnerable location of the tunnel lining, overall internal forces along the periphery should be used.
- Dynamic bending moment distribution shows that the maxima occur at shoulders (e.g., 45^0 and 315^0) and knees (e.g., 135^0 and 225^0) locations of the lining causing the ovalization phenomena. The greater BM at these points may produce joint openings, thus threatening the moisture movement inside the tunnel.
- In the actual field conditions, the higher overburden pressure will multiply this phenomenon.
- A tunnel with a crack has a very different behavior as compared to the weak zone. The lining with weak zones has a higher tunnel and ground response as compared to the crack scenario. A tunnel with a weak zone has a higher tendency of elongation as indicated by

the ratios of vertical and diagonal lengths as compared to the case of a cracked tunnel however, in the case of crack the maximum ground response was recorded after placing it on the crown position.

- The quantitative and qualitative results attained from this study, in general, agree with those reported in the literature. The change in bending moment, volumetric strain, and ground shear strain are close to those previously reported for tunnels in granular soils.
- Before shaking (without earthquake), if the internal strain at a specific point is increasing over time, and the neighboring points show a decrease in internal strain then, it will indicate the possibility of a weak zone behind the lining at that point.
- Before shaking (without earthquake), if the internal strain increases at more than half part of the tunnel, it will indicate the possibility of lining crack.
- Between two seismic activities, if the internal strain is decreasing it will represent the position of that crack.

7.2 Future Research

However, there exist some limitations in this study. The experiments are conducted on a small-scale model and the outcomes of this small-scaled model cannot be simply extended to relate to field performance. The weak zone was formed by extracting the soil particles in this study. A more realistic weak zone formation mechanism can be used in the future. The soil used in this study was like dry sand but a material closer to reality incorporating the effect of pore pressure can be studied. High gravitational stresses cannot be produced in shaking table tests because of limited height. Although only a circular tunnel with uniform thickness and buried inhomogeneous soil has been tested in this study, many tunnels may have a box or horseshoe shape with variable thickness constructed in multi-layered soil. The tunnel construction method was different from the practical construction. What is essential to understand is that weak zones or voids can produce serious harm to the tunnel lining, but their existence may not be readily spotted by traditional tactics such as tunnel convergence. So usually, they are detected following the lining structure has been critically broken. It is also vital to recognize that all tunnels are vulnerable and fragile against weak zones and this research can be a good reference to study further considering the complicating factors.

- Actual soil can be placed to incorporate the effect of the pore water pressure.

- The effect of retrofitting can be checked, and results can be compared with the available field observations, and it is also essential to consider the vertical component as well.
- High overburden and different geometries of the tunnel can be explored.
- The stresses due to weak zones properly are included in design and field data must be collected to accumulate experience.
- It is also vital to recognize that all tunnels are vulnerable and fragile against weak zones and this research can be a good reference to study further considering the complicating factors.

Reference

Adrian, Ronald J. 1991. “Particle-Imaging Techniques for Experimental Fluid Mechanics.” *Annual Review of Fluid Mechanics* 23 (1): 261–304.

Aggelis, D. G., T. Shiotani, and K. Kasai. 2008. “Evaluation of Grouting in Tunnel Lining Using Impact-Echo.” *Tunnelling and Underground Space Technology* 23 (6): 629–37.

Allersma, H. G.B. 1996. “Using Digital Image Processing in Field Measurement.” *Geotechnique* 46 (3): 561–63.

Asakura, and Kojima. 2003. “Tunnel Maintenance in Japan.” *Tunnelling and Underground Space Technology* 18 (2–3): 161–69.

Asakura, Toshihiro, and Yutaka Sato. 1996. “Damage to Mountain Tunnels in Hazard Area.” *Soils and Foundations*, no. Special: 301–10.

Baba, Hamoudy Ould, and Stephan Peth. 2012. “Large Scale Soil Box Test to Investigate Soil Deformation and Creep Movement on Slopes by Particle Image Velocimetry (PIV).” *Soil and Tillage Research* 125: 38–43.

Bobet, Antonio. 2010. “Drained and Undrained Response of Deep Tunnels Subjected to Far-Field Shear Loading.” *Tunnelling and Underground Space Technology* 25 (1): 21–31.

Cai, M. 2008. “Influence of Stress Path on Tunnel Excavation Response - Numerical Tool Selection and Modeling Strategy.” *Tunnelling and Underground Space Technology* 23 (6): 618–28.

Chau, K. T., C. Y. Shen, and X. Guo. 2009. “Nonlinear Seismic Soil-Pile-Structure Interactions: Shaking Table Tests and FEM Analyses.” *Soil Dynamics and Earthquake Engineering* 29 (2): 300–310.

Chen, Jun, Luzhen Jiang, Jie Li, and Xiaojun Shi. 2012. “Numerical Simulation of Shaking Table Test on Utility Tunnel under Non-Uniform Earthquake Excitation.” *Tunnelling and Underground Space Technology* 30: 205–16.

Chen, Jun, Xiaojun Shi, and Jie Li. 2010. “Shaking Table Test of Utility Tunnel under Non-Uniform Earthquake Wave Excitation.” *Soil Dynamics and Earthquake Engineering* 30 (11): 1400–1416.

Cilingir, Ulas, and S. P. Gopal Madabhushi. 2011. “A Model Study on the Effects of Input Motion on the Seismic Behaviour of Tunnels.” *Soil Dynamics and Earthquake Engineering* 31 (3): 452–62.

Clot, Arnau, Robert Arcos, Jordi Romeu, and Teresa Pàmies. 2016. “Dynamic Response of a Double-Deck Circular Tunnel Embedded in a Full-Space.” *Tunnelling and Underground Space Technology* 59: 146–56.

Cui, Ying, and Makoto Kimura. 2010. “Model Test and Numerical Analysis Methods in Tunnel Excavation Problem.” *Soils and Foundations* 50 (6): 915–23.

Davis, Allen G., Malcolm K. Lim, and Claus Germann Petersen. 2005. “Rapid and Economical Evaluation of Concrete Tunnel Linings with Impulse Response and Impulse Radar Non-Destructive Methods.” *NDT and E International* 38 (3): 181–86.

Delatte, N., et al. 2003. “Application of Nondestructive Evaluation to Subway Tunnel Systems.” *Transportation Research Record* 1845: 127–35.

Einstein, H. H., and C. Schwartz. 1980. “Discussion on Simplified Analysis for Tunnel Supports.” *Journal of the Geotechnical Engineering Division, ASCE, No. GT7*, 835–38.

Eisenstein, Z, F El-Nahhas, and S Thomson. 1979. “Pressure-Displacement Relations in Two Systems of Tunnel Lining.” In *Proceedings of 6th PanAmencan Conference on Soi1 Mechanics, Lima*, 85–94.

Fenner, R. A. 2000. “Approaches to Sewer Maintenance: A Review.” *Urban Water, 2,* 343–56.

Fu, Jinyang, Jiawei Xie, Junsheng Yang, Shuying Wang, and Feng Yang. 2019. *The Effects of Local Cavities on the Cracking Performance of an Existing Tunnel Lining*. *Sustainable Civil Infrastructures*. Vol. 2. Springer International Publishing.

Gomes, Rui Carrilho, Fátima Gouveia, Diogo Torcato, and Jaime Santos. 2015. “Seismic Response of Shallow Circular Tunnels in Two-Layered Ground.” *Soil Dynamics and Earthquake Engineering* 75: 37–43.

Guoxing, Chen, Chen Su, Zuo Xi, Du Xiuli, Q. I. Chengzhi, and Wang Zhihua. 2015. "Shaking-Table Tests and Numerical Simulations on a Subway Structure in Soft Soil." *Soil Dynamics and Earthquake Engineering* 76: 13–28.

H. Mashimo, T. Ishimura. 2003. "Evaluation of the Load on Shield Tunnel Lining in Gravel." *Tunnelling and Underground Space Technology* 18 (2–3): 233–41.

Hashash, Youssef M.A., Jeffrey J. Hook, Birger Schmidt, and John I-Chiang Yao. 2001. "Seismic Design and Analysis of Underground Structures." *Tunnelling and Underground Space Technology* 16 (4): 247–93.

Hashash, Youssef M.A., Duhee Park, and John I.Chiang Yao. 2005. "Ovaling Deformations of Circular Tunnels under Seismic Loading, an Update on Seismic Design and Analysis of Underground Structures." *Tunnelling and Underground Space Technology* 20 (5): 435–41.

Hassanzadeh, Mehran, Masoud Hajialilue Bonab, and Akbar A. Javadi. 2018. "Experimental and Numerical Study of the Behaviour of Shallow Rectangular Tunnels." *Journal of Vibroengineering* 20 (4): 1783–96.

Helfrich, Steven C. 1997. "Investigation of Sewer Line Failure." *Journal of performance of constructed facilities* 42 (11): 42–44.

Hoffman, M. And Lerner, D. 1992. "Leak Free Sewers: Who Needs Them." *Water and Waste Treatment Journal* 35 (8): 18–19.

Howard, and Chairman. 1991. "Report on the Damaging Effects of Water on Tunnels during Their Working Life." *Tunnelling and Underground Space Technology*. Vol. 6.

Huang, Feng, Hehua Zhu, Qianwei Xu, Yongchang Cai, and Xiaoying Zhuang. 2013. "The Effect of Weak Interlayer on the Failure Pattern of Rock Mass around Tunnel - Scaled Model Tests and Numerical Analysis." *Tunnelling and Underground Space Technology* 35: 207–18.

Iai, Susumu. 1989. "Similitude for Shaking Table Tests on Soil-Structure-Fluid Model in 1g Gravitational Field." *Soils and Foundations* 29 (1): 105–18.

ITA. 1991. "Report on the Damaging Effects of Water on Tunnels During Their Working Life." *Tunnelling and Underground Space Technology* 6 (1): 11–76.

Kheradi, Hamayoon, Keisuke Nagano, Haruki Nishi, and Feng Zhang. 2018. "1-g Shaking Table

Tests on Seismic Enhancement of Existing Box Culvert with Partial Ground-Improvement Method and Its 2D Dynamic Simulation." *Soils and Foundations* 58 (3): 563–81.

Kishida, Kiyoshi, Ying Cui, Masaichi Nonomura, Tomomi Iura, and Makoto Kimura. 2016. "Discussion on the Mechanism of Ground Improvement Method at the Excavation of Shallow Overburden Tunnel in Difficult Ground." *Underground Space (China)* 1 (2): 94–107.

Koyama, Yukinori. 2003. "Present Status and Technology of Shield Tunneling Method in Japan." *Tunnelling and Underground Space Technology* 18 (2–3): 145–59.

Lee, K. M., R. K. Rowe, and K. Y. Lo. 1992. "Subsidence Owing to Tunnelling. I. Estimating the Gap Parameter." *Canadian Geotechnical Journal* 29 (6): 929–40.

Leung, C., and M. A. Meguid. 2011. "An Experimental Study of the Effect of Local Contact Loss on the Earth Pressure Distribution on Existing Tunnel Linings." *Tunnelling and Underground Space Technology* 26 (1): 139–45.

Li, Tianbin. 2012. "Damage to Mountain Tunnels Related to the Wenchuan Earthquake and Some Suggestions for Aseismic Tunnel Construction." *Bulletin of Engineering Geology and the Environment* 71 (2): 297–308.

MATLAB Reference Guide. The Math Works, Inc., Natic, MA. 2003. "."

McDonald, S. E., and J. Q. Zhao. 2001. "Condition Assessment and Rehabilitation of Large Sewers." In *International Conference on Underground Infrastructure Research*, 361–69.

McKenna, S. P., and W. R. McGillis. 2002. "Performance of Digital Image Velocimetry Processing Techniques." *Experiments in Fluids* 32 (1): 106–15.

Meguid et al. 2008. "Physical Modeling of Tunnels in Soft Ground: A Review." *Tunnelling and Underground Space Technology* 23 (2): 185–98.

Meguid, M. A., and H. K. Dang. 2009a. "The Effect of Erosion Voids on Existing Tunnel Linings." *Tunnelling and Underground Space Technology* 24 (3): 278–86.

Meguid, M. A., and H. K. Dang. 2009b. "The Effect of Erosion Voids on Existing Tunnel Linings." *Tunnelling and Underground Space Technology* 24 (3): 278–86.

Meguid, Mohamed A., and Sherif Kamel. 2014. "A Three-Dimensional Analysis of the Effects of Erosion Voids on Rigid Pipes." *Tunnelling and Underground Space Technology* 43: 276–89.

Mitsuhiro, MORI, ASANO Isamu, TOKASHIKI Masaru, and NISHIHARA Masahiko. 2001. "Destructive Model Test of Irrigation Horseshoe-Shaped Tunnel That Has Different Scale of Void behind the Lining."

Moore, I. D. 2008. "Assessment of Damage to Rigid Sewer Pipes and Erosion Voids in the Soil, and Implications for Design of Liners." In *North American Society for Trenchless Technologies Conference and Exhibition, C-2-01.*

Munro, Scott M., Ian D. Moore, and Richard W.I. Brachman. 2009. "Laboratory Testing to Examine Deformations and Moments in Fiber-Reinforced Cement Pipe." *Journal of Geotechnical and Geoenvironmental Engineering* 135 (11): 1722–31.

Nakai, Teru, Hiromichi Kawano, Kouki Murata, Masaaki Banno, and Tadashi Hashimoto. 1999. "Model Tests and Numerical Simulation of Braced Excavation in Sandy Ground: Influences of Construction History, Wall Friction, Wall Stiffness, Strut Position and Strut Stiffness." *Soils and Foundations* 39 (3): 1–12.

Nakai, Teruo, Marcio M. Farias, Daniela Bastos, and Yasuharu Sato. 2007. "Simulation of Conventional and Inverted Braced Excavations Using Subloading Tij Model." *Soils and Foundations* 47 (3): 597–612.

Nakai, Teruo, and Masaya Hinokio. 2004. "A Simple Elastoplastic Model for Normally and over Consolidated Soils with Unified Material Parameters." *Soils and Foundations* 44 (2): 53–70.

Nejati, Hamid Reza, Morteza Ahmadi, and Hamid Hashemolhosseini. 2012. "Numerical Analysis of Ground Surface Vibration Induced by Underground Train Movement." *Tunnelling and Underground Space Technology* 29: 1–9.

Niedostatkiewicz, M., D. Lesniewska, and J. Tejchman. 2011. "Experimental Analysis of Shear Zone Patterns in Cohesionless for Earth Pressure Problems Using Particle Image Velocimetry." *Strain* 47 (2): 218–31.

Pakbaz, Mohammad C., and Akbar Yareevand. 2005. "2-D Analysis of Circular Tunnel against Earthquake Loading." *Tunnelling and Underground Space Technology* 20 (5): 411–17.

Peck. 1969. "Deep Excavations and Tunneling in Soft Ground." In *Proceedings of the Seventh International Conference on Soil Mechanics and Foundation Engineering, Mexico City*, 225–90.

Peck, R. B., A. J. Hendron, and B Mohraz. 1972. “State of the Art of Soft-Ground Tunneling.” In *RETC Proceedings*, 259–86.

“Rekindled NATM Debate.” 2008. 2008.

Sedarat, Hassan, Alexander Kozak, Youssef M.A. Hashash, Anoosh Shamsabadi, and Alex Krimotat. 2009. “Contact Interface in Seismic Analysis of Circular Tunnels.” *Tunnelling and Underground Space Technology* 24 (4): 482–90.

Serpente, P. E. 1994. “Understanding the Modes of Failure for Sewers.” In *Urban Drainage Rehabilitation Programs and Techniques Selected Papers on Urban Drainage Rehabilitation from 1988 – 1993. New York: ASCE.*

Shahin et al. 2004. “Influence of Surface Loads and Construction Sequence on Ground Responce Due to Tunneling.” *Soils and Foundations* 44 (2): 71–84.

———. 2011. “Behavior of Ground and Response of Existing Foundation Due to Tunneling.” *Soils and Foundations* 51 (3): 395–409.

Slominski, Cezary, Maciej Niedostatkiewicz, and Jacek Tejchman. 2007. “Application of Particle Image Velocimetry (PIV) for Deformation Measurement during Granular Silo Flow.” *Powder Technology* 173 (1): 1–18.

Spasojevic, A. D., Mair, R. J., and Gumbel, J. E. 2007. “Centrifuge Modelling of the Effects of Soil Loading of Flexible Sewer Liners.” *Géotechnique* 57 (4): 331–41.

Sun, Jizhu, and Jinyuan Liu. 2014. “Visualization of Tunnelling-Induced Ground Movement in Transparent Sand.” *Tunnelling and Underground Space Technology* 40: 236–40.

Sun, Tiecheng, Zurun Yue, Bo Gao, Qiang Li, and Yungang Zhang. 2011. “Model Test Study on the Dynamic Response of the Portal Section of Two Parallel Tunnels in a Seismically Active Area.” *Tunnelling and Underground Space Technology* 26: 391–97.

Talesnick, M., and Baker, R. 1999. “Investigation of the Failure of a Concrete-Lined Steel Pipe.” *Geotechnical and Geological Engineering* 17: 99–121.

Talesnick, M., and R. Baker. 1999. “Investigation of the Failure of a Concrete-Lined Steel Pipe.” *Geotechnical and Geological Engineering* 17 (2): 99–121.

Tan, Z. and Moore, I.D. 2007 “Effect of Backfill Erosion on Moments in Buried Rigid Pipes.” In

Transportation Research Board Annual Conference, Washington D.C. January, 29. Tobar Valencia, T. (2009). "An Experiment.

Tan, Z. 2007. "Effect of Soil Voids on Sewer Repair Using Liners. MSc Thesis, Department of Civil Engineering, Queen's University at Kingston, Ontario, Canada."

Terzaghi, Karl. 1946. *Rock Defects and Loads on Tunnel Supports*. Rock Tunnelling with Steel Supports, The Youngstown/Ohio, Printing Co.

"U.S. Department of Transportation Federal Highway Administration. Highway and Rail Transit Maintenance and Rehabilitation Manual." 2005.

Wang et al. 2014. "Void-Induced Liner Deformation and Stress Redistribution." *Tunnelling and Underground Space Technology* 40: 263–76.

Wang, W. L., T. T. Wang, J. J. Su, C. H. Lin, C. R. Seng, and T. H. Huang. 2001. "Assessment of Damage in Mountain Tunnels Due to the Taiwan Chi-Chi Earthquake." *Tunnelling and Underground Space Technology* 16 (3): 133–50.

Wang, Z. Z., Y. J. Jiang, C. A. Zhu, and T. C. Sun. 2015. "Shaking Table Tests of Tunnel Linings in Progressive States of Damage." *Tunnelling and Underground Space Technology* 50: 109–17.

Wang, Zhan, Lizhong Wang, Lingling Li, and Jingchang Wang. 2014. "Failure Mechanism of Tunnel Lining Joints and Bolts with Uneven Longitudinal Ground Settlement." *Tunnelling and Underground Space Technology* 40: 300–308.

Ward, W. H., and M. J. Pender. 1981. "Tunneling in Soft Ground-General Report." In *Proceedings of the Tenth International Conference on Soil Mechanics and Foundation Engineering*.

White, D. J., W. A. Take, and M. D. Bolton. 2003. "Soil Deformation Measurement Using Particle Image Velocimetry (PIV) and Photogrammetry." *Geotechnique* 53 (7): 619–31.

White, D., and A. Take. 2002. "GeoPIV: Particle Image Velocimetry (PIV) Software for Use in Geotechnical Testing." *CUED/D-SOILS/TR322. Cambridge, UK.*

Xiao, J. Z., F. C. Dai, Y. Q. Wei, H. Min, Chong Xu, X. B. Tu, and M. L. Wang. 2014. "Cracking Mechanism of Secondary Lining for a Shallow and Asymmetrically-Loaded Tunnel in Loose Deposits." *Tunnelling and Underground Space Technology* 43: 232–40.

Xin et al. 2018. “Shaking Table Tests on Seismic Response and Damage Mode of Tunnel Linings in Diverse Tunnel-Void Interaction States.” *Tunnelling and Underground Space Technology* 77: 295–304.

Xu, Hua, Tianbin Li, Lei Xia, John X. Zhao, and Dong Wang. 2016. “Shaking Table Tests on Seismic Measures of a Model Mountain Tunnel.” *Tunnelling and Underground Space Technology* 60: 197–209.

Yan, Xiao, Haitao Yu, Yong Yuan, and Juyun Yuan. 2015. “Multi-Point Shaking Table Test of the Free Field under Non-Uniform Earthquake Excitation.” *Soils and Foundations* 55 (5): 985–1000.

Yashiro, Kazuhide, Yoshiyuki Kojima, and Mitsuru Shimizu. 2007. “Historical Earthquake Damage to Tunnels in Japan and Case Studies of Railway Tunnels in the 2004 Niigataken-Chuetsu Earthquake.” *Quarterly Report of RTRI (Railway Technical Research Institute) (Japan)* 48 (3): 136–41.

Yasuda et al. 2017. “Elastic Solutions for Circular Tunnel with Void behind Lining.” *Tunnelling and Underground Space Technology* 70: 274–85.

Yasuda et al. 2019. “Three-Dimensional Seismic Response of a Cylindrical Tunnel with Voids behind the Lining.” *Tunnelling and Underground Space Technology* 84: 399–412.

Yu, Haitao, Juntao Chen, Antonio Bobet, and Yong Yuan. 2016. “Damage Observation and Assessment of the Longxi Tunnel during the Wenchuan Earthquake.” *Tunnelling and Underground Space Technology* 54: 102–16.

Zhang, Weiwei, Xianlong Jin, and Zhihao Yang. 2014. “Combined Equivalent & Multi-Scale Simulation Method for 3-D Seismic Analysis of Large-Scale Shield Tunnel.” *Engineering Computations (Swansea, Wales)* 31 (3): 584–620.

Zhang, Xu, Zijian Ye, Bo Min, and Youjun Xu. 2019. “Effect of Voids behind Lining on the Failure Behavior of Symmetrical Double-Arch Tunnels.” *Symmetry* 11 (10): 1–16.

Zhang, Xuepeng, Yujing Jiang, and Satoshi Sugimoto. 2018. “Seismic Damage Assessment of Mountain Tunnel: A Case Study on the Tawarayama Tunnel Due to the 2016 Kumamoto Earthquake.” *Tunnelling and Underground Space Technology* 71 (July 2017): 138–48.

Appendix A

A-1 Input Acceleration Wave

Apart from the displacement, the input table acceleration was also recorded by placing the accelerometer at the top of the horizontal platform and the results have been resented in Figure A-1. The values recorded by the accelerometer are closer to the theoretical as explained by Eq. (10), where;

a = acceleration recorded in 'm/s^2'

f = frequency in 'Hz'

x = displacement from the mean position measured in 'm'

$$a = -(2\pi f)^2 x \tag{10}$$

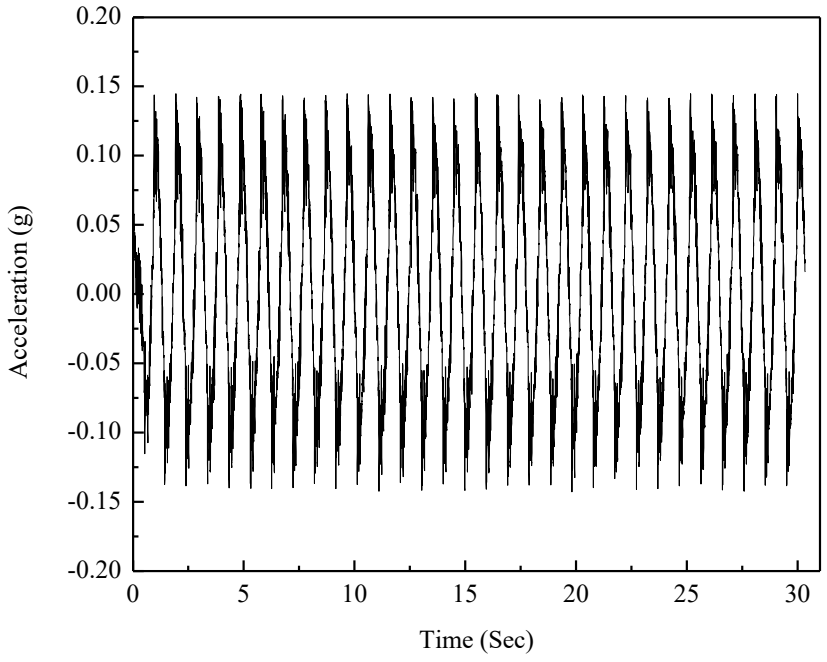

Figure A-1. Input acceleration wave

A-2 Particle Image Velocimetry Technique

For two consecutive images with image intensities of the interrogation cells I_1 & I_2, the quantity of correlation (R) can be measured with the help of Eq. (11). The 2D array of R values provides the correlation values for all displacements (Δx, Δy) between two interrogation cells. Then a bicubic interpolation function calculates simply possible displacements by correlating the first image with the second image (Sun and Liu, 2014; Hamoudy and Peth, 2012).

$$R\ (\Delta x, \Delta y) = \sum_{x=0,y=0}^{x<n,y<n} I_1(x,y) I_2(x+\Delta x, y+\Delta y) \qquad (11)$$

wherein x and y – coordinates in image 1, Δx, and Δy – displacement increments from image 1 to image 2, and n – the size of the interrogation cell, respectively.

The movement of soil particles was recorded in the form of a digital image series which were then processed to measure the displacement vectors $\{u\}$ using Flownizer 2D software. Strain vectors were then measured using strain-displacement matrix $[B]$ as expressed in Eq. (13). The calculated strains were then integrated through gauss integration to get the strain of the element. For the plane strain problem, the vector consists of three different strain components:

$$\{\varepsilon\} = \{\varepsilon_x \quad \varepsilon_y \quad \gamma_{xy}\} = \left\{ {}^{\partial u}/_{\partial x} \quad {}^{\partial v}/_{\partial y} \quad {}^{\partial u}/_{\partial x} + {}^{\partial v}/_{\partial y} \right\} \qquad (12)$$

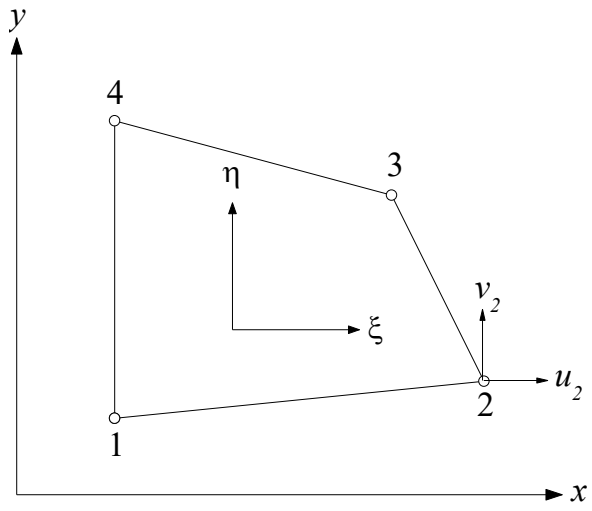

Figure A-2. Two-dimensional quadrilateral element

$$\{\varepsilon\} = [B]\{u\} \tag{13}$$

$$[B] = [D][N] \tag{14}$$

$$[D] = \begin{bmatrix} \partial/\partial x & 0 \\ 0 & \partial/\partial y \\ \partial/\partial y & \partial/\partial x \end{bmatrix} \tag{15}$$

where $[B]$, $[D]$ and $[N]$ are the geometric matrix, matrix differentiation, and shape function matrices respectively. For a plane strain condition, there will be four shape functions which are as follows.

- $N_1 = \frac{1}{4}(1-\xi)(1-\eta)$
- $N_2 = \frac{1}{4}(1+\xi)(1-\eta)$
- $N_3 = \frac{1}{4}(1+\xi)(1+\eta)$
- $N_4 = \frac{1}{4}(1-\xi)(1+\eta)$

As, shape functions are expressed in local coordinates (ξ, η) so they have to convert them into global coordinates (x, y). Derivatives can be converted from one coordinate system to the other through the chain rule of partial differentiation:

$$\begin{Bmatrix} \partial N_i/\partial \xi \\ \partial N_i/\partial \eta \end{Bmatrix} = \begin{Bmatrix} \partial x/\partial \xi & \partial y/\partial \xi \\ \partial x/\partial \eta & \partial y/\partial \eta \end{Bmatrix} \begin{Bmatrix} \partial N_i/\partial x \\ \partial N_i/\partial y \end{Bmatrix} = [J] \begin{Bmatrix} \partial N_i/\partial x \\ \partial N_i/\partial y \end{Bmatrix} \tag{16}$$

where $[J]$ is the Jacobian matrix.

$$[N] = \begin{bmatrix} N_1 & 0 & N_2 & 0 & N_3 & 0 & N_4 & 0 \\ 0 & N_1 & 0 & N_2 & 0 & N_3 & 0 & N_4 \end{bmatrix} \tag{17}$$

$$[B] = \begin{bmatrix} \partial N_1/\partial x & 0 & \partial N_2/\partial x & 0 & \partial N_3/\partial x & 0 & \partial N_4/\partial x & 0 \\ 0 & \partial N_1/\partial y & 0 & \partial N_2/\partial y & 0 & \partial N_3/\partial y & 0 & \partial N_4/\partial y \\ \partial N_1/\partial y & \partial N_1/\partial x & \partial N_2/\partial y & \partial N_2/\partial x & \partial N_3/\partial y & \partial N_3/\partial x & \partial N_4/\partial y & \partial N_4/\partial x \end{bmatrix} \quad (18)$$

As we cannot find the strain at nodal points, so we have to perform Gauss integration with the help of shape function. The Gauss quadrature formula for the volume integral in a two-dimensional case is of the form:

$$I = \int_{-1}^{1}\int_{-1}^{1} f(\xi, \eta)\ d\xi d\eta = \sum_{i=1}^{n}\sum_{j=1}^{n} f(\xi_i, \eta_j)\, w_i w_j \quad (19)$$

where ξ_i, η_j are abscissae and w_i , w_j are weighting coefficients of the Gauss integration rule and have been listed in Table A-1.

Table A-1. Abscissae and weights of the Gauss quadrature for n=1,2,3,4,5.

Gaussian point (n)	The abscissa (ξ_i)	Weight (w_i)
1	0	2
2	$\pm\ 1/\sqrt{3}$	1
3	0	$8/9$
	$\pm\sqrt{3/5}$	$5/9$
4	$\pm\sqrt{3/7 - 2/7\sqrt{6/5}}$	$\frac{18+\sqrt{30}}{36}$
	$\pm\sqrt{3/7 + 2/7\sqrt{6/5}}$	$\frac{18-\sqrt{30}}{36}$
5	0	$128/225$

	$\pm\ {}^{1}/_{3}\sqrt{5-2\sqrt{{}^{10}/_{7}}}$	$\frac{322+13\sqrt{70}}{900}$
	$\pm\ {}^{1}/_{3}\sqrt{5+2\sqrt{{}^{10}/_{7}}}$	$\frac{322-13\sqrt{70}}{900}$

$$\varepsilon_{1,2}=\frac{\varepsilon_x+\varepsilon_y}{2}\pm\sqrt{(\frac{\varepsilon_x-\varepsilon_y}{2})^2+\gamma_{xy}^2} \tag{20}$$

$$\gamma_{max}=\sqrt{(\varepsilon_x-\varepsilon_y)^2+\gamma_{xy}^2} \tag{21}$$

$$Volumetric\ strain,\ \varepsilon_v=\varepsilon_x+\varepsilon_y=\varepsilon_1+\varepsilon_2 \tag{22}$$

$$Diviator\ strain,\ \varepsilon_d=\varepsilon_1-\varepsilon_2 \tag{23}$$

wherein, ξ_i, η_j are abscissae, and w_i , w_j are weighting coefficients of the Gauss integration rule, $\varepsilon_x, \varepsilon_y$ and γ_{xy} are strain in the x-direction, strain in the y-direction, and the shear strain respectively.

A-3 Repeatability Analysis

The reliability of the seismic analysis depends upon the repeatability of the results. In this research, the repeatability has been checked at two-stage. At the first stage, the repeatability of the raw data is checked. To complete this step the raw data of the inner and outer strain was plotted and checked the variation between the consecutive tests. As a sample the raw data in the form of internal strain for two cases has been plotted and shown in Figure A-3 and Figure A-4. These graphs include the data for three tests conducted under the same conditions. From the plotted figure it can be seen that all three tests are close to each other which shows reasonable repeatability. At this stage, only those tests were chosen which were showing good repeatability.

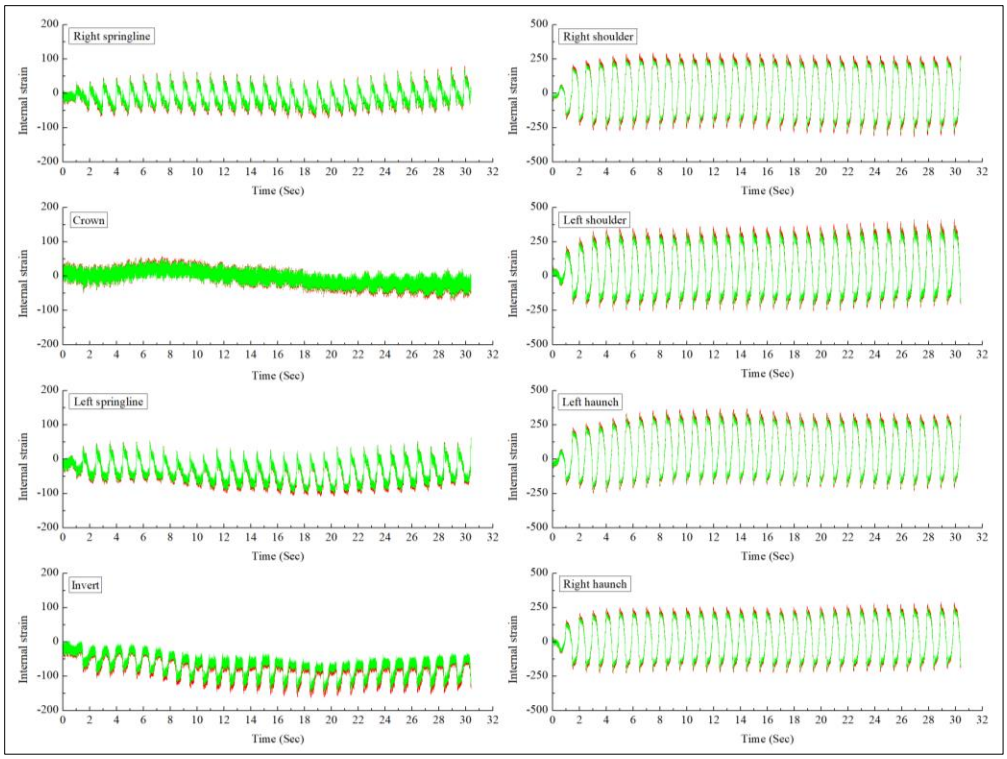

Figure A-3. Repeatability plots for no weak zone (overburden height = 2D)

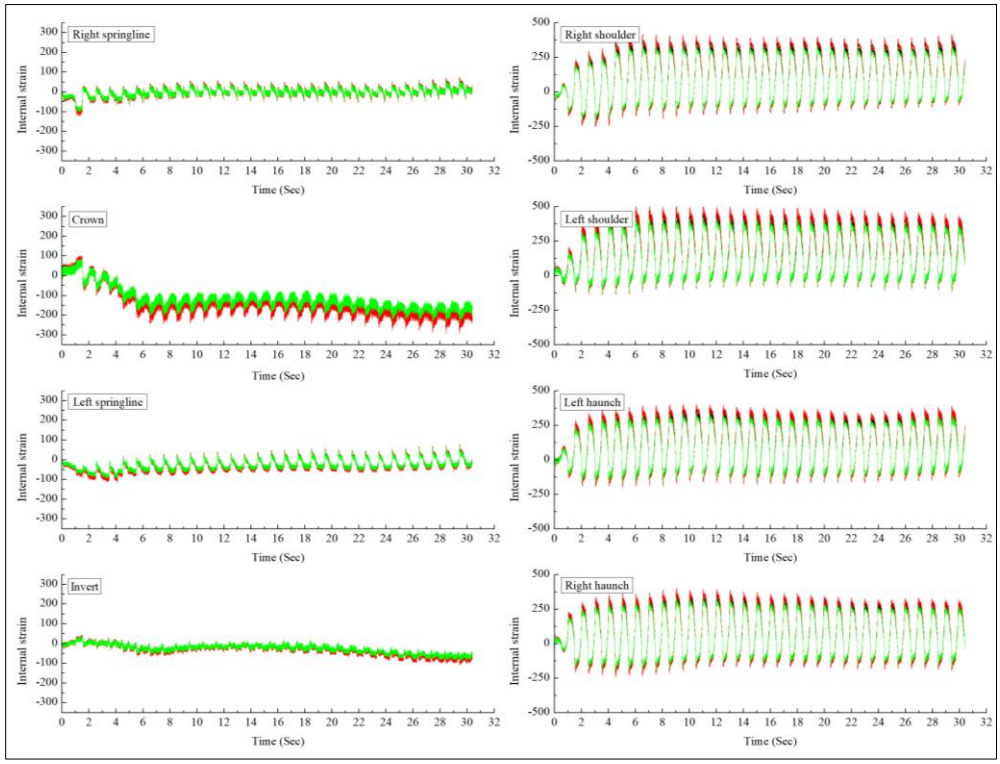

Figure A-4. Repeatability plots for weak zone having void ratio 0.30 and positioned at the crown (overburden height = 2D)

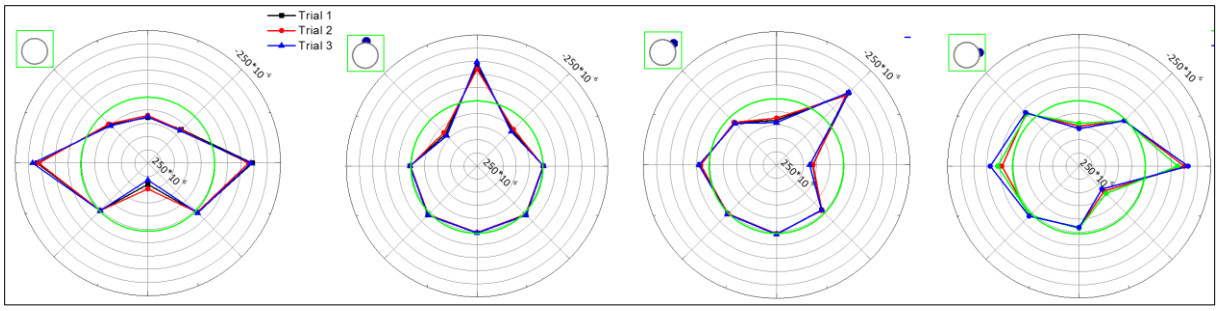

Figure A-5. Summary of results for void ratio 0.30 before shaking

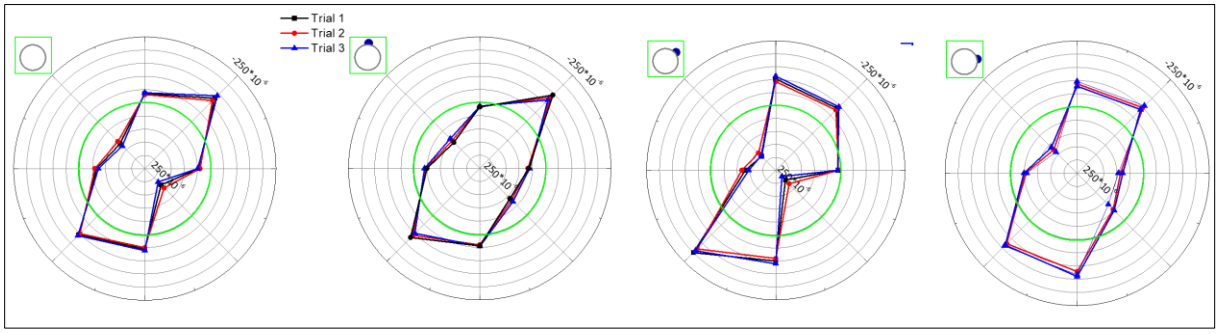

Figure A-6. Summary of results for void ratio 0.30 at maximum shear displacement

After confirming the reasonable repeatability at the first stage then the data was checked at the second stage. In the second stage, the repeatability of the specific data was checked. In this step, the values at the required time steps were chosen and plotted and then the repeatability was checked. For example, for the case of the weak zone at the crown, shoulder, and springline having the void ratio of 0.30 the data before shaking and at maximum shear displacement has been shown in Figure A-5 and Figure A-6 respectively. The plotted data shows that all three trials are fairly close to each other which means the tests have reasonable repeatability. After analyzing at the second stage one case was chosen for further analysis.